

This document is confidential and is proprietary to the American Chemical Society and its authors. Do not copy or disclose without written permission. If you have received this item in error, notify the sender and delete all copies.

Water: a Tale of Two Liquids

Journal:	<i>Chemical Reviews</i>
Manuscript ID	Draft
Manuscript Type:	Thematic Review
Date Submitted by the Author:	n/a
Complete List of Authors:	Gallo, Paola; Universita` di Roma Tre, Dipartimento di Fisica Amann-Winkel, Katrin; Stockholm University, Department of Physics Angell, Charles; Arizona State University, Department of Chemistry and Biochemistry Anisimov, Mikhail; The University of Maryland, Inst. for Physical Science & Technology Caupin, Frédéric; Université Claude Bernard Lyon 1, Département de Physique Chakravarty, Charusita; Indian Institute of Technology-Delhi, Chemistry Lascaris, Erik; Boston University, physics Loerting, Thomas; University of Innsbruck, Institute of Physical Chemistry Panagiotopoulos, Athanassios; Princeton University, Chemical Engineering Russo, John; Tokyo Daigaku Seisan Gijutsu Kenkyujo Sellberg, Jonas A.; Uppsala Universitet, Biomedical Center, dept. of Cell and Molecular biology Stanley, H.; Boston University, Department of Physics Tanaka, Hajime; Institute of Industrial Science, Dept. of Fundamental Engineering Vega De Las Heras, Carlos; Facultad de Ciencias Quimicas, Departamento de Quimica Fisica Xu, Limei; Peking University, International Center for Quantum Materials Pettersson, Lars; Stockholm University, Department of Physics

SCHOLARONE™
Manuscripts

WATER: A TALE OF TWO LIQUIDS

P. Gallo

*Dipartimento di Matematica e Fisica,
Università Roma Tre, via della Vasca Navale 84,
I-00146 Rome, Italy and INFN Sez. Roma Tre,
Via della Vasca Navale 84, I-00146 Rome, Italy*

K. Amann-Winkel

*Department of Physics, AlbaNova University Center,
Stockholm University, SE-106 91, Stockholm, Sweden*

C. A. Angell

*Department of Chemistry and Biochemistry,
Arizona State University, Tempe, Arizona 85287, USA*

M. A. Anisimov

*Institute for Physical Science and Technology and
Department of Chemical and Biomolecular Engineering,
University of Maryland, College Park, MD 20742, USA*

F. Caupin

*Institut Lumière Matière, UMR5306 Université Claude Bernard Lyon 1-CNRS,
Université de Lyon, Institut Universitaire de France, 69622 Villeurbanne, France*

C. Chakravarty

*Department of Chemistry, Indian Institute of Technology Delhi,
Hauz Khas, New Delhi 110016, India*

E. Lascaris

*Center for Polymer Studies and Dpt. of Physics,
Boston University, Boston, MA 02215, USA*

T. Loerting

1
2
3 *Institute of Physical Chemistry, University of Innsbruck, 6020 Innsbruck, Austria*
4
5

6 A. Z. Panagiotopoulos
7

8 *Department of Chemical and Biological Engineering,*
9 *Princeton University, Princeton, NJ 08544, USA*
10
11

12 J. Russo
13

14 *Inst. of Industrial Science, University of Tokyo,*
15 *4-6-1 Komaba, Meguro-ku, Tokyo 153-8505, Japan*
16
17
18

19 J. A. Sellberg
20

21 *Laboratory of Molecular Biophysics,*
22 *Department of Cell and Molecular Biology,*
23 *Biomedical Center, SE-752 37 Uppsala Sweden*
24
25
26
27

28 H. E. Stanley
29

30 *Center for Polymer Studies and Department of Physics,*
31 *Boston University, Boston, MA 02215, USA*
32
33

34 H. Tanaka
35

36 *Institute of Industrial Science, University of Tokyo,*
37 *4-6-1 Komaba, Meguro-ku, Tokyo 153-8505, Japan*
38
39
40

41 C. Vega
42

43 *Departamento de Química Física, Facultad de Ciencias Químicas,*
44 *Universidad Complutense de Madrid, 28040 Madrid, Spain*
45
46

47 L. Xu
48

49 *International Center for Quantum Materials,*
50 *Peking University, Beijing 100871, China*
51
52
53

54 L. G. M. Pettersson
55

56 *Dept. of Physics, AlbaNova University Center,*
57 *Stockholm University, SE-106 91, Stockholm, Sweden*
58
59
60

Abstract

Water is the most abundant liquid on earth and also the substance with the largest number of anomalies in its properties. It is a prerequisite for life and as such a most important subject of current research in chemical physics and physical chemistry. In spite of its simplicity as a liquid it has an enormously rich phase diagram where different types of ices, amorphous phases and anomalies disclose a path that points to unique thermodynamics of its supercooled liquid state that still hides many unraveled secrets. In this review we describe the behavior of water in the regime from ambient conditions to the deeply supercooled region. The review is divided into sections that describe simulations and experiments on this anomalous liquid. Several scenarios have been proposed to explain the anomalous properties that become strongly enhanced in the supercooled region and they are described in the first section. Among those the second critical point scenario has been investigated extensively and at present most experimental evidence point to this scenario and it is described in the second section. Starting from the very low temperatures a coexistence line between a high density amorphous phase and a low density amorphous phase would continue in a coexistence line between a high density and a low density liquid phase terminating in a liquid-liquid critical point, LLCP. On approaching this LLCP from the one-phase region a crossover in thermodynamics and dynamics can be found. Two liquid structures of water, nucleation of ice from supercooled water, stretched water, thermodynamics and dynamics of bulk water, confined water and aqueous solutions are discussed through results from experiments and simulations using the most sophisticated and advanced techniques. These findings represent tiles of a global picture that still needs to be completed. The future direction section explores some of the possible experimental lines of research that are essential to complete this picture.

CONTENTS

I. INTRODUCTION	5
II. SEVERAL SCENARIOS	6
III. LIQUID-LIQUID TRANSITION	9
IV. MICROSCOPIC STRUCTURE AND THERMODYNAMICS	17
V. COMPETITION BETWEEN TWO ALTERNATIVE STRUCTURES	24
The order parameter	28
VI. MODE COUPLING THEORY AND DYNAMICAL CROSSOVERS	33
VII. NUCLEATION OF ICE FROM SUPERCOOLED WATER	35
Local structural ordering in water has an impact on ice nucleation	41
VIII. RELATION BETWEEN DYNAMICS AND THERMODYNAMICS	45
IX. STRETCHED WATER	49
X. THERMODYNAMICS AND DYNAMICS OF CONFINED WATER	52
XI. THERMODYNAMICS AND DYNAMICS OF AQUEOUS SOLUTIONS	54
XII. FUTURE DIRECTIONS	59
A. Ultrafast probing.	60
B. Second component studies.	62
C. Studies at negative pressure.	63
XIII. ACKNOWLEDGEMENTS	68
References	69

I. INTRODUCTION

Water is the most abundant liquid, exhibits the most anomalous behavior, and is a prerequisite for life on this planet and probably for life elsewhere [1–10]. It shows a density maximum at 4°C (277 K) under ambient conditions and the solid phase has a lower density than the liquid (ice floats on top of liquid water) [11–13]. Its thermodynamic response functions, such as specific heat C_P , compressibility κ_T , and thermal expansion coefficient α , all of which can be determined by entropy or volume fluctuations, i.e.

$$\langle(\Delta V)^2\rangle = V k_B T \kappa_T, \quad (1)$$

$$\langle(\Delta S)^2\rangle = N k_B C_P,$$

and

$$\langle\Delta V \Delta S\rangle = V k_B T \alpha,$$

also show anomalous behaviors [4–6, 13–18].

For example, at atmospheric pressure κ_T increases when $T < 46^\circ\text{C}$ (319 K) but exhibits normal behavior when $T > 46^\circ\text{C}$. Similarly, at atmospheric pressure C_p increases when $T < 35^\circ\text{C}$ (308 K) and the value of α becomes negative, indicating that the volume expands below 4°C. One characteristic of the three thermodynamic properties shown in Eq. (1) is that they are related to fluctuations in liquid water that *increase* upon cooling below a certain temperature instead of decrease as in simple liquids. Figure 1 shows how this anomalous behavior becomes more pronounced in the deeply supercooled region and seems to diverge when T approaches -45°C (228 K) [12].

Here we review the behavior of water in the anomalous regime from ambient conditions to the deeply supercooled region. The regime above 232 K (temperature of homogeneous ice nucleation) and below the crystallization temperature 160 K (at ambient pressure) has provided the most information since it is more accessible. Among several theoretical scenarios, a liquid-liquid phase transition and an associated critical point (LLCP) are conjectured [19] and are assumed to lie in the regime between 232 K and 160 K, the so-called “no-man’s land” in the phase diagram, so called because ice nucleation occurs too rapidly for conventional measurement techniques. We connect the thermodynamic behavior of liquid water—its restructuring, anomalous behavior, and dynamics in the ambient and moderately supercooled

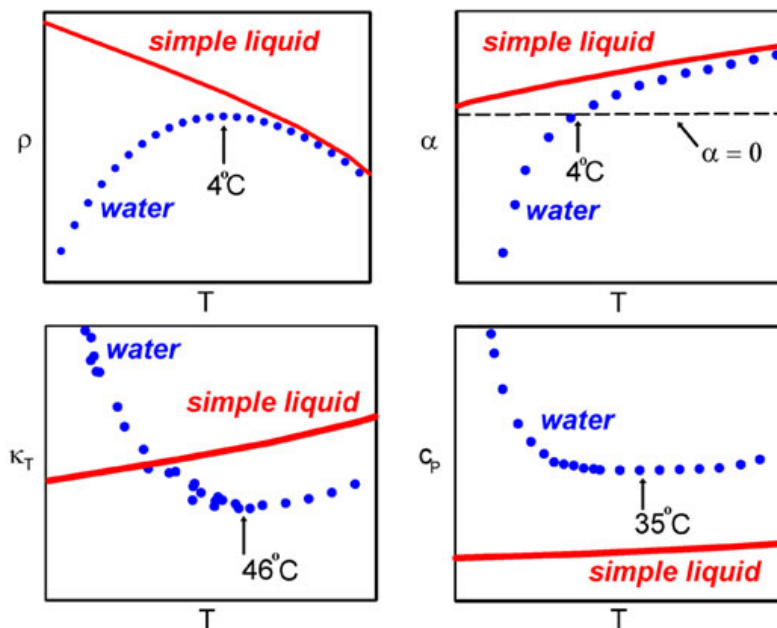


FIG. 1. Anomalous thermodynamic properties of water compared to simple liquids. Schematic comparison of the isobaric temperature dependence of the density ρ , thermal expansion coefficient α , isothermal compressibility κ_T , and isobaric heat capacity C_P for water and a simple liquid. Reproduced with permission from ref. [4].

regimes where experimental and simulation data are more accessible—to its behavior in the deeply supercooled region where an LLCP, real or virtual, may be located.

II. SEVERAL SCENARIOS

Over the past years, different scenarios have been proposed to explain the origin of the anomalies briefly described in the preceding section [19–24]. The first was in 1982 in a remarkable paper by Robin Speedy [25], which has become known as the “Speedy stability limit conjecture”. It has the same form of metastable water phase diagram as that yielded by empirical equations of state for water produced by the water and steam engineers. It was followed in 1992 by the famous “second critical point hypothesis” of Poole et al. [19] on the basis of molecular dynamics simulations of the ST2 model. This has been by far the most influential scenario and has been supported, explained, and contested, by various authors, e.g., Tanaka [26–28], Anisimov [29–31], Stanley and coworkers [19, 32–34], Limmer and Chandler [35, 36], Nilsson and Pettersson [37] to name a few. Then, among scenarios

1
2
3 that are qualitatively distinct, there is the “critical-point-free” scenario, initially presented
4 in 1994 as one of two cases within a bond-modified van der Waals model of the tetrahedral
5 liquid state by Poole et al. [38] and recently revisited by one of the present authors [24].
6
7 This was followed in 1996 by the “singularity free” scenario of Sastry et al. [23], based on
8
9 lattice model calculations.
10
11

12 The essential differences between these four scenarios are depicted in the series of phase
13 diagrams of Figure 2, adapted from the recent paper of Pallares et al. [39], and may be
14 summarized as follows (see also the Figure caption).
15
16

17 In the “stability limit conjecture” scenario, Figure 2A, the boundary of the liquid state at
18 high temperatures, (the well-known spinodal limit to the stability of the superheated liquid
19 state that terminates at the liquid gas critical point) is seen as reversing its temperature
20 dependence where the line of density maxima meets the liquid-vapor spinodal at negative
21 pressure. It then retraces to establish the limit to supercooling of the ambient pressure
22 and low pressure liquid. Debenedetti [4] correctly argues that the intersection between a
23 liquid-vapor spinodal and the metastable continuation of the liquid-vapor equilibrium line
24 must be a critical point, whose existence is not expected. However, we note that this is not
25 necessary if the line of instability at positive pressure is not a liquid-vapor spinodal, but
26 rather a line of instability toward another phase. The critical-point free scenario [23, 24]
27 (Fig. 2C) provides such a line (see below).
28
29
30
31
32
33
34
35
36

37 Figure 2B shows the second critical point scenario in its most familiar form, wherein
38 a second critical point exists at positive pressure, which terminates a line of liquid-liquid
39 transition. From the second critical point emanates a Widom line, the locus of extrema of
40 the correlation length. This scenario also includes other lines of response function maxima,
41 extending to lower and negative pressures. Near the critical point these lines asymptotically
42 approach the Widom line, but they fan out further away from the critical point.
43
44
45
46
47

48 In Fig. 2C is depicted the “critical point free” scenario by which is meant that the liquid-
49 liquid transition exists but the LLCP has moved sufficiently to negative pressures that it
50 meets the liquid-vapor spinodal and the fluctuations characteristic of each merge and lose
51 identity.
52
53
54

55 Finally, the “singularity-free” scenario (Fig. 2D), is characterized by sharp but non-
56 divergent maxima in the different response functions, occurring at different temperatures
57 but without a liquid-liquid transition and with a critical point only at 0 K.
58
59
60

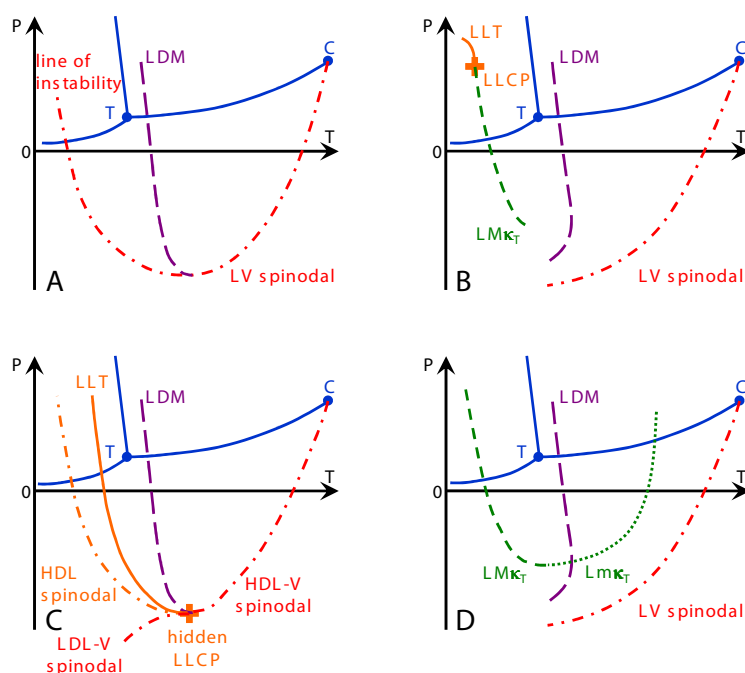


FIG. 2. Scenarios that might account for the behavior observed in Figure 1. **A.** Speedy's reentrant spinodal, **B.** Poole et al.'s 2nd critical point **C.** Poole et al.'s "weak bond" modified van der Waals model, now the "critical point free" scenario **D.** Sastry et al.'s "singularity free" scenario. Continuous blue curves show the known equilibrium coexistence lines between liquid, solid and vapor with the triple point marked as T. Liquid-vapor equilibrium terminates at the critical point C. The long-dashed purple line shows the line of density maxima (LDM), the short-dashed and dotted green line the lines of isothermal compressibility maxima (LMkT) and minima (LmkT), respectively. The dash-dotted lines show lines of instability. When the scenario comprises a liquid-liquid transition, it is displayed with a continuous orange line (LLT) and the liquid-liquid critical point is shown as an orange plus. Adapted from ref. [39].

Only in the first of the above scenarios does the form agree with that of the various multiparameter empirical equations of state, for which the spinodal limit to liquid stability reverses its position in pressure and retraces to positive pressures. Only in the second and third of these scenarios does a liquid-liquid coexistence line exist. And only in one of these does a second critical point exist.

III. LIQUID-LIQUID TRANSITION

Among the scenarios presented in Section II, the second critical point scenario [19] (Fig. 2B) with the possible existence of a liquid-liquid critical point (LLCP) and its associated critical fluctuations, which are considered as the source of water anomalies [5, 6, 20–22, 33, 40, 41], has been investigated extensively both in amorphous glassy water and in deeply supercooled liquid water, see for example [41–44]. The second critical point scenario and its associated liquid-liquid phase transition (LLPT) will be the focus of the present review.

In 1985, Mishima et al. [45] amorphized ice Ih at 77 K by compression beyond 1.1 GPa, and observed a first-order-like phase transition from high-density amorphous ice (HDA) to low-density amorphous ice (LDA) by heating the pressure-amorphized material at ambient pressure. LDA and HDA differ in structure and density where both states consist of fully hydrogen bonded, tetrahedral networks, but in HDA five first neighbors exist where the fifth molecule sits on an interstitial place between the first and second shell [46]. The radial distribution functions of LDA and HDA are examined in the article “X-ray and Neutron Scattering of Water” [47] contained within this volume.

The idea that water is a “mixture” of two different structures dates back to the 19th century [48, 49] and was reinvigorated in the late 20th century [50–52]. In 1992, in a seminal paper [19], using molecular dynamics simulations on the ST2 model of water, Poole, Sciortino, Essman, and Stanley found a first-order phase transition from low-density liquid (LDL) to high-density liquid (HDL) with an LLCP located at $T_C \sim 235$ K and $P_C \sim 200$ MPa [20–22]. In this scenario the LLPT is determined by extending the HDA and LDA first-order phase transition into the higher temperature and lower pressure region of the phase diagram [32, 45, 53–58], see Fig. 3. Mishima and Stanley base their estimate of the LLCP location on the discontinuity of the melting curve of ice IV at $T_C = 220$ K and $P_C = 100$ MPa [40]. Using neutron diffraction, first Bellissent-Funel [58] and then Soper and Ricci [57] verified the structure transformation in liquid water from LDL to HDL with increasing pressure, see Fig. 4. They found that the main difference between LDL and HDL lies in the second shell, i.e. the second shell of LDL sits at approximately the tetrahedral distance, but the second shell of HDL substantially collapses with interstitial molecules and contributions from less specific, bifurcated hydrogen bonds [59]. Using similar techniques, Bellissent-Funel et al. further demonstrated that the structure of liquid water becomes HDA

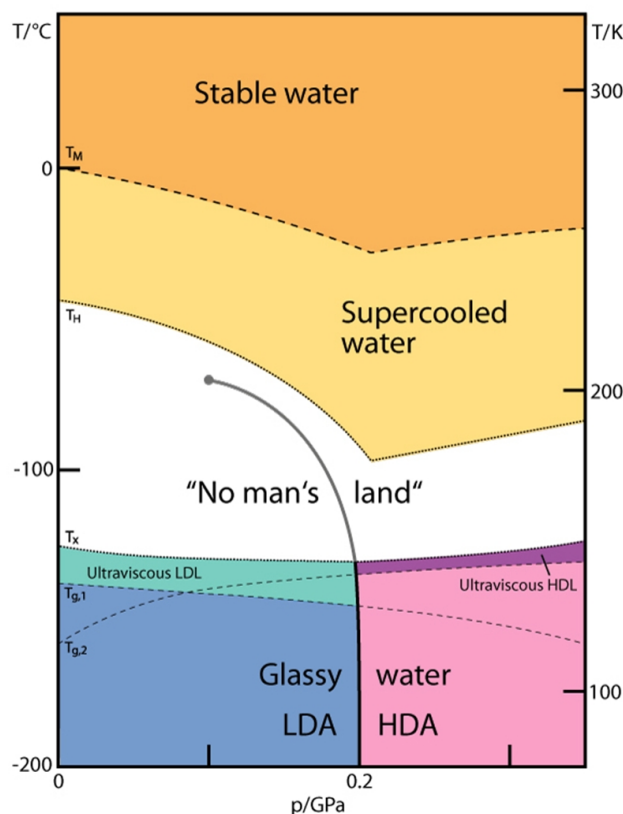


FIG. 3. Phase diagram of non-crystalline water (adapted from ref. [60], courtesy of Stephan Fuhrmann and Thomas Loerting). The "No man's land" indicates the region in which only crystalline ices have been observed so far. It is enclosed by the homogeneous crystallization line T_H from the top and the crystallization line T_X from the bottom. Two ultraviscous liquid domains, low- and high-density liquid water (LDL and HDL), can be found just below T_X . The two corresponding glass transition temperatures $T_{g,1}$ and $T_{g,2}$ separating the glassy solids LDA and HDA from the ultraviscous liquids LDL and HDL are taken from refs. [61] and [62], respectively. Please note the metastable extension of $T_{g,1}$ into the stability region of HDA and of $T_{g,2}$ into the stability region of LDA/LDL. A first-order liquid-liquid phase transition line (LLPT) ends in the purported liquid-liquid critical point (LLCP).

when cooled at high pressures but changes to LDA when cooled at low pressures. This again indicates a continuation of the LDA–HDA transition line to a LLPT in water [54, 55], and is consistent with results obtained using dilatometry and powder x-ray diffraction [56, 57].

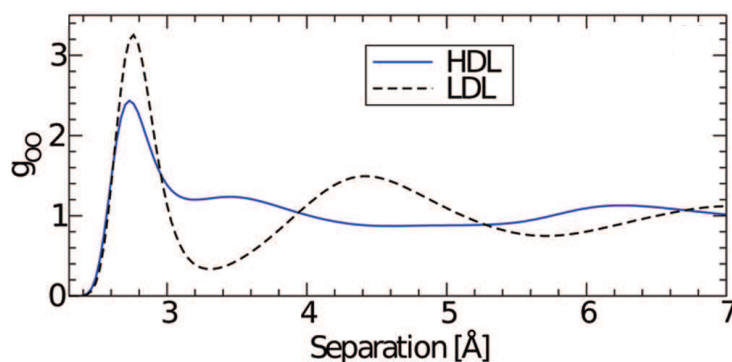


FIG. 4. Radial oxygen-oxygen pair-distribution functions for HDL and LDL demonstrating the structural difference between high- and low-density water. Adapted from ref. [57].

The transition between HDA and LDA under pressure was studied by Mishima and Suzuki [63], Klotz et al. [64], and Yoshimura et al. [65]. Their experiments demonstrate the first-order nature of the transition by revealing phase-boundaries between two phases, phase-coexistence, and a discontinuous change of structural properties at the transformation. Going beyond these studies Winkel et al. [66, 67] saw evidence of a first-order transition in the ultraviscous liquid domain at ≈ 140 K and 100 MPa on the downstroke. The location of the ultraviscous liquid domains for HDL and LDL is mapped by several experiments on the glass transition of amorphous ices, see Fig. 4 in Ref. 62 and Refs. 61 and 68.

A glass transition onset temperature of ≈ 136 K was detected in LDA by following the change in heat capacity upon heating LDA ice at ambient pressure at a rate of 10 K/min [69–71]. Although LDA can be prepared in several ways—by vapor deposition, by hyperquenching, and by the transformation from HDA described above—all studies find a similar increase in heat capacity, ΔC_p of ≈ 1 JK⁻¹mol⁻¹ [72]. The real nature of this extremely weak signal has been discussed for decades [24, 73]. The main point of the controversy concerns the question of whether a liquid nature is reached prior to crystallization [74] and the question whether translational motion [75] or rather defect-dynamics as in a crystalline system [76] is observed above T_g . More recently the interpretation that LDA undergoes a glass-liquid transition at the calorimetric glass transition near 136 K has received considerable support [77–79]. In the most recent scenario, the feeble signal is explained by the suspected strong or even superstrong nature of the low-density liquid near the glass transition temperature [24, 73, 80]. This suspicion found recent confirmation by dielectric

1
2
3 measurements indicating that LDL is actually the strongest of all known liquids [81, 82].
4

5 The glass transition of high-density amorphous ices was studied by *in situ* high-pressure
6 methods by Mishima [83, 84], Andersson [68, 85, 86], and Loerting et al. [87, 88]. These
7 measurements were recently reviewed in Ref. 62. All measurements indicate that the glass
8 transition at elevated pressures of $p > 200$ MPa appears to be at $T_g > 140$ K. These mea-
9 surements also indicate that the glass transition in HDA can be observed even at pressures
10 < 200 MPa, where LDA is thermodynamically favored over HDA [89], i.e. metastability
11 alone does not preclude the observation of glass transitions if the time scale of the trans-
12 formation to the thermodynamically more stable phase is significantly longer than the time
13 scale of equilibration. The transformation time scales can in fact greatly exceed those re-
14 quired for the equilibration of HDA, even at ambient pressure. Thus measurements of HDA
15 become possible in an extended temperature range and reveal an ambient-pressure heat ca-
16 pacity step and a dielectric relaxation time that indicates a glass transition at 116 K [81].
17 This glass transition in HDA is 20 K lower than the glass transition in LDA and thus rep-
18 represents water’s second glass transition. The possibility that two distinct glass transitions
19 occur has been further supported by the simulation results of Xu et al. [90, 91] and Gio-
20 vambattista et al. [61], which indicate that the experimental observations are qualitatively
21 consistent with water and water-like models having a LLPT, e.g., the ST2 water model, but
22 not with models lacking two liquid phases, e.g., SPC/E water.
23
24
25
26
27
28
29
30
31
32
33
34
35
36

37 The hypothesized LLCP is located in the deeply supercooled region, the “No-Man’s Land”
38 below the temperature of homogeneous nucleation [19–22, 33, 40, 41]. Various potential
39 model studies [20–22, 29, 30, 92–107] have demonstrated the existence of an LLCP, and
40 Table I provides the reported locations of the LLCP in the various long-range all-atom
41 models.
42
43
44
45

46 Some models show a number of water’s anomalies but do not have an LLCP, e.g., the
47 short-range monoatomic mW model [108, 109].
48
49

50 On the other hand other short-range monoatomic models, e.g., the Jagla model, do show
51 the presence of an LLCP [110]. The use of the technique of successive umbrella sampling
52 grand canonical Monte Carlo and of finite-size scaling has allowed to prove rigorously that
53 the Jagla LLCP is a second-order critical point that belongs to the Ising universality class
54 and to determine with great precision its location [111]. Importantly the estimate of the
55 LLCP position that was previously obtained by molecular dynamics (MD) simulation [110]
56
57
58
59
60

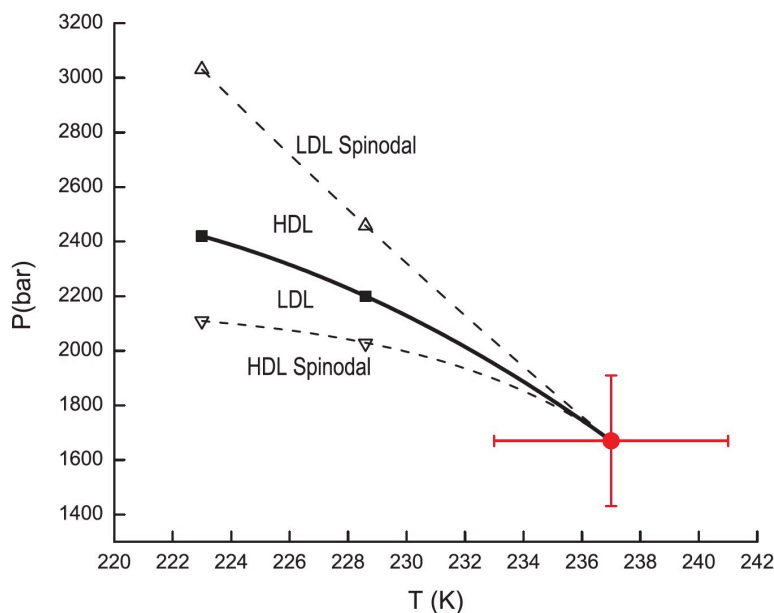


FIG. 5. Pressure-temperature projection of the metastable phase behavior of the ST2b model for water from Liu et al. [112] showing the liquid-liquid coexistence curve (black squares), the LDL spinodal (up-triangles), and the HDL spinodal (down-triangles). Solid and dashed lines are a guide to the eye and the red circle is the critical point from Ref. [113]. Copyright ©2012 by the American Institute of Physics.

is in very good agreement with the true location of the LLCP in the model, as found with the rigorous finite-size scaling approach [111]. These results prove that the techniques for locating the LLCP at the maximum temperature of the spinodals in MD finite size simulations are valid and lead to the same result as the rigorous technique.

The liquid-liquid transition phenomenon for a one-component liquid also applies to other network-forming, tetrahedrally-coordinated liquids where simulations show the possible existence of an LLCP, see for example Refs. [114–119].

The landmark paper by Poole, Sciortino, Essman and Stanley [19] that first proposed the possibility of an LLPT in a molecular model of water described their molecular dynamics simulations as using the 5-site, rigid ST2 model [120] that includes both Coulombic and van der Waals forces. Long-range interactions for the Coulombic forces were taken into account using the reaction-field method. We label this variant of the model ST2c to distinguish it from the two other variants that we will introduce below. Poole et al. observed that

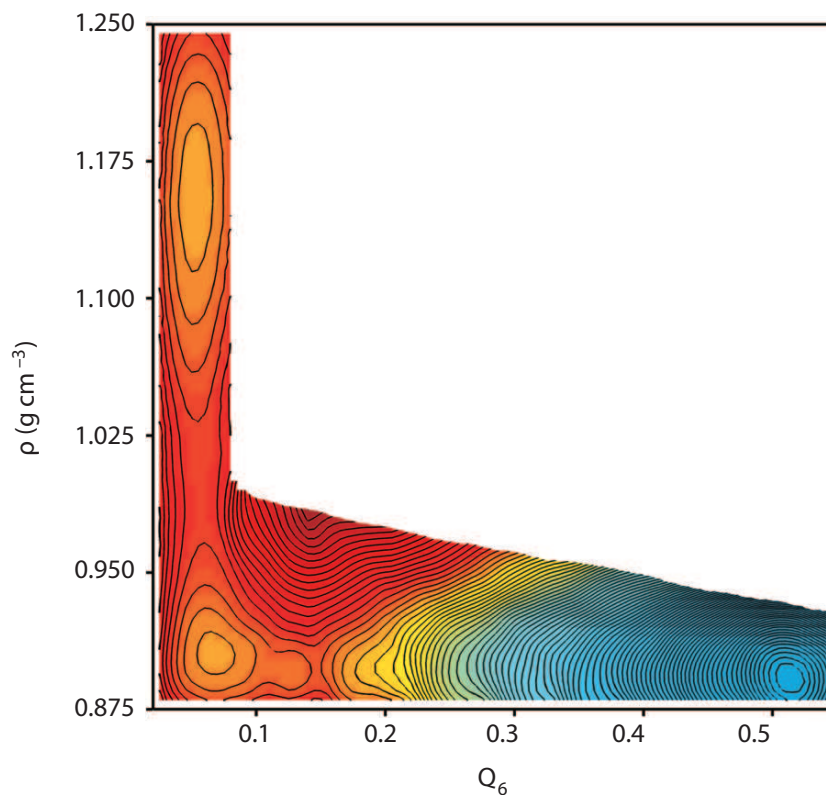


FIG. 6. The free energy surface of the ST2 model with vacuum boundary conditions at 228.6 K and 2.4 bar from Palmer et al. [121]. These conditions correspond to liquid-liquid equilibrium. Contours are spaced $1 k_B T$ apart. Copyright ©2014 by Macmillan Publishers.

at sufficiently low temperatures the liquid isotherms exhibit behavior consistent with an approach to a critical point, which they proposed would terminate a liquid-liquid coexistence line in the deeply supercooled region of the phase diagram. More recently Liu et al. [113] used grand canonical Monte Carlo to study the ST2 model with an Ewald summation of electrostatic interactions. This approach determines the free energy of the system as a function of density, but does not permit the precise control of other order parameters.

An Ewald summation of Coulombic interactions requires an assumption about the dielectric properties of the medium surrounding the system at infinite distance. Reference [113] used vacuum boundary conditions ($\epsilon_\infty = 1$), which we will refer to as the ST2b model. Limmer and Chandler [35, 36] studied different versions of the ST2 model using a hybrid Monte Carlo approach in which both the density ρ and the orientational order parameter Q_6 that discriminates between disordered liquid and crystalline environments can be controlled. They did not find evidence of an LLPT for any model variation and suggested that

Potential	T_c (K)	P_c (MPa)	ρ_c (g/cm ³)
ST2 [19]	235	200	1
ST2 [94]	245	180	0.94
ST2a [112]	-	-	-
ST2b [97]	237 ± 4	167 ± 24	0.99 ± 0.02
ST2c [122]	247 ± 3	185 ± 15	0.955 ± 0.010
TIP4P [107]	190	150	1.06
TIP4P/2005 [98]	193	135	1.012
TIP4P-EW [96]	210	310	1.09
TIP5P [93]	217 ± 3	340 ± 20	1.13 ± 0.04
TIP5P-E [95]	210	310	1.09
SPC/E [92]	160	200	1.07

TABLE I. Critical temperature T_c , pressure P_c and density ρ_c reported using different water potentials. ST2a, ST2b and ST2c are variants of ST2 as described in the text.

results pointing to an LLPT were due to insufficient equilibration and sampling. A subsequent study by Liu et al. [112] used NPT Monte Carlo sampling and a weighted histogram analysis method to obtain the free energy as function of ρ , Q_6 , and temperature T . The existence of an LLPT for the ST2b ($\epsilon_\infty = 1$) model was confirmed (see Fig. 5). For the ST2a ($\epsilon_\infty \rightarrow \infty$) model, rapid crystallization to an unphysical high-density ($\rho \sim 1.5$ to 1.7 g/cm³) dipolar-ordered ice phase was observed. A phase diagram similar to that shown in Fig. 5 (shifted to slightly higher temperatures and pressures) was obtained by Cuthbertson and Poole [122] and Poole et al. [123] for the ST2c (reaction field) model using molecular dynamics and umbrella sampling Monte Carlo, respectively. The most comprehensive study to date of an LLPT in a molecular model of water was reported recently by Palmer et al. [121] who focused on the ST2b ($\epsilon_\infty = 1$) model. Six different computational protocols were used to obtain the free energy as a function of ρ , Q_6 , and temperature T , and all three basins (HDL, LDL, and crystal) were sampled reversibly (see Fig. 6). The free energy barrier between HDL and LDL was obtained as a function of system size and found to be consistent with the $N^{2/3}$ scaling law expected for a first-order phase transition.

At LLPT conditions, both liquids are metastable with respect to crystallization, and if

1
2
3 the time is sufficiently long and the system size sufficiently large, crystallization will occur.
4 Unlike the mW model [124], crystallization time scales for the ST2 model of water are longer
5 than the time scales for equilibration of the liquid. For example, in a study of the ST2c
6 (reaction field) model using an $N = 4000$ molecule system, Yagasaki et al. [125] observed
7 liquid-liquid coexistence at $T = 235$ K for approximately 800 ns, followed by ice nucleation
8 and crystal growth. In that study a rectangular simulation box was used to minimize the
9 interfacial energy and allow liquid-liquid coexistence to develop. These results were later
10 criticized by Overduin and Patey [126] who found that the density differences that are
11 observed for TIP4P/2005 and TIP5P water using smaller simulation cells disappear when
12 larger cells ($N = 32,000$) are considered.
13
14

15 Using the same force-field model as Yagasaki et al., Kesselring et al. [127, 128] performed
16 many 1 μ s simulations of systems ranging in size from 216 to 729 molecules, and found
17 LDL to be stable with respect to the crystal in over 98% of their runs. Small crystal
18 nuclei ("crystallites") are easily detected using the bond order parameter d_3 introduced by
19 Ghiringhelli et al. [129]. This parameter characterizes the bond between two molecules and
20 is designed to distinguish between a fluid and a diamond structure. A molecule is typically
21 considered part of a crystal if three of its four bonds exhibit $d_3 < 0.87$. In the simulations
22 done by Kesselring et al., tiny crystallites grew and then melted within 1 μ s. Based on the
23 few crystallization events that occurred, they estimated that the critical size of a crystallite
24 is approximately 70 ± 10 molecules before spontaneous crystallization occurs.
25
26
27
28
29
30
31
32
33
34
35
36
37
38
39

40 Two recent studies by Sciortino and coworkers rigorously examine the LLPT for a general
41 model of tetrahedrally coordinated liquids [115] and for variations of the ST2 model of water
42 [130]. They show that bond flexibility affects the relative stability of the liquid and crystal
43 phases. On increasing bond flexibility, the liquid-liquid critical point moves to a temperature
44 where the liquid is more stable than ice. Taken together with the work of Palmer et al.
45 [121], these studies conclusively show that the claim of Limmer and Chandler—that the
46 liquid-liquid transition is a misinterpreted crystallization transition in all atomistic models
47 of water—is incorrect in its generality. It is certainly true for the mW model, while for
48 TIP4P/2005 water the situation is unclear [125, 126]. The origin of the discrepancy between
49 different simulations using the ST2 model has still not been clearly identified, but potential
50 contributions are discussed in Ref. [131]. We conclude this section by noting that the strong
51 debate about the potential existence of a LLPT in real and simulated supercooled water
52
53
54
55
56
57
58
59
60

1
2
3 has driven a rapid development of computational methodologies and has led to rigorous
4 sampling of low-temperature properties in several water models. However, to conclusively
5 determine which case describes real water we will need new experimental data that go deeper
6 into "no-man's land".
7
8
9

10 11 12 13 **IV. MICROSCOPIC STRUCTURE AND THERMODYNAMICS** 14 15

16 The thermodynamic behavior of water suggests that it consists of at least two structurally
17 distinct species with relative populations varying with pressure and temperature. Beginning
18 with the mixture models of Whiting and Röntgen [48, 49], two-scale models [110, 132] have
19 often been invoked as possible explanations of the thermodynamic and dynamic anomalies
20 of liquid water. These models posit a separation of the energy states available to water
21 molecules into two distinct groups: one corresponding to low-energy/low entropy ordered
22 configurations, and the other to high-energy/high entropy configurations. In this picture
23 the complexity of water is thus modeled by a mixture of these two structural motifs.
24
25
26
27
28
29

30 Conceptually similar but differently formulated approaches have been taken using two-
31 state models. Tanaka [26, 28, 133] recognizes that, in any liquid, locally-favored structures
32 with low configurational entropy are formed in a sea of random, normal-liquid structures with
33 high configurational entropy. A phenomenological two-state model approximates this picture
34 as a bimodal distribution of possible molecular configurations and sees cold and supercooled
35 liquid water as a "mixture" of two distinct competitive states, where the fraction of each state
36 is controlled by pressure and temperature. Anisimov and coworkers [30, 31, 134] describe a
37 competition between an ideal entropy of mixing and a non-ideal part of the Gibbs energy of
38 mixing. From a phenomenological point of view, even without a microscopic understanding
39 of the differences between these alternative configurations, this two-state model yields an
40 equation of state of supercooled water that can be fitted to agree remarkably well with
41 experimental results [26, 31, 133, 135] (see Fig. 7).
42
43
44
45
46
47
48
49
50
51

52 A difficulty associated with correlating data that are obtained in the experimentally
53 accessible region (above the ice homogeneous nucleation temperature) is accurately locating
54 the liquid-liquid critical point and determining the critical pressure based on these data.
55 Using the optimization shown in Fig. 8, any critical pressure value above 100 MPa is excluded
56 and the lower limit is uncertain. This is in contrast to the extensively-studied water models,
57
58
59
60

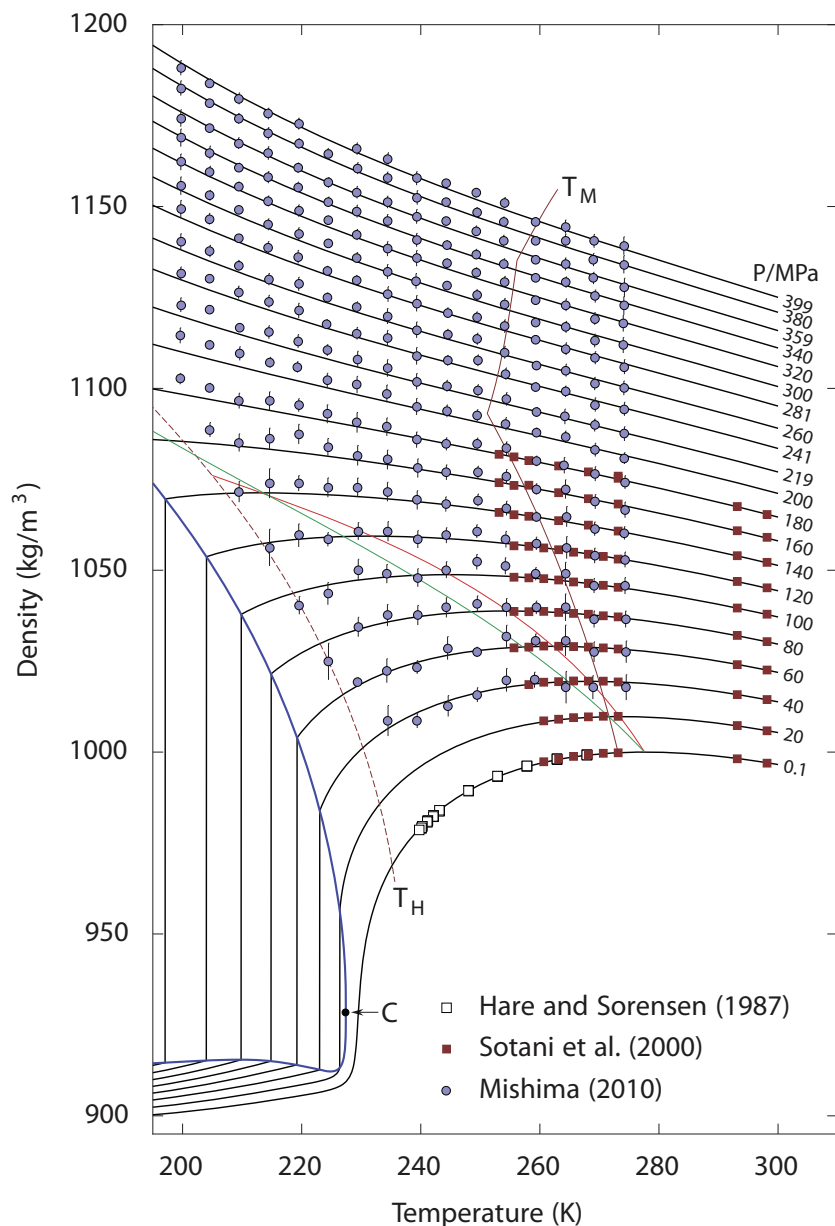


FIG. 7. Density of cold and supercooled water as a function of temperature along isobars. Symbols represent experimental data [136–138]. Black curves are the predictions of the two-state model [31]. T_M (dark red) indicates the melting temperature and T_H indicates the homogeneous nucleation temperature. The thick blue line is the predicted liquid-liquid equilibrium curve, with the critical point C. The red line is the line of maximum density, and the green line is the line of a constant LDL fraction of about 0.12.

the ST2 model and the TIP4P/2005 model proposed by Abascal and Vega [139], for which the critical points are located at about 180 and 135 MPa, respectively, see Table I. However,

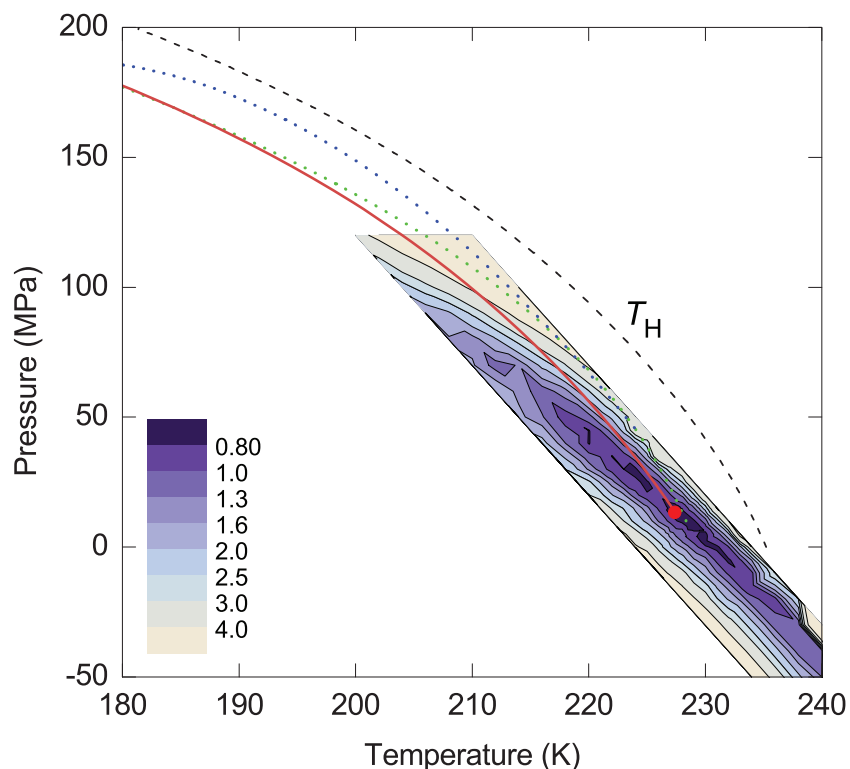


FIG. 8. Optimization of the critical-point location [31]. The colored map shows the reduced sum of squared residuals. The solid red line is the hypothesized liquid-liquid transition curve. The dashed curve shows the temperature of homogeneous ice nucleation. The blue dotted curve is the liquid-liquid transition curve suggested by Mishima [137] and the green dotted curve is the 'singularity' line suggested by Kanno and Angell [18].

any attempt to predict the location of a possible LLCPP becomes highly uncertain because the anomalous behavior intensifies as it moves into regions of lower temperature and higher pressure where measurements are lacking (see Fig. 8). Indeed, we note the uncertainty in the location of a possible LLCPP in the TIP4P/2005 model as there have been different proposals [98, 125] and the existence of an LLCPP in the model has even been questioned [126, 140].

Thus pseudo-binary models are used to explain both the anomalies and the possible liquid-liquid phase transition. From a molecular point of view, water does not consist of distinct species. It is the nature of the hydrogen-bonding network that implies that fluctuations in density, correlated with local tetrahedral ordering, give rise to structurally distinct regions of local order that in turn give rise to pseudo-binary behavior. Indeed, data from small-angle x-ray scattering (SAXS) have been interpreted in terms of density inhomogeneities

1
2
3 in the liquid—with an average spatial extent of ~ 1 nm at ambient conditions [141]—that
4 grow upon supercooling [142]. Although this has not avoided controversy [143–145], it has
5 received support from a purely statistical mechanical perspective [146].
6
7

8
9 X-ray absorption spectroscopy (XAS) has also indicated the presence of two types of local
10 structure in liquid water: very tetrahedral and very disordered [147–149]. The former would
11 correspond to LDL and the latter to HDL. There is general agreement that the pre- (535
12 eV) and main-edge peaks (537 to 538 eV) in the XAS of liquid water are fingerprints of
13 distorted H-bonds, whereas the post-edge (540 to 541 eV) is associated with strong H-bonds
14 and is further enhanced for tetrahedral H-bond structures [147–152]. Interpretations of the
15 spectra in terms of structure either emphasize the ultrafast nature of the x-ray probe and
16 suggest small, instantaneous distortions around a mainly tetrahedral network [152–155] or
17 propose fluctuations that are of a sufficiently long duration and are sufficiently extended
18 that a distinction in terms of local HDL and LDL environments becomes meaningful [141,
19 143, 156, 157].
20
21
22
23
24
25
26
27

28
29 The most direct evidence of bimodality in terms of local structures is found in x-ray
30 emission spectroscopy (XES) in which the sharp, non-bonding lone-pair peak of gas phase
31 water becomes broadened and shifted down in energy in crystalline ice. In water we observe
32 *two* sharp peaks that interconvert but do not broaden with increasing temperature [141, 158–
33 163] (see Fig. 9). The peak close to the peak in tetrahedral ice is assigned to local LDL-like
34 tetrahedral coordination and the other peak, close to the gas phase position, is assigned
35 to disordered HDL-like local structures with broken or weakened H-bonds. The origin of
36 the split is under debate [165, 166], with one interpretation in terms of differences in final
37 state [158, 159] and the other in terms of differences in the initial state [141, 162, 167].
38 However both interpretations require the existence of two different local environments. As
39 further support for a bimodal distribution of structures, we note the recent time-resolved
40 Optical Kerr Effect (OKE) measurements by Taschin et al. [168]. OKE involves low-energy
41 vibrations in the H-bonding network where there are clearly identified signatures of HDL
42 and LDL with the same temperature dependence as in the other spectroscopies.
43
44
45
46
47
48
49
50
51
52
53

54 A two-order parameter model [28] provides a framework for understanding the spec-
55 troscopic results and the various thermodynamic features in terms of two competing order
56 parameters: a density-dependent order metric that promotes close-packed structures in both
57 the crystal and the liquid and an anisotropic or bond-driven order parameter that promotes
58
59
60

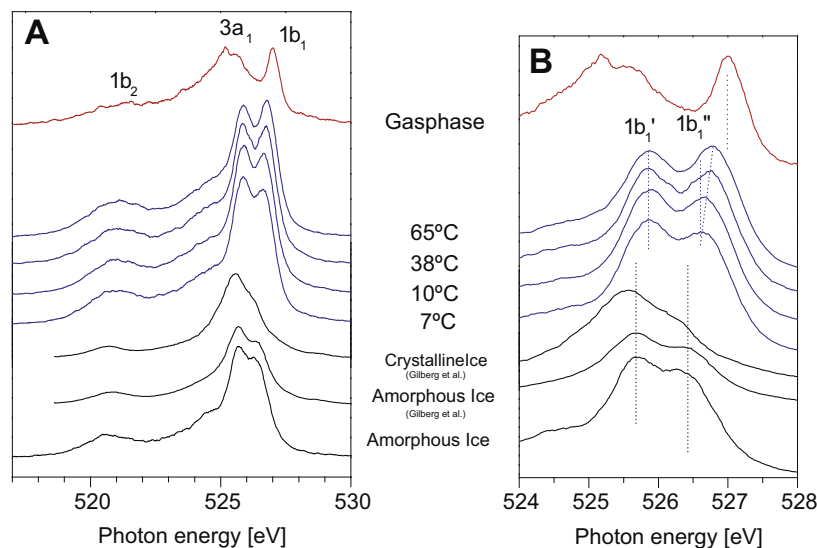


FIG. 9. O 1s soft x-ray emission spectra of gas phase water, liquid water at different temperatures and amorphous and crystalline ice, with an energy scale displaying the full spectrum (A) or only the lone-pair, $1b_1$ region (B). The excitation energy is 550 eV, well above the ionization threshold. Peak components are labeled based on the molecular orbitals for a water molecule. The highest peak ($1b_1$) splits into double peaks ($1b_1'$ and $1b_1''$). The XES spectra of amorphous (-190°C (83 K)) and crystalline ice from Gilberg et al. [164] are included for comparison. Figure adapted from ref. [162].

open, tetrahedral local order.

The local structure of the liquid tends to correspond to that of the underlying crystalline phase, and a triple point is seen, i.e. a point where the low-density crystal, the high-density crystal, and the liquid are in equilibrium [27]. Glass-forming tendencies are most pronounced in the neighborhood of the triple point [169, 170] where structural frustration due to competition between the two order metrics is most pronounced [28].

The connection between the two-order parameter description of water-like liquids and an atomistic picture of liquid state structure and dynamics was first provided by Errington and Debenedetti using the rigid-body SPC/E water model [171]. This connection requires that local order metrics be defined in terms of particle positions. A suitable order metric that defines density-driven local order applicable to both simple and complex fluids is the translational- or pair-ordering metric in terms of the atom-atom pair-correlation function

g(r) [172]. In the case of H₂O, this order parameter may be defined as

$$\tau = 1/\xi_C \int_0^{\xi_C} |g_{oo}(\xi) - 1| d\xi, \quad (2)$$

where $\xi = r\rho^{1/3}$ is the distance r between the oxygen atoms of a pair of molecules divided by the mean pair separation $\rho^{1/3}$ where ρ is the number density N/V , and $g_{oo}(\xi)$ is the oxygen-oxygen pair-correlation function. A convenient measure of local tetrahedrality associated with a given oxygen atom i is given by

$$q_{\text{tet}} = 1 - \frac{3}{8} \sum_{j=1}^3 \sum_{k=j+1}^4 \left(\cos(\psi_{jk}) + \frac{1}{3} \right)^2, \quad (3)$$

where ψ_{jk} is the angle between the bond vectors r_{ij} and r_{ik} where j and k label the four nearest oxygen atoms. At low densities or temperatures the probability distributions of tetrahedral order $P(q_{\text{tet}})$ have a peak at high tetrahedrality. At intermediate densities or temperatures $P(q_{\text{tet}})$ has a bimodal or shoulder structure with a second peak at intermediate tetrahedrality. Order maps displaying the correlation between translational and tetrahedral order provide an interaction-independent summary of the variation of structural order over a wide range of state points. In the case of SPC/E and other rigid-body models of water, one can define a structurally anomalous region in the phase diagram such that all state points in this regime fall on essentially the same curve in the (q_{tet}, T) plane. This strong correlation between tetrahedral- and pair-order indicates that distortions from local tetrahedrality in the hydrogen-bonded network reduce pair-correlations and enhance disorder in the anomalous regime. At high densities, tetrahedral order ceases to be significant and the system behaves as a simple liquid dominated by pair-ordering.

Figure 10 uses simulations of the TIP4P/2005 water model [173] to show the structurally anomalous regime in water that encloses the region of diffusional anomaly which in turn encloses the region of density anomaly. This nested structure gives rise to the idea of a cascade of anomalies, where progressive enhancement of the degree of structural anomaly gives rise to various transport and thermodynamic anomalies. Comparisons of the cascade structure and the order maps of a number of tetrahedral liquids are now available [177–179].

Connecting entropy with structure-based order parameters for fluids, particularly in the context of biomolecular simulations, has been an active area of research [180–186]. A useful route in the context of simple and anomalous liquids is provided by the multiparticle

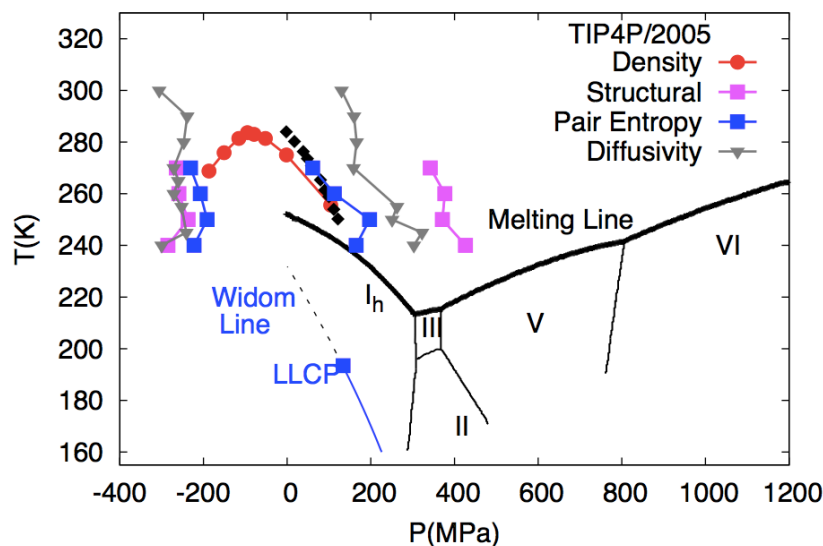


FIG. 10. Thermodynamics of the condensed phases of water, illustrated for the TIP4P/2005 rigid-body model of water [173]. The data for the phase boundaries are taken from ref. [174]. The boundaries of the structural, density, pair-entropy and diffusivity anomalies are taken from ref. [175]. The experimental TMD line shown in filled black diamonds is taken from ref. [176]. The Widom line (see the definition in sec. VIII) is taken from ref. [98].

correlation expansion of the entropy. $S_e = S_2 + S_3 + \dots$, where S_n denotes the entropy contribution due to n -particle correlations [187–191]. Since the thermodynamic excess entropy can be obtained from simulations or from calorimetric data, the multiparticle expansion serves to highlight the role of pair-, triplet-, and higher-order correlations in determining the liquid entropy. The behavior of simple liquids is dominated by pair-correlations which contribute 85–90% of S_e . For multi-atomic systems, the pair-entropy term can be generalized in terms of atom-atom pair-distribution functions accessible from simulations, x-ray, or neutron scattering. For tetrahedral liquids such as water, however, the three-body or triplet correlations can be significant since they are associated with the locally anisotropic nature of the liquid-state network.

Stillinger-Weber liquids with a variable tetrahedrality parameter can be used to model molten phases of Group 14 elements (C, Si, Ge, Sn, Pb) as well as provide a coarse-grained, monoatomic (mW) model for water [108, 124, 192–195]. As a function of increasing tetrahedrality, the triplet contribution to the excess entropy is significantly higher than the pair-entropy contribution [196]. Transformation to a triplet-dominated fluid strongly favors the

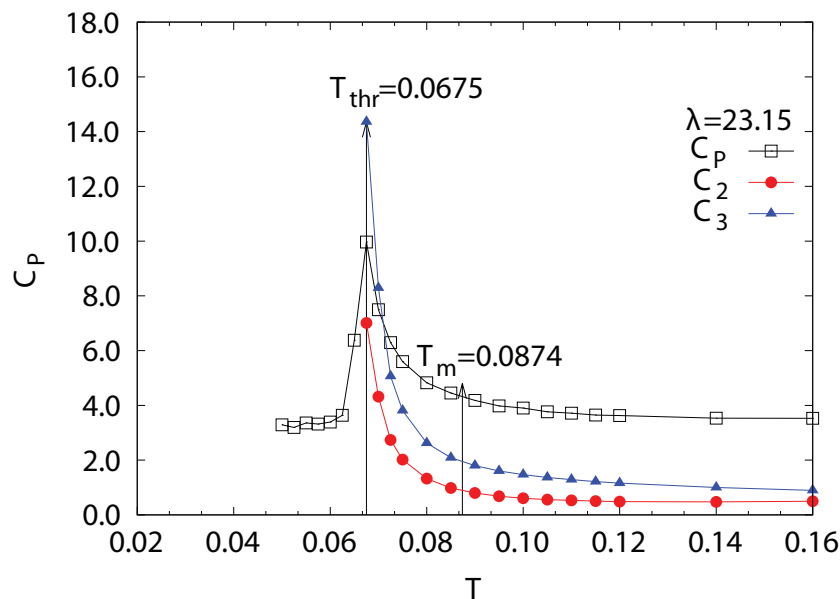


FIG. 11. Multiparticle correlation. Contributions to the entropy and the heat capacity anomaly. The total (C_P), pair (C_2), and triplet (C_3) contributions as a function of temperature (T) for the monoatomic water (mW) model at 1 atm pressure [196].

formation of a tetrahedral crystal, as well as the existence of a heat capacity anomaly, and the local order within the first neighbor shell is a critical factor in determining the behavior upon supercooling. The characteristic rise in heat capacity on the isobaric cooling of tetrahedral liquids is closely tracked by the pair- and triplet-contributions to the entropy (see Fig. 11), and thus provides a direct connection between structural correlations and thermodynamics. Preliminary results for triplet O–O–O correlations in pair-additive, rigid-body, atomistic models of water strongly resemble the mW water model [197].

In the section linking dynamics to thermodynamics the behavior of the two-body excess entropy s_2 will be discussed for the TIP4P water model upon supercooling [198, 199]. This quantity is easily measurable in experiments and it is connected to a dynamic crossover that in supercooled water is associated with the presence of an LLCP.

V. COMPETITION BETWEEN TWO ALTERNATIVE STRUCTURES

The anomalies of supercooled water and the possibility of metastable liquid-liquid separation in water can be explained if water is viewed as a mixture of two inter-convertible

1
2
3 organizations of hydrogen bonds whose ratio is controlled by thermodynamic equilibrium
4 [30, 31, 133, 200]. The existence of two structures does not necessarily mean that they will
5 phase-separate [31, 134, 200]. If these structures form an ideal solution, the liquid will re-
6 main homogeneous at any temperature or pressure, while the competition between the two
7 structures may cause the density maximum and non-diverging anomalies of the response
8 functions [200]. However, if the solution is non-ideal, a positive excess Gibbs energy of
9 mixing could lead to phase separation if the nonideality of mixing of these two states is
10 strong enough. If the excess Gibbs energy is primarily associated with a heat of mixing,
11 the separation will be energy-driven. If the excess Gibbs energy is primarily associated
12 with excess entropy, the separation will be entropy-driven. The entropy-driven nature of
13 this separation means that if the two states were unmixed they would allow more possible
14 statistical configurations and thus a higher entropy.

15
16 One example of this is the Woodcock-Angell-Cheeseman (WAC) model [201] modified
17 by Lascaris [202]. The original WAC model was for liquid silica (SiO_2), a close relative
18 of water. Both liquids are tetrahedral and consist of large four-coordinated atoms (O in
19 water, Si in silica) surrounded by twice as many smaller atoms (H in water, O in silica), but
20 unlike most water models the WAC model has no explicit bonds and is simply a mixture
21 of Si^{+4} and O^{-2} ions. It was recently found that the WAC model is remarkably close to
22 having a LLCPP [203], and it was subsequently demonstrated that by decreasing the ion
23 charge the model can be tuned such that a LLCPP appears, as indicated by the crossing
24 of the isochores and the diverging response function maxima at the state point where the
25 LLCPP is located [34, 94]. Increasing the charge separates the isochores and greatly reduces
26 the magnitude of the response function maxima. In addition, the response function maxima
27 move to separate state points, indicating that the LLCPP has disappeared [202]. Changing
28 the ion charge in the WAC model has this effect due to the Gibbs free-energy of mixing,
29 $\Delta G_{\text{mix}} = \Delta H_{\text{mix}} - T\Delta S_{\text{mix}}$. Because increasing the charge makes the Si–O bond more
30 attractive, more Si ions are drawn into the first coordination shell. This increases the HDL
31 entropy and thus the ΔS_{mix} . The result is that ΔG_{mix} becomes negative at all temperatures
32 and pressures, and no liquid-liquid transition occurs. A decrease in the ion charge reverses
33 this effect. These considerations suggest that the liquid-liquid transition in the modified
34 WAC model may be entropy-driven, a scenario that has also been proposed for water [31].

35
36 More generally, two-state thermodynamics can explain “liquid polymorphism,” defined
37
38
39
40
41
42
43
44
45
46
47
48
49
50
51
52
53
54
55
56
57
58
59
60

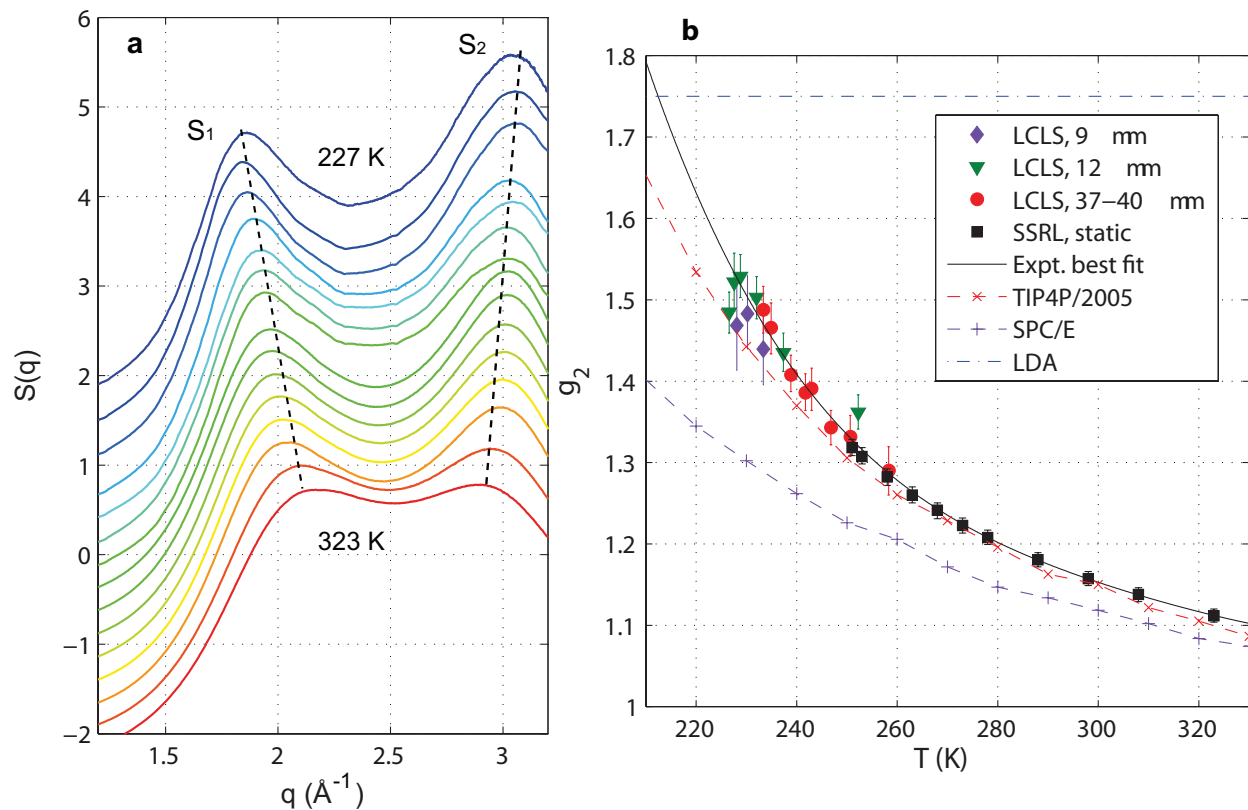


FIG. 12. Ultrafast x-ray probing of water structure below the homogeneous ice nucleation using micron-sized water droplets falling in vacuum [209] **a.** Scattering structure factor, $S(q)$. The data reveal a continuously increasing split of the principal $S(q)$ maximum into two well-separated peaks, S_1 and S_2 (dashed lines). **b.** Experimental tetrahedrality (g_2) values, derived from the measured split, Δq , between the two peaks in **a** as calibrated against a fit to molecular dynamics data. g_2 is the height of the second peak in the O-O pair-distribution function. Error bars are estimated from the maximum and minimum Δq values allowed by the uncertainty in the S_1 and S_2 peak positions. Also shown is the fourth-order polynomial least-squares fit to the experimental data (black solid line), where the last (that is, low-T) two data points for the 12- μm -diameter droplets and the last data point for the 9- μm -diameter droplets are ignored owing to high nonlinearity in the detector response (see ref. [209]). For comparison, the temperature dependences of g_2 for the TIP4P/2005 (red dashed line) and SPC/E (purple dashed line) models are depicted along with the characteristic value of g_2 for LDA ice [210] (blue dashdot line).

as the existence of a single-component substance in two different liquid forms [133, 200,

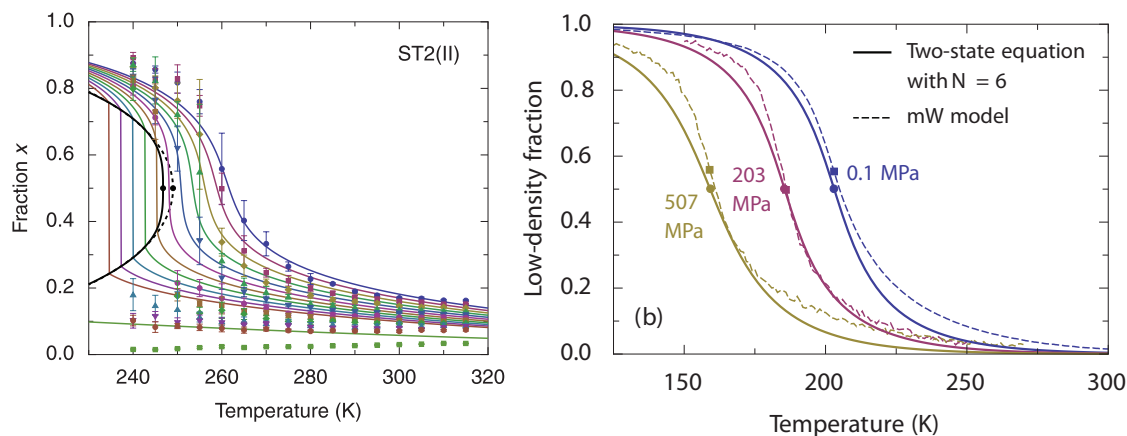


FIG. 13. Low-density fraction from simulations of water-like models and the predictions from the two-state thermodynamics: **a.** ST2(II), a version of the ST2 model [219]. Symbols are simulation data. Solid curves are theoretical predictions. Dashed curve is a mean-field approximation. **b.** mW model [109]. Solid curves are theoretical predictions which include clustering of water molecules with average aggregation number $N = 6$.

204–207, 211]. Liquid polymorphism has been experimentally observed or theoretically suggested in molten silicon, liquid phosphorus, triphenyl phosphate, and in some other molecular-network-forming substances [119, 178, 200, 204, 205]. Recent experiments [147, 156, 162, 163, 168, 208, 209] suggest the existence of a bimodal distribution of molecular configurations in water. In particular, the transformation of water structure in micrometer-sized water droplets has been observed [209] using an x-ray free-electron laser (see Fig. 12). The droplets are injected into vacuum where they almost instantly cool through evaporation, and a diffraction pattern is obtained from individual droplets when they are hit by the 50 fs duration, fully-coherent intense x-ray pulses. The temperature of the droplets can be controlled by varying the distance between the nozzle where the droplets are generated and the region where they interact with the x-rays. If the diffraction pattern exhibits Bragg spots the droplets are ice-containing, and if it exhibits diffuse rings the droplets are liquid. The lowest temperature at which liquid droplets are still present is 227 K, i.e. 5 K below the previous upper boundary of the "no-man's land". Analysis of the data shows a continuous, but accelerated transformation of the structure towards an LDL dominated liquid [209]. Thus the structure of water is LDA when it cools through the "No-Man's Land" (to $T < 136$ K) without crystallization [72, 212–215].

1
2
3 According to Mishima and Stanley [33], if the intermolecular potential of a pure fluid
4 exhibits two minima, the interplay between the two indicates that a liquid-liquid separation
5 may be present. Another possibility is a double-step potential caused by hydrogen-bond
6 bending, as shown by Tu et al. [216]. A liquid-liquid transition in the two-scale spherically-
7 symmetric Jagla ramp model of anomalous liquids has been demonstrated [110], and the
8 LLCP has rigorously been proven to be second-order and belonging to the Ising universality
9 class [111]. Ponyatovsky et al. [217] and Moynihan [218] assume that water is a “regular
10 binary solution” of two states, and this implies that the phase separation is driven by
11 energy. Cuthbertson and Poole [122] and Holten et al. [219] apply the energy-driven version
12 of the two-state thermodynamics to describe the fraction of molecules in the high-density
13 structure of two versions of the ST2 model of water, which exhibits liquid-liquid separation.
14 Holten et al. [109] also describe the thermodynamic anomalies of the mW model with the
15 same equation of state as used in Ref. [31] to correlate thermodynamic anomalies in real
16 supercooled water. Although the direct computations of the fraction of molecules involved
17 in the low-density structure in the ST2 and mW models are in agreement with the prediction
18 of the two-state thermodynamics [109, 134] (see Fig. 13), in the mW model the athermal,
19 entropy-driven non-ideality of mixing of the two alternative structures is not sufficiently
20 strong to cause liquid-liquid phase separation. The situation in real water remains less
21 certain, but the recent correlation of available experimental data [31, 135] (see Fig. 7) favors
22 a nonideality in entropy-driven mixing of the alternative molecular configurations.
23
24
25
26
27
28
29
30
31
32
33
34
35
36
37
38
39
40

41 **The order parameter**

42
43
44 The phenomenological order parameter in the two-state model is the extent of the “reac-
45 tion” between the two alternative structures [31, 134, 219] (see Fig. 13). Thermodynamically,
46 this order parameter belongs to the Ising model universality class and it is a non-conserved
47 dynamic property [207]. However, two-state thermodynamic models cannot microscopically
48 describe the alternative liquid structures in water, thus hindering attempts to build the
49 two-state thermodynamics from purely microscopic information.
50
51
52
53
54

55 The most popular order parameters used in microscopic two-state models of water are
56 the tetrahedral order parameter [109, 172] (defined in Eq. 3), $g_5(r)$ (the average density of
57 fifth-nearest neighbor) [122], ζ (the distance between the first and second shell) [220], and
58
59
60

1
2
3 the local structure index (LSI) [221–225].
4

5 Here we consider several properties of supercooled liquid water that can be defined using
6 the order parameter. In reference to a possible liquid-liquid phase transition in water,
7 evidence has been found that there are two different forms of the liquid that differ in the
8 structure of their second-nearest neighbor shell [57]. The low-energy/low-entropy state is
9 characterized by an open tetrahedral structure, and the high-energy/high-entropy state by
10 a collapsed second-nearest neighbor shell with substantial shell interpenetration [33]. The
11 microscopic pathway to the crystallization of supercooled water is also relevant in that
12 hydrogen bonding causes water to acquire a high degree of translational order prior to
13 crystallization, i.e. in supercooled water molecules progressively organize themselves in
14 well-defined shells. In contrast, simple liquids such as hard-sphere fluids have a high degree
15 of orientational order prior to crystallization and acquire translational order only after a
16 liquid-to-solid transition [226]. Thus to detect locally-favored, ~~LDL-like~~ states in water, the
17 order parameter must take into account the structure up to the second-nearest neighbor
18 shell, defined in terms of the network of hydrogen bonds, and be based on translational
19 order rather than orientational order. Thus tetrahedral order only takes into account the
20 first coordination shell and is obtained from bond angles rather than bond distances, and
21 $g_5(r)$ ignores the underlying hydrogen bond network.
22
23
24
25
26
27
28
29
30
31
32
33
34
35

36 We thus next consider the order parameter ζ [220], which measures the distance between
37 the shells of the second and first nearest neighbors. This is obtained by reconstructing
38 the network of hydrogen bonds and then computing for each water molecule the difference
39 between the radial distance of the closest oxygen in the second shell and that of the farthest
40 oxygen atom in the first shell. Locally favored ~~LDL-like~~ states are represented by a Gaussian
41 population centered around a finite value of ζ , and the disordered state is characterized by a
42 Gaussian population centered around a null value of ζ , with substantial shell interpenetration
43 ($\zeta < 0$).
44
45
46
47
48
49

50 Figure 14(a) shows that by decomposing the two populations for many state points it is
51 possible to extract the fraction s of locally-favored states, where s is the order parameter that
52 indicates the degree of structural order. This fraction can then be fitted with a two-state
53 model [see the lines in Fig. 14(a)], which is obtained solely from microscopic information.
54 Note that the isobars become mechanically unstable at high pressure and low temperature,
55 indicating the presence of a liquid-liquid critical point (full symbol).
56
57
58
59
60

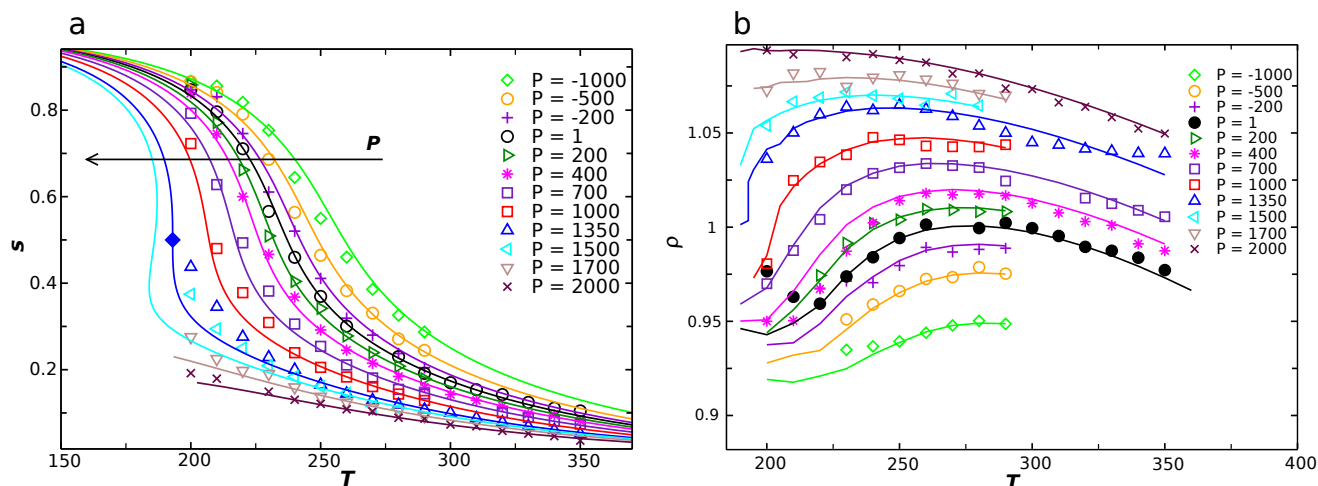


FIG. 14. Two-state model for TIP4P/2005 water. a) Values of the fraction of the locally favored S state (s) as function of temperature for all simulated pressures. The symbols mark the values obtained by decomposition of the order parameter distribution, $P(\zeta)$, at the corresponding state point. Continuous lines are fits according to the two-state model. b) Temperature dependence of density for several pressures. Continuous lines are simulation results, while symbols are obtained from the two-state model. Reproduced from Ref. [220].

The structural order parameter estimated using microscopic measurements enables us to predict quantitatively the magnitude of the anomalies and compare them with those obtained in simulations. Figure 14(b) compares the simulations (symbols) with the two-state model predictions (lines) for the density anomaly of TIP4P/2005. The two-state model agrees with the measured anomalies, indicating that a microscopic two-state description of the phase behavior of water is possible. Reference [220] carries out extended analyses for both the TIP4P/2005 and TIP5P models of water.

Although it was recently proposed that a liquid-liquid phase separation can only occur on time-scales shorter than the equilibration time of the simulated (or real) liquid—and thus only liquid-solid transitions are possible [35, 36]—results from several water models showing strong fluctuations between high- and low-density liquid indicate the presence of an HDL-LDL transition [111, 122, 127]. The extensive study by Palmer et al. [121] using several different computational protocols verifies a metastable liquid-liquid coexistence for the ST2 model. For other simulation models the situation is less clear. The studies above were performed in the deeply supercooled and pressurized region of the phase diagram while water

1
2
3 anomalies set in already under ambient conditions. As already discussed, these anomalies
4 find a simple description in a two-state model and evidence of a bimodal distribution of local,
5 instantaneous structures has been found in ambient real water both from x-ray spectroscopies
6 [141, 147, 162, 163] and from measurements of the optical Kerr effect [168]. However, no
7 molecular dynamics simulation has so far shown a bimodal structural distribution under
8 ambient conditions.

9
10
11
12
13
14 On the other hand, Sciortino and coworkers [223, 225] applied the local-structure index
15 (LSI) of Shiratani and Sasai [221, 222] to the *inherent* structure of SPC/E water and found
16 that the resulting distribution of this order parameter was bimodal in terms of HDL and
17 LDL at all investigated temperatures.

18
19
20
21 The LSI for each molecule i is acquired by putting the distances of the nearest neighbors
22 j from the reference molecule i in increasing order, i.e. $r_1 < r_2 < r_3 < \dots < r_{n(i)} < 3.7\text{\AA}$
23 $< r_{n(i)+1}$, where $n(i)$ is the number of molecules within 3.7\AA from molecule i (using the
24 positions of the oxygen atoms). The LSI distinguishes molecules with well-separated first and
25 second coordination shells from molecules in a disordered environment, containing molecules
26 in interstitial positions, using the parameter $I(i)$ defined by

$$I(i) = \frac{1}{n(i)} \sum_{j=1}^{n(i)} [\Delta(j; i) - \Delta_{mean}(i)]^2. \quad (4)$$

27
28 Here $\Delta(j; i) = r_{j+1} - r_j$ and $\Delta_{mean}(i)$ is the average of $\Delta(j; i)$ over all neighbors j of
29 molecule i within the cutoff. A low LSI value indicates a disordered local environment (HDL),
30 and a high LSI value indicates a highly structured, tetrahedrally coordinated environment
31 (LDL). The inherent structure [227] is obtained by removing thermal disorder, i.e. quenching
32 the instantaneous structure to the nearest local minimum through minimizing the energy
33 in an optimization of the geometry. The LSI measures the degree of order in the pair-
34 correlation function out to the second shell for a given oxygen; a high value indicates a
35 highly structured, locally favored tetrahedral or LDL-like, local environment while a low
36 value indicates a highly disordered, more close-packed or HDL-like structure [221, 222]. A
37 connection between the inherent structure of the more realistic TIP4P/2005 water model
38 and the phase diagram of water was made by Wikfeldt et al. [224]. They found a perfectly
39 bimodal distribution of structures separated at the same LSI value for all temperatures and
40 pressures (Fig. 15A-C). The fraction in each distribution is plotted in Fig. 15D where a
41 weak dependence on temperature is seen in the ambient regime, but as the temperature is
42
43
44
45
46
47
48
49
50
51
52
53
54
55
56
57
58
59
60

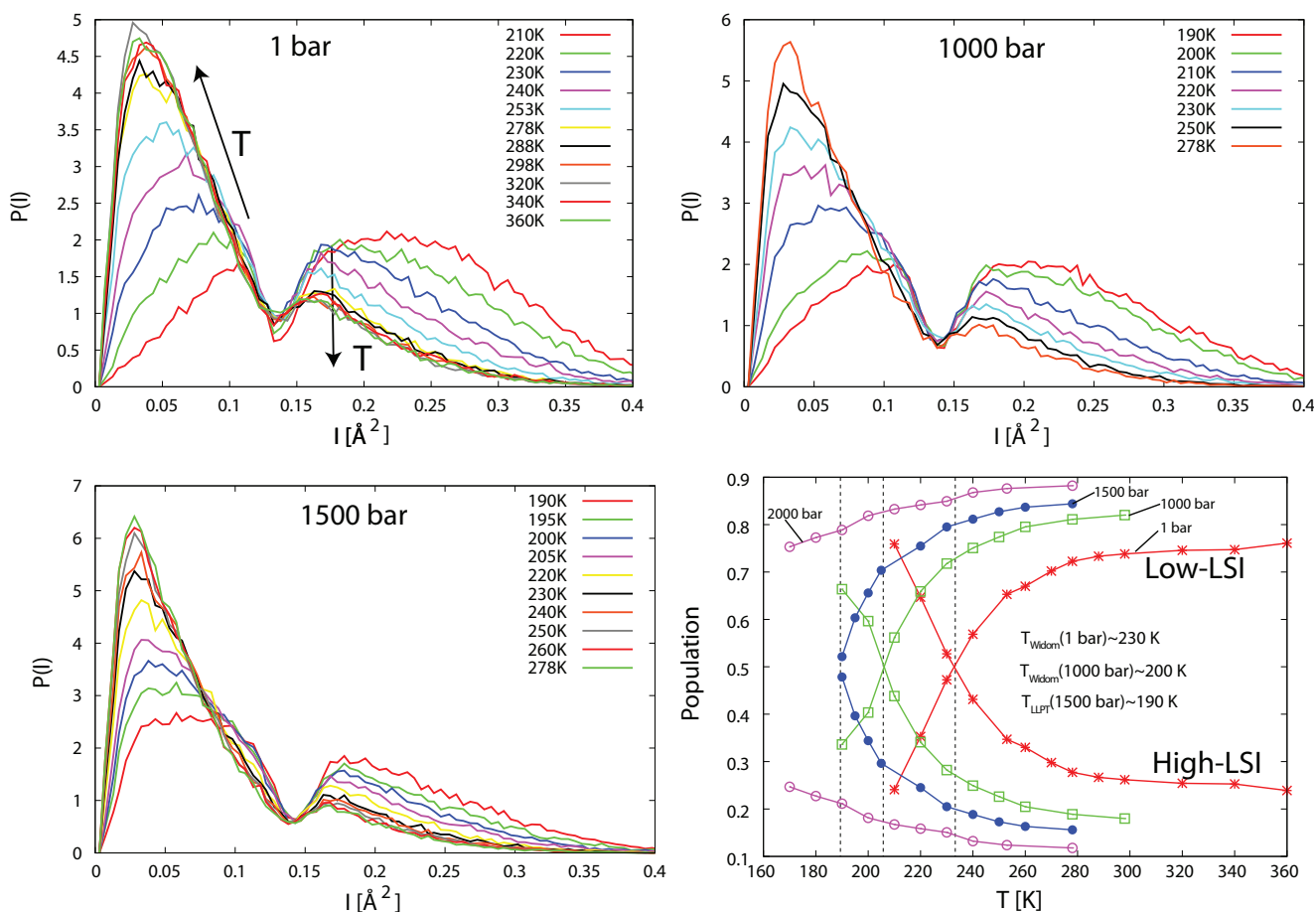


FIG. 15. Analysis of the inherent structure in simulations of TIP4P/2005 water. (A-C) Plot of the temperature dependent distributions of LSI values at (A) 1 bar, (B) 1000 bar and (C) 1500 bar. (D) Number of molecules in each distribution as function of temperature and pressure. The Widom line (see the definition in sec. VIII) at each pressure is indicated by a vertical line and corresponds to the crossing point between the high- and low-LSI distributions. Figure adapted from ref.[224].

decreased into the supercooled regime, an accelerated conversion of low-LSI (HDL) species into high-LSI (LDL) is observed fully consistent with recent measurements on micron-sized water droplets where a continuous, but accelerated transformation to a highly tetrahedral liquid was observed down to 227 K [209]. Interestingly, the 3:1 ratio between HDL- and LDL-like local environments in the inherent structure at ambient conditions is very close to what has been concluded from spectroscopic measurements [141, 147, 162, 163, 168].

A direct connection with thermodynamics is found for the crossing point, i.e. where the

1
2
3 populations in the two distributions are equal. At each investigated pressure this coincides
4 with the Widom line (see the definition in section VIII) in the model where fluctuations
5 are maximal. A further observation regarding the inherent structure can be made from
6 the temperature dependence within each distribution where, with increasing temperature,
7 the low-LSI (HDL-like) species exhibit increasing disorder (shift to lower LSI values) while
8 the maximum of the high-LSI (LDL-like) distribution remains at fixed LSI value while
9 the magnitude decreases. This is consistent with the temperature-dependence of the two
10 lone-pair peaks in x-ray emission spectroscopy [141, 162, 163] as well as the temperature
11 evolution of x-ray absorption spectra of water [149]. However, in simulations of ambient
12 water published so far the bimodality of the inherent structure becomes smeared out and
13 more of an average is observed.
14
15
16
17
18
19
20
21
22
23
24
25
26

27 VI. MODE COUPLING THEORY AND DYNAMICAL CROSSEOVERS

28
29
30 The dynamical behavior of bulk water simulated upon supercooling [228, 229] fits in
31 the framework of the idealized version of mode coupling theory (MCT) [230]. The normal
32 diffusive behavior of a liquid is Brownian. At $t=0$ the single particle starts with a ballistic
33 diffusion and then switches to a Brownian regime. When a simple liquid is cooled below the
34 melting line the dynamics starts to be dominated by the “cage effect” which that after the
35 initial ballistic behavior the particle is trapped by the transient caging by its first neighbors
36 and rattles in this cage until the cage relaxes and the particle is free to diffuse away and
37 restore the Brownian regime. Upon supercooling the relaxation time of the cages becomes
38 longer and longer and relaxation times of the liquid stretch by orders of magnitude. The
39 ideal version of the theory predicts that at the MCT crossover temperature T_C all cages
40 are frozen. If structural relaxations were the only relaxation channels for having an ergodic
41 liquid then T_C would be the glass transition temperature. When the relaxation time of the
42 cage is stretched enough, already slightly above T_C , hopping processes start and the liquid
43 does not lose ergodicity even below T_C where cages are frozen and these activated processes
44 become the only source of diffusion.
45
46
47
48
49
50
51
52
53
54
55
56

57 Glass-former liquids which are described by MCT show relaxation times with a super-
58 Arrhenius behavior. This behavior can either be phenomenologically fitted with the Vogel-
59
60

1
2
3 Fulcher-Tamman (VFT) relation [232]

4
5
6
$$\tau = \tau_0 e^{\frac{BT_0}{T-T_0}}$$
 (5)
7

8 or with the MCT power law [230],

9
10
11
$$\tau \sim (T - T_C)^{-\gamma}$$
 (6)
12

13 and this behavior is termed “fragile”. Below T_C , according to the idealized version of
14 MCT, the system is frozen but since in real structural glasses, hopping processes restore
15 ergodicity, around T_C the liquid turns its behavior to that of a strong liquid [230, 231]. The
16 relaxation time of strong liquids increases upon decreasing temperature with an Arrhenius
17 behavior [233].
18
19
20
21

22
23
$$\tau = \tau_0 e^{\frac{E_A}{k_B T}}$$
 (7)
24

25 The crossover from non-Arrhenius to Arrhenius behavior is referred to as a fragile-to-
26 strong (FTS) crossover and it is a feature of many glass formers, see for example refs. 234
27 and 235.
28

29
30 The MCT crossover temperature, which falls close to the FTS transition temperature,
31 is very close to the singular temperature T_s [228, 229] which is the temperature where
32 thermodynamic and dynamic quantities show power law divergences [1, 12]. This finding
33 points to a connection between dynamics and thermodynamics for water.
34
35

36
37 Experimental observations have demonstrated that bulk water behaves as a fragile liq-
38 uid, [4, 236]. The translational region of Raman spectra of water has been interpreted in
39 terms of scaling behavior predicted by MCT with a T_C close to T_S [237]. Relaxation times
40 from time resolved spectroscopy follow MCT predictions [238] and show a T_C close to T_S in
41 agreement with simulations [228, 229]. However, we note that very recently Dehaoui et al.
42 [239] found that viscosity and diffusivity are not coupled in water as predicted by MCT.
43
44
45
46

47 It is important to stress that in water, a network-forming liquid, the caging phenomenon
48 is due to the breaking and re-forming of the hydrogen bond local network [240].
49

50 The change in behavior from fragile to strong in water was experimentally discussed
51 [241] also pointing out that the FTS crossover in water is connected to the presence of a
52 thermodynamic event. An FTS crossover in water was also observed in computer simulations
53 for SPC/E water [242]. We will discuss further the fragile to strong transition in water and
54 the connection between dynamics and thermodynamics in Sec.s VIII, X and XI.
55
56
57
58
59
60

VII. NUCLEATION OF ICE FROM SUPERCOOLED WATER

Below the melting point, water is metastable and will eventually freeze into its thermodynamically stable phase (ice). The transformation involves overcoming a free energy barrier so that the freezing is an activated process. Often the transformation into ice occurs on the surface of solid impurities (heterogeneous nucleation). Some solid compounds, such as AgI [243], or feldspar [244] are quite efficient in reducing the free energy barrier for nucleation. Dust particles of the Sahara desert play a key role in the freezing of water in the upper atmosphere [244]. In the absence of impurities, metastable liquid water can survive even at temperatures well below the melting point, until a critical nucleus of ice appears in the bulk (homogeneous nucleation). By condensing micrometer-sized water droplets (microdroplets) in expansion cloud chambers, it has been possible to prepare metastable liquid water at temperatures down to 232 K [245–247]. Below this temperature (known as the homogeneous nucleation temperature T_H) water freezes too quickly for traditional measurement techniques.

From the fraction of droplets containing ice as a function of time at a given temperature, it is possible to experimentally determine the nucleation rate, J , i.e. the number of critical ice clusters per unit of volume and time. Classical nucleation theory (CNT) has often been used to describe the experimental results. According to CNT, J is given by [248–250] $J = K^* \exp(-\Delta G^*/(k_B T))$ where K^* is a kinetic prefactor related to the time required for a particle of the fluid to be incorporated into a solid cluster and ΔG^* is the free energy barrier. In CNT ΔG^* is related to the interfacial free energy γ_{sl} between the two phases, ice Ih and liquid, and to their chemical potential difference $\Delta\mu$ and is given by the relation $\Delta G^* \propto (\gamma_{sl})^3/(\Delta\mu)^2$. $\Delta\mu$ is well known from experiments and increases as the temperature decreases (thus reducing the free energy barrier), but the experimental value of γ_{sl} for the ice Ih-water interface is not so well known (values between 25 and 35 mN/m have been reported [251, 252]). By inserting solid clusters of ice Ih (seeds) in simulations of supercooled water, and using CNT to interpret the results it has been possible to estimate J from computer simulations [253, 254] in a range of temperatures larger than previous studies [255–261].

Various experimental techniques to determine J are compared in Fig. 16. Above T_H , 232 K, microdroplets have been produced in (water-in-oil) emulsions using microfluidic devices by Stan et al. [262] and Riechers et al. [263], whereas Stöckel et al. [272] levitated single

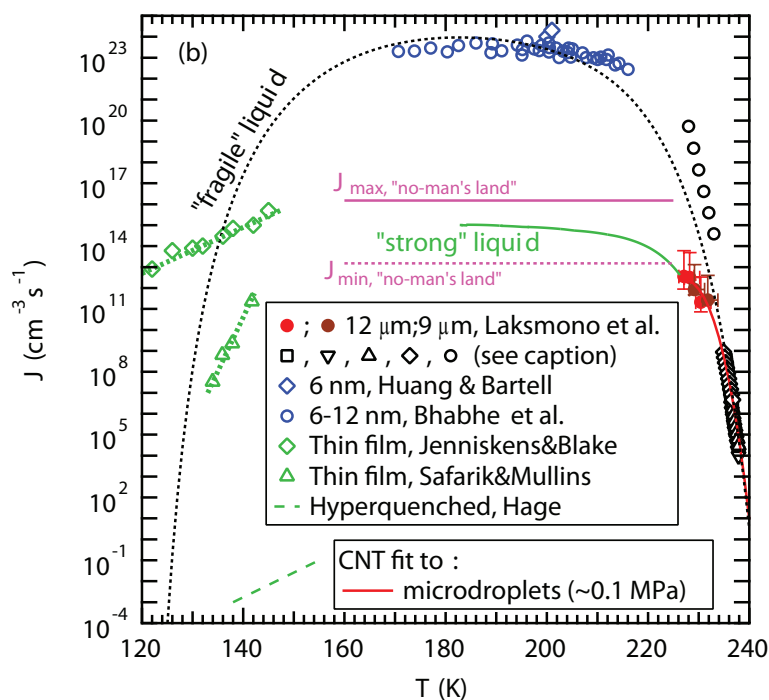


FIG. 16. Comparison of experimentally determined nucleation rates J of water using microdroplets (black hollow markers [262–264, 272, 273] and red and brown filled dots [265]), nanodroplets (blue hollow markers [266, 267]), thin films (black filled diamonds and triangles [268, 269], and hyperquenched water [270, 271]). The data of microdroplets (red solid line) and nanodroplets (blue symbols) follow different trajectories where the nanodroplet data might be affected by the large surface area to volume ratio and elevated internal pressure. An upper limit for the nucleation rate maximum within “no-man’s land” J_{max} (pink solid line) and a corresponding lower limit J_{min} (pink dashed line) were calculated from hyperquenching experiments on microdroplets [72, 212–215]. The expected CNT behavior for a “fragile” (black dotted line) and a “strong” (green solid line) liquid are included as guides to the eye. We follow Jenniskens and Blake [268] to obtain the “fragile liquid” CNT curve and also include an expected extension nucleation rate into “no-man’s land” (green curve) based on the requirement to lie between the upper and lower limits from hyperquenched microdroplets. Figure adapted from Ref. [265].

water droplets in an electrodynamic balance and Murray et al. [273] determined the nucleation rate from microdroplets supported on a hydrophobic substrate. All these techniques agree within the error of the experiments [273] and have determined J within an order of

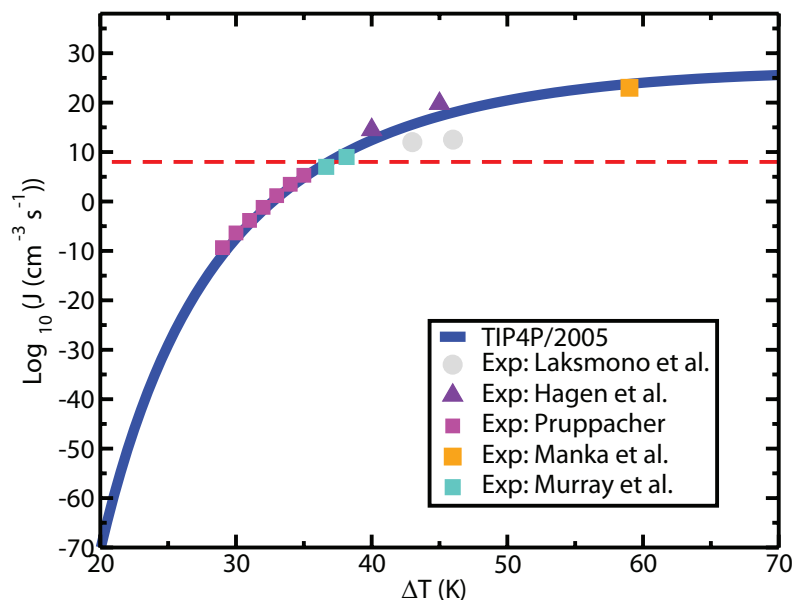


FIG. 17. Nucleation rate J as determined for the TIP4P/2005 model (blue solid line) compared to experiments (filled squares) of Pruppacher [274], Murray et al. [273] and Manka et al. [275]. Experimental results from Laksmono et al. [265] (filled circles) and from Hagen et al. [264] (filled triangles) were also included. The horizontal line corresponds to $\text{Log}_{10} J$ ($\text{cm}^{-3} \text{s}^{-1}$) = 8 which is the approximate value of J at the homogeneous nucleation temperature in experiments (i.e. about 38 K below the melting point). Figure adapted from Ref. [254].

magnitude between 235 K and 244 K to $7 \times 10^8 \text{ cm}^{-3} \text{s}^{-1}$ and $5 \times 10^{10} \text{ cm}^{-3} \text{s}^{-1}$, respectively [262, 263, 272–274]. If CNT is applied to the experimental data in this temperature regime, the fit closely resembles that of a “fragile” liquid. Below 232 K, however, non-conventional techniques that cool water rapidly and simultaneously detect ice nucleation have to be applied to overcome the homogeneous nucleation temperature, which has resulted in that various measurements do not agree. Hagen et al. [264] used an expansion cloud chamber to nucleate microdroplets between 228 K and 233 K, and obtained J of $2 \times 10^{17} \text{ cm}^{-3} \text{s}^{-1}$ and $2 \times 10^{12} \text{ cm}^{-3} \text{s}^{-1}$, respectively. Hagen et al. relied on using a droplet growth model [264] that may introduce large uncertainties in the estimation of the temperature and droplet size [273]. Very recently, Sellberg et al. [209] exploited the intense and fully coherent 50 fs x-ray pulses from the Linac Coherent Light Source (LCLS) free-electron x-ray laser to measure the structure of water in microdroplets evaporatively cooled in vacuum to a range of tempera-

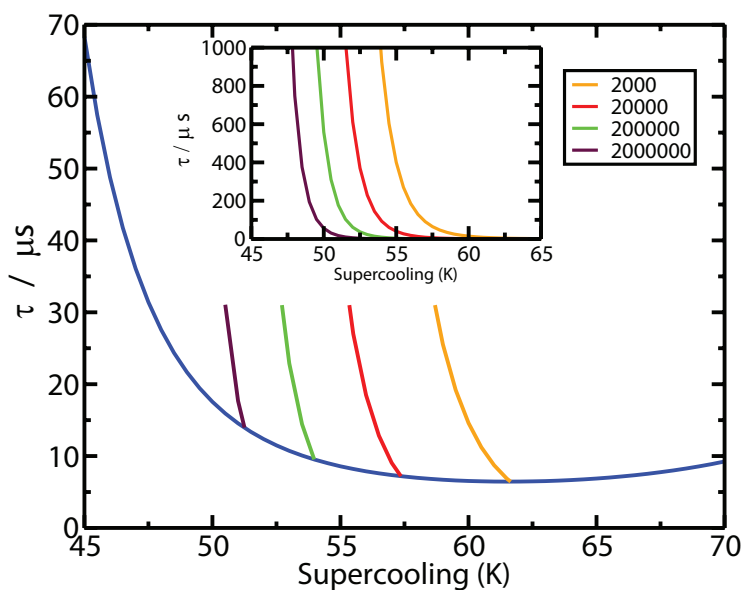


FIG. 18. τ_x for $\phi = 0.7$ for the TIP4P/2005 model as a function of the supercooling. τ_x is the time necessary to crystallize 70% of the system in an infinitely large system (blue line). Inset: plot of the nucleation time, τ_ν , versus the supercooling for systems having different numbers, N , of molecules of water. Figure taken from Ref. [254].

tures down to 227 K, i.e. 5 degrees below T_H . Based on these data Laksmono et al. [265] analyzed the ice fraction and obtained J ranging from $2 \times 10^{11} \text{ cm}^{-3}\text{s}^{-1}$ to $4 \times 10^{12} \text{ cm}^{-3}\text{s}^{-1}$ as the temperature decreased from 232 K to 227 K [265]. Sellberg et al. and Laksmono et al. determined the droplet diameters through *ex situ* optical microscopy and scanning electron microscopy, but were forced to rely on Knudsen theory of evaporation, which was calibrated toward reference data above 250 K to determine the droplet temperature as well as to MD simulations of droplet cooling to verify the Knudsen model [209].

Huang and Bartell [266], Manka et al. [275], and Babhe et al. [267] used a different approach and condensed water vapor in a supersonic flow, which reduced the droplets to nanometer-sized dimensions (nanodroplets). This reduces the probability of nucleation, but also increases the surface-to-volume ratio and internal Laplace pressure and therefore may not be representable of bulk water at ambient pressure [265]. These measurements have yielded J of $\sim 10^{23} \text{ cm}^{-3}\text{s}^{-1}$ between 170 K and 215 K with nearly no temperature dependence [266, 267, 275], which would be the expected behavior if water behaves as

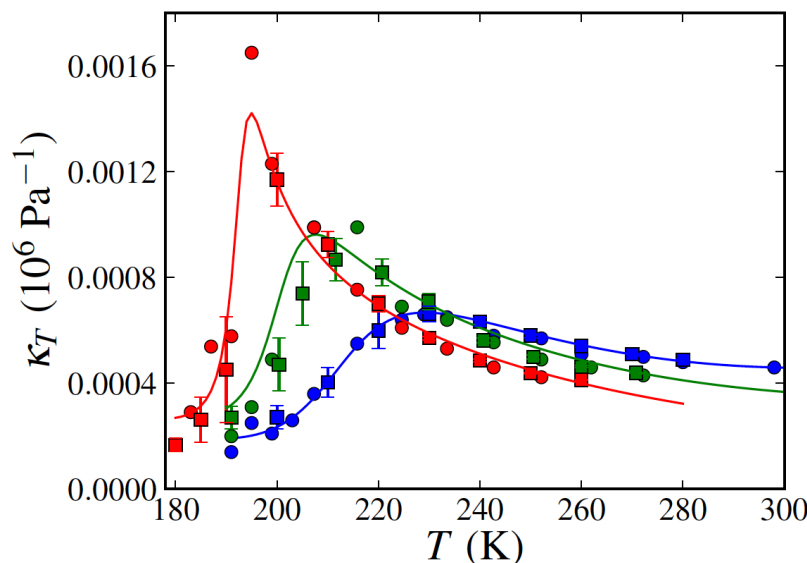


FIG. 19. Isothermal compressibility of TIP4P/2005 water at 1 (blue), 70 (green) and 1200 bar (red) as function of temperature. The symbols indicate the simulated values: squares (with error bars) obtained by Bresme et al. [281] and circles (without error bars) obtained previously by Abascal and Vega [98]. The curves represent values calculated from the two-structure equation of state. Figure taken from Ref.[281]

a “fragile” liquid in this temperature regime. However, additional information obtained from hyperquenching experiments using micrometer-sized water droplets can be used to place upper and lower limits on the maximum nucleation rate [72, 212–215] at temperatures further into “no-man’s land”. These limits can be defined based on the observation that essentially *all* droplets crystallize in huge ensembles of droplets of 3 μm in diameter, when they are cooled at 10^4 K/s, whereas crystallization was *not detected* when cooled at 10^7 K/s through the 70 K broad “no-man’s land” [72, 212–215]. These limits are included in Fig. 16.

Finally, the crystallization rate has also been measured in the temperature range between 122 K and 143 K using thin films of amorphous ice created by vapor deposition. Jenniskens and Blake [268] obtained J ranging from $4 \times 10^{12} \text{ cm}^{-3}\text{s}^{-1}$ to $7 \times 10^{14} \text{ cm}^{-3}\text{s}^{-1}$ between 122 K and 140 K, respectively, in support of water behaving as a “strong” liquid around the glass transition temperature of 136 K [69, 71, 276] and in agreement with dielectric relaxation and calorimetric measurements [81]. In contrast, Safarik and Mullins [269] obtained much

1
2
3 lower values of J ranging from $3 \times 10^7 \text{ cm}^{-3} \text{ s}^{-1}$ to $2 \times 10^{11} \text{ cm}^{-3} \text{ s}^{-1}$ between 134 K and 142
4
5 K. These measurements are clearly inconsistent with each other and may be affected by the
6
7 growth rate that limits the crystallization rate at these temperatures and therefore renders
8
9 it difficult to obtain J .

10
11 Results for the TIP4P/2005 model of water are shown in Fig. 17. The agreement with
12
13 experiment is good. From the computer simulation, it has been estimated that K^* is of the
14
15 order of $10^{31} \text{ cm}^{-3} \text{ s}^{-1}$ at 235 K, and γ_{sl} of about 29 mN/m at the melting point (decreasing
16
17 with temperature). At moderate supercooling, the growth rate of ice, u , is fast, so that
18
19 the limiting step for crystallizing a certain fraction of the sample ϕ into ice is the time,
20
21 τ_ν , required for the formation of a critical cluster. However, at low T , u is small [277] and
22
23 the time τ_x required to crystallize a certain fraction ϕ of the sample provides an important
24
25 measure. According to Avrami's equation [2, 278] this time depends on J and u as $\tau_x \propto$
26
27 $(Ju^3)^{-1/4}$. Since J increases while u decreases as the temperature becomes lower, the time
28
29 scale τ_x has a minimum. The existence of this minimum has been obtained from brute force
30
31 simulations for the mW model of water [108]. It has also been estimated for the TIP4P/2005
32
33 model for which results are presented in Fig. 18. For this model τ_x reaches a value of about
34
35 $10 \mu\text{s}$ at the minimum. To avoid crystallization one must cross the 50 K region around
36
37 this minimum at least 10 times faster, which means that the cooling rate must be about
38
39 $50 \text{ K}/(1\mu\text{s}) = 5 \times 10^7 \text{ K/s}$. This estimate is in reasonable agreement with the experimental
40
41 finding that to form water in the glassy state (thus avoiding crystallization) the liquid phase
42
43 must be cooled at rates higher than 10^6 - 10^7 K/s [72] and is also consistent with the maximum
44
45 J in "no-man's land" discussed in connection with Fig. 16.

46
47 Obviously, water is not an easy glass former as one requires high cooling rates to form
48
49 the glass (i.e. amorphous water). In computer simulations it has been found that certain
50
51 response functions (as compressibility, heat capacity) reach a maximum when the liquid
52
53 is cooled at constant pressure. For TIP4P/2005 (at 1 bar) a maximum in the isothermal
54
55 compressibility has been found [98, 279–281] at 232 K indicating crossing of the Widom line
56
57 (see the definition and discussion about the Widom line in water in sec. VIII). Results for
58
59 this maximum are shown in Fig. 19 where it is shown that the results of several groups
60
61 are in agreement. As discussed above, for this model Wikfeldt et al. [224] have evaluated
62
63 the amount of HDL and LDL as a function of T at room pressure with assignment based
64
65 on the inherent structure. At 232 K, the populations of the two species cross. An issue

1
2
3 with simulations at low temperatures is equilibration and whether this maximum may be
4 due to the transient formation of ice [36]. However, as can be seen in Fig. 17, the value of
5 J at 232 K and 1 bar (where the maximum in compressibility occurs and 20 K below the
6 melting point of the model) is terribly small (i.e. $10^{-70} \text{ cm}^{-3}\text{s}^{-1}$) so that no ice formation
7 is observed in the simulations. In fact a key question concerning the possible existence of
8 a liquid-liquid critical point in supercooled water [19, 112, 121] (and/or the existence of
9 a Widom line in response functions), is if the liquid can be equilibrated before it freezes.
10 Limmer and Chandler [35] have pointed out that a relevant magnitude is the ratio between
11 τ_x and τ_e (i.e. the time required to equilibrate the system). If this ratio is large/small, the
12 system can/cannot be equilibrated before it freezes. It is also important to point out that
13 both τ_x and τ_e may depend on the system size [282]. For the mW model the maximum in
14 the compressibility at ambient pressure cannot be reached since water freezes first. This
15 is a clear case where the ratio of τ_x to τ_e is close to one and one cannot observe some of
16 the water anomalies because water simply freezes first. However, for TIP4P/2005 water at
17 room pressure this seems not to be the case and the maximum in compressibility occurs
18 without any indication of ice formation. It would be of interest to analyze this ratio at
19 higher pressures. Thus it is difficult to establish definite conclusions. The fact that two
20 different water models behave differently means that “chemistry matters” and one cannot
21 expect universal behavior for all water models. Further studies both from experiment and
22 from simulations determining both equilibration and nucleation times in droplets between
23 the nanometer and the micrometer scale would be very useful to clarify the value of the
24 ratio between τ_x and τ_e in real water.
25
26
27
28
29
30
31
32
33
34
35
36
37
38
39
40
41
42
43
44

45 **Local structural ordering in water has an impact on ice nucleation**

46
47
48 Structural ordering in water involves both translational and orientational ordering, re-
49 flecting the nature of hydrogen bonding that selects not only distance but also orientation.
50 It has been proposed that the local structural ordering in water controls not only water’s
51 anomaly but also ice nucleation and that this feature may be generic to so-called water-type
52 liquids [27, 28].
53
54
55
56

57 An analysis of locally favored, ~~LDL-like~~ structures in simulated water reveals that a
58 large fraction of second-nearest neighbors participates in five-membered rings of hydrogen
59
60

1
2
3 bonded molecules, and that this fraction increases with decreasing temperature and pressure.
4
5 These five-membered rings, being absent in the stable crystalline phases of ice (the cubic and
6
7 hexagonal polytypes), have been proposed to be responsible for the long lifetime of the locally
8
9 favored ~~LDL-like~~ states [28, 200], and act as a source of frustration against crystallization
10
11 to ice I [220, 261]. As the temperature decreases, the lifetime of hydrogen bonds increases,
12
13 and the opening of five-membered rings to form six-membered rings becomes increasingly
14
15 rare. This can partly explain why water has such a large metastability gap, in which, in
16
17 absence of impurities, it can persist in its liquid form down to 40 degrees ($^{\circ}\text{C}$ or K) below
18
19 the melting temperature.

20
21 Work by Molinero and collaborators has shown that homogeneous crystal nucleation
22
23 starts from tetrahedrally ordered regions inside the liquid phase [108]. In the language
24
25 of two-state models, crystallization should thus be initiated from locally favored, ~~LDL-like~~
26
27 structures, which already have the full translational symmetry of the crystal up to the
28
29 second shell. These locally favored structures have long lifetimes at supercooled conditions
30
31 due to the inclusion of five-membered rings of hydrogen bonded molecules, which severely
32
33 constrains the orientational degrees of freedom of the involved water molecules, and thus
34
35 stops the development of the orientational order necessary to trigger the liquid-to-ice I
36
37 transition. The differences in local structure between the supercooled liquid phase and the
38
39 ice I phase can be measured with quantities such as the dipole-dipole spatial correlation, or
40
41 the topology of hydrogen bond loops (see Fig. 20).

42
43 To overcome frustration effects, the pathway to crystallization can occur through inter-
44
45 mediate steps, in line with Ostwald's empirical step rule of phases [283] (see, e.g., Ref. [284]
46
47 for a theoretical basis in terms of minimum entropy production). In fact, in many molecular
48
49 and soft-matter systems, crystallization does not occur directly into the stable crystalline
50
51 phase, but instead involves one or more intermediate steps where the melt crystallizes first
52
53 in metastable phases [283]. These metastable crystals are structurally more similar to the
54
55 melt than to the stable phase. This structural similarity leads to a significant reduction of
56
57 the interfacial energy, although the bulk free energy of metastable states is only intermediate
58
59 between the one of the melt and of the stable phase.

60
The idea of two-step water crystallization involving a metastable phase was recently put
forward in Ref. [261]. The authors identified a novel metastable phase, called ice 0, with
a tetragonal unit cell with 12 molecules, the thermodynamic and structural properties of

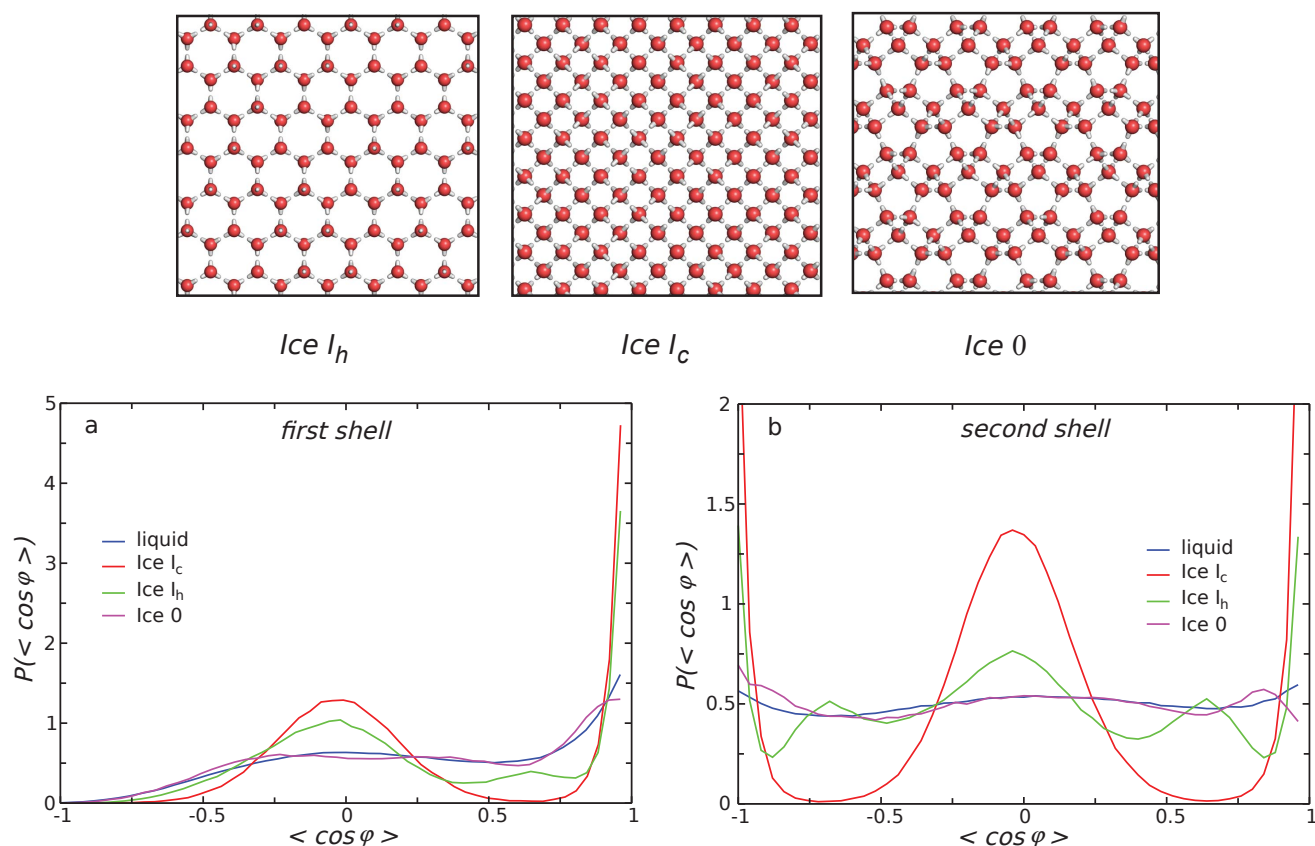


FIG. 20. (top row) Crystal planes for the stable phases and ice 0. (left panel) Distribution of the average angle $\langle \cos \theta \rangle$ between the dipole moment of a molecule and its hydrogen-bonded neighbors for TIP4P/2005 water at $T = 200$ K and $P = 1$ bar in the liquid phase and the ice I_c , I_h and ice 0 phases. (right panel) The same as in the left panel but for second-nearest neighbors. Adapted from Ref. [261].

which are intermediate between the melt and the solid crystalline phase. This is shown for example in Fig. 20, where the average dipole-dipole orientation is computed between molecules which are first neighbors (left panel) and second-nearest neighbors (right panel). The angle distribution is very similar between the supercooled phase and ice 0, in contrast with the distributions of both the hexagonal and cubic ice forms. Moreover, ice 0 is rich in five-membered rings, which are also very common within the locally favored ~~LDL-like~~ structures where crystallization first originates.

The structural similarity between supercooled water and the metastable ice 0 form, plays

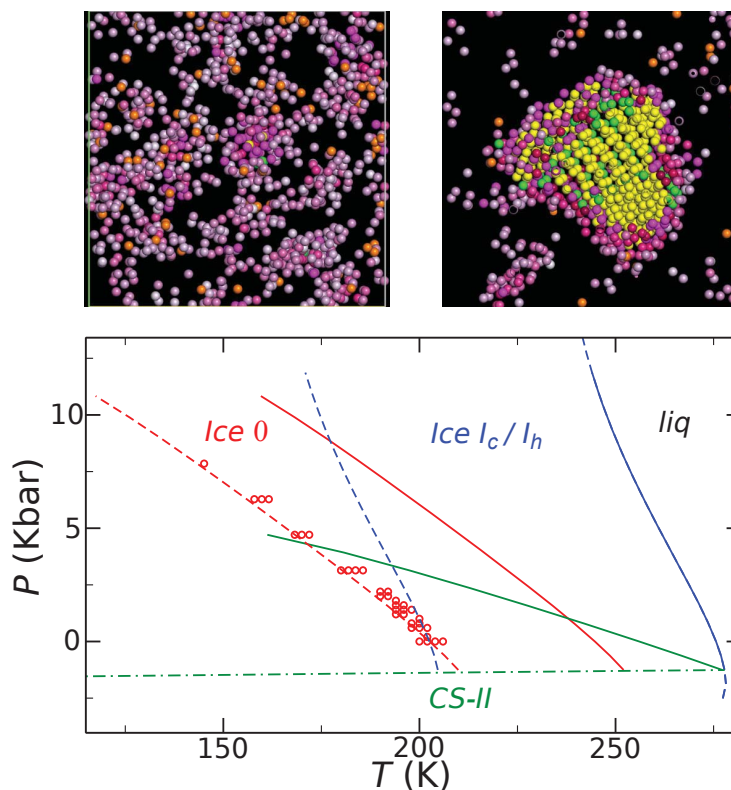


FIG. 21. (top row) Snapshot of two configurations with the birth of a small crystalline nucleus (left panel) and a section of a nucleus of critical size (right panel). The color code is: yellow for ice I_c , green for ice I_h , and magenta for ice 0. (bottom) P - T phase diagram of mW water. Continuous lines indicate coexistence between the liquid phase and different crystal structures: ice I_h/I_c (blue), ice 0 (red) and clathrate CS-II (green). Dashed lines indicate constant chemical potential differences between the liquid and ice I_h/I_c ($\beta\Delta\mu = -0.721$, in blue), and the liquid and ice 0 ($\beta\Delta\mu = -0.365$, in red). The green dashed-dotted line is the $I_c/CS-II$ coexistence line. The red open circles indicate state points where homogeneous nucleation is observed in simulations. Adapted from Ref. [261].

an important role in homogeneous ice nucleation. According to Ostwald's step rule of phases, first a small nucleus of the metastable phase should form, which later converts to the stable ice I form. It is thus natural to expect that, close to the homogeneous nucleation line, where the size of the critical nucleus is negligible, the rate of ice nucleation should be controlled by the thermodynamic properties of ice 0. Reference [261] has indeed shown that the homogeneous nucleation line for the mW model of water coincides with a line of constant

thermodynamic driving force with respect to ice 0 (i.e. the homogeneous nucleation line is the locus of constant chemical potential difference between the melt and ice 0). This scenario was confirmed both by direct simulations and by computation of the nucleation rates of ice.

In Fig. 21 the phase diagram of mW water is reported, with dots representing the locus of homogeneous nucleation, and the dashed line that of constant driving force with respect to ice 0. This suggests that it is possible to derive the homogeneous nucleation line from purely thermodynamic arguments. Furthermore, by adopting translational order of the second shell as the order parameter, it is possible to describe the phase behavior of liquid water to a good approximation from purely microscopic information.

Locally favored, ~~LDL-like~~ states are stabilized by five-membered rings of hydrogen bonded molecules, which act as a source of frustration against crystallization to ice I. This dynamical pathway reflects in the crystallization transition, in which the metastable crystalline phase can play an important role. In particular, there is evidence that a novel metastable phase, ice 0, being structurally similar to the supercooled melt, can act as an intermediate step during crystallization. Water would first transform into small nuclei of this phase, that then grow into the stable crystalline phases. According to this scenario, the homogeneous nucleation line would then be controlled by the thermodynamic properties of ice 0.

VIII. RELATION BETWEEN DYNAMICS AND THERMODYNAMICS

Though simulation studies and experimental results approaching the “no-man’s land” region of bulk water have shown evidence supporting the existence of LLPT, advanced experimental techniques are still needed to reach this “no-man’s land” region [209, 285], in order to establish whether an LLPT exists in deeply supercooled water. Experiments on water in confinement have shown that a fragile-to-strong (FTS) transition line as a function of pressure was pointing to where the LLCP is supposedly located [285]. Based on a simulation study on the two-scale Jagla model with an accessible LLCP, Xu et al. proposed an alternative way to detect the LLCP from the one-phase region above the LLCP at higher temperature and lower pressure [34, 94, 110, 286]. Generally speaking in a fluid, when moving away from a critical point into the single-phase region, the correlation length keeps a maximum reminiscent of the critical divergence. On approaching the critical point from this region, thermodynamic quantities such as the specific heat and the isothermal

1
2
3 compressibility show maxima that are expected to merge on a pseudo-critical single line
4 terminating at the critical point. The maxima of those response functions collapse on the
5 same line on approaching the critical point because they become proportional to power laws
6 of the correlation length. This line, called the Widom line, is defined as the loci of maxima
7 extending from the critical point into the single-phase region. Moving away from the critical
8 point into the single-phase region, the maxima are progressively smeared out and their values
9 decrease [287]. If a second critical point exists in water, the system undergoes a continuous
10 transition from HDL-like to LDL-like liquid upon cooling at constant pressure in the one-
11 phase region [34, 94, 110, 286]. Thermodynamic response functions, such as the isobaric
12 heat capacity C_P , isothermal compressibility κ_T and thermal expansion coefficient α , show
13 extrema in this region, the loci of which asymptotically approach one another and converge
14 to the Widom line in the vicinity of the LLC. This phenomenon has been clearly detected
15 in numerous water simulation studies: the Widom line pointing to the LLC has been
16 found for the ST2 and Jagla potentials [34, 94, 110, 286], for the TIP4P potential [107, 288],
17 and for the TIP4P/2005 potential [98]. It has also been found in simulations of aqueous
18 solutions [107, 288, 289] as will be discussed in Sec. XI. In experiments on supercooled
19 water, the Widom line is of particular interest since it can be used to trace the hypothesized
20 LLC from the one-phase region, thus avoiding the two-phase region where crystallization
21 occurs easily. Across the Widom line not only the structural response functions but also
22 dynamic properties change and a unified picture of slow dynamics and thermodynamics
23 emerges where a FTS dynamic crossover happens for water upon crossing the Widom line
24 as explicitly found in bulk water for the ST2 and Jagla potentials [34, 110, 286], the TIP4P
25 potential [291] and more recently for the TIP4P/2005 potential [292]. A recent study of the
26 Van Hove self-correlation function for TIP4P/2005 water explicitly connects the freezing of
27 the structural relaxations and the start of activated processes to the FTS transition. This
28 coincidence between the FTS and the Widom line also persists in solutions [290, 293] (see
29 discussion in Sec. XI).

30
31
32 We note here that these findings clarify the connections between glassy dynamics and
33 thermodynamics that are peculiar to water and that were hypothesized from the past studies
34 discussed in Sec. VI.

35
36
37 Xu et al. [294] and later Wikfeldt et al. [224] showed that the populations of LDL-
38 like and HDL-like structures in simulated water change upon crossing the Widom line and,
39
40
41
42
43
44
45
46
47
48
49
50
51
52
53
54
55
56
57
58
59
60

1
2
3 due to these structural changes the system shows the dynamic crossover from non-Arrhenius
4 (fragile) behavior at higher temperature to Arrhenius (strong) behavior at lower temperature
5 [34, 94, 110, 286, 290, 291, 293].
6
7

8
9 The structural change is observed experimentally by infrared (IR), Nuclear Magnetic
10 Resonance (NMR), Quasi-Elastic Neutron Scattering (QENS) experiments on confined wa-
11 ter, and by x-ray scattering measurements in bulk water [209] at ambient pressure. This
12 is consistent with the results of model studies upon crossing the Widom line from the one-
13 phase region in water. Using QENS and NMR on water confined in MCM-41, Liu et al.
14 observed a cusp-like dynamic transition [285], from non-Arrhenius (fragile) behavior at high
15 T to Arrhenius (strong) behavior at low temperature. This transition was linked to the
16 FTS transition upon crossing the Widom line in the vicinity of the LLCP with the high-
17 and low-temperature liquids corresponding to the HDL and LDL, respectively. The picture
18 of water confined in MCM41 undergoing a FTS was reproduced, linked to bulk water and
19 framed in the MCT context by a simulation study [296–298] (see also the section on con-
20 fined water here below). Fourier Transform InfraRed (FTIR) experiments on confined water
21 also showed that an HDL-like to LDL-like continuous transition occurs upon crossing the
22 Widom line [294]. According to these experiments, we should be able to trace the LLCP – if
23 it exists – as the terminal point of the dynamic crossover in the one-phase region, located at
24 $P_c = 1600 \pm 400$ bar and $T_c = 200 \pm 10$ K. However, it must be noted that the cited pressure
25 is that applied to water using a fluid outside the pores. The actual pressure in water might
26 be different, and even negative due to the Laplace pressure effect [295, 299].
27
28
29
30
31
32
33
34
35
36
37
38
39
40

41 A convenient conceptual bridge connecting thermodynamic and dynamic properties of
42 dense fluids is also provided by excess entropy scaling relationships for transport properties.
43 In dense fluids, diffusion proceeds by a combination of binary collisions and cage relaxations.
44 Transport properties can be conveniently reduced to dimensionless form using reduction
45 factors based on kinetic theory. Rosenfeld and others [300–315] showed that for a wide
46 range of simple liquids, the following semi-empirical scaling relationship was valid: $X^* =$
47 $A \exp(\alpha S_e)$ where X^* are dimensionless transport properties, including diffusivity, viscosity
48 and thermal conductivity. The scaling parameters A and α depend on both the nature of
49 the interactions and the transport property.
50
51
52
53
54
55
56

57 For example, for simple liquids, the scaled diffusivity, $D_R^* = D r^{1/3} / (k_B T / m)^{1/2}$, obeys
58 excess entropy scaling with quasiuniversal values of A and α . Rosenfeld-type exponential
59
60

1
2
3 scaling relationships between transport properties and excess entropies hold for a much wider
4 variety of dense liquids in the stable and supercritical regimes than was originally assumed,
5 including liquid metals, molecular fluids, ionic melts, core-softened model fluids, chain fluids,
6 room temperature ionic liquids and colloidal fluids, even though the exact scaling parameters
7 may vary substantially. Deviations from Rosenfeld-scaling behavior arise as a consequence
8 of cooperative effects, but for a large number of fluids, transport properties from a wide
9 range of state points scale with the excess entropy.

10
11 Given the idea behind Rosenfeld scaling, it was shown in a recent study on TIP4P water
12 that if s_e is approximated with s_2 , i.e. the two-body term of the excess entropy, the same
13 FTS transition of the diffusion coefficient is found for s_2 [198, 199]. This result can be tested
14 experimentally by measuring the radial distribution function. The relation between s_2 and
15 the radial distribution function is in fact straightforward and for a one-component fluid it
16 is:

$$s_e \approx s_2 = -2\pi\rho k_B \int \{g(r)\ln[g(r)] - [g(r) - 1]\} r^2 dr \quad (8)$$

17
18
19
20
21
22
23
24
25
26
27
28
29
30
31
32
33
34 where $g(r)$ for water is the Oxygen-Oxygen $g(r)$.

35
36
37 We note also that the phenomenon of the Widom line extends is of interest also in the
38 supercritical state i.e. in the one-phase region above the well known liquid gas critical point
39 both in water [316] and in other liquids [317, 318]. In supercritical water the Widom line
40 is clearly found both in experiments and in simulations [316, 319]. A dynamic crossover
41 passing through the Widom line has also been shown to exist in the supercritical state of
42 water where changes in trends in diffusion coefficient and viscosity have been observed upon
43 crossing this line on isobaric paths [316, 319].

44
45
46
47
48
49
50 Finally, we note that there is yet another approach to make a link between structure
51 and dynamics on the basis of a two-order-parameter model [28, 320]. In this approach, it
52 is assumed that locally favored structures have a higher activation energy than the normal
53 liquid structures. Then, the total activation energy is given by their average. In this way,
54 the dynamic anomaly can be described by the same order parameter used for explaining the
55 thermodynamic anomaly.

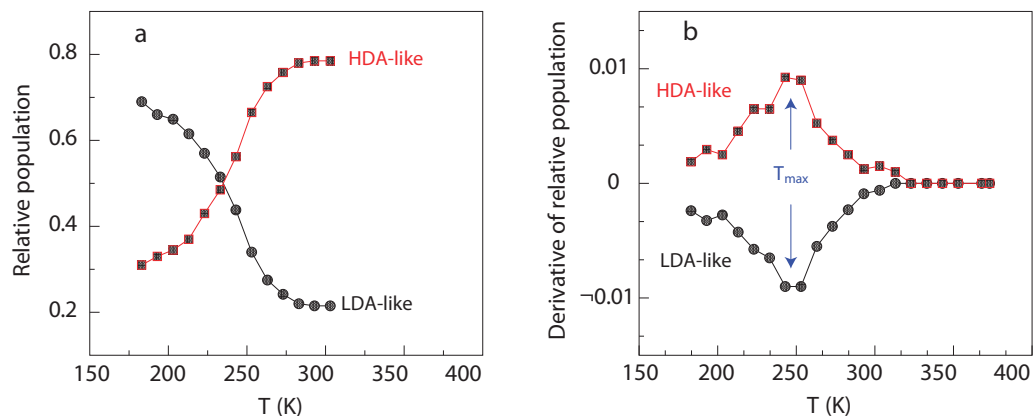


FIG. 22. Experimental IR results for structural change of confined water upon crossing the Widom line (adapted from ref. [294]). (a) Relative population of HDA-like and LDA-like water species as function of temperature. (b) Derivative of the relative population for HDA-like and LDA-like water species. The maximal change occurs at the temperature T_{max} where the Widom line is crossed.

IX. STRETCHED WATER

Water, like any liquid, can resist mechanical traction and become metastable with respect to its vapor [2]. We will not be able to claim that we understand the "most anomalous liquid" properly until we have learned to measure and understand the properties of water and its solutions accurately in the negative pressure domain. In particular, the behavior of the line of density maxima (LDM) at negative pressure can help discriminate between the proposed theoretical scenarios, depending on whether, when the pressure decreases, the LDM reaches a maximum temperature, or its temperature keeps increasing (see Fig.2). Moreover, a region exists, at negative pressure and temperature below the melting point of ice, where water is doubly metastable, with respect to both ice and vapor. Is it possible to observe the Widom line (or one of the lines of maxima in a thermodynamic response function) in the doubly metastable region? A comparison between the experimental line of homogeneous nucleation of ice and simulations with the TIP4P/2005 potential (Fig. 23) suggests that it might be possible [39, 299].

Whereas negative pressures are routinely accessible in simulations, experiments are notoriously difficult because a small perturbation can trigger the rupture of the liquid by nucleation of a bubble (cavitation). The most documented quantity is the largest negative pressure that could be reached. For water, all experimental techniques but one are limited

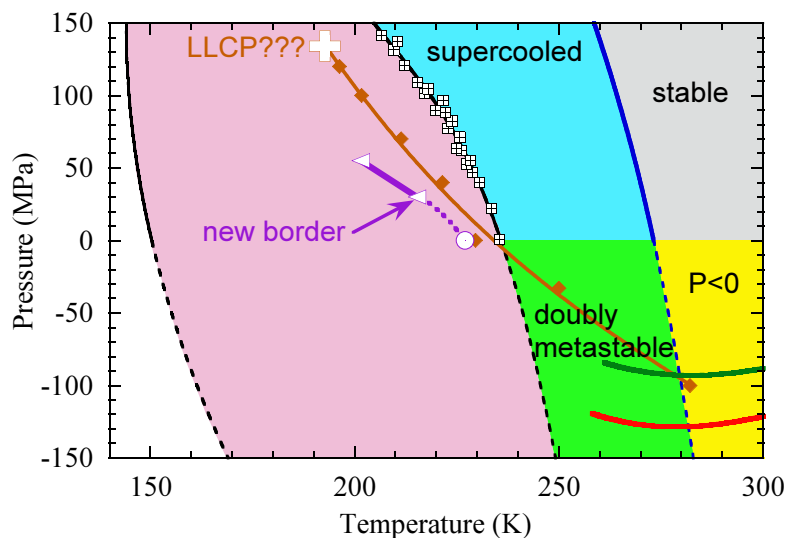


FIG. 23. Pressure-temperature phase diagram of water from Ref. [39]. Colored areas are used to identify the different possible states for liquid water. The melting line of ice I_h is shown at positive pressure by a solid blue curve and its extrapolation to negative pressure by a dashed blue curve. The black crossed white squares show the experimental supercooling limit [321]. They define the homogeneous nucleation line based on conventional experimental techniques (solid black curve), which is extrapolated here to negative pressure (dashed black curve). The isochores of TIP4P/2005 water for the two densities used in a recent experiment [39] are shown by the red circles and curve, and green diamonds and curve, respectively. Simulations of TIP4P/2005 water are performed to find the maximum of κ_T along several isobars (white triangles), defining the line of maxima in κ_T (brown curve), that might emanate from an LLCPP (white plus symbol). Because the predictions of TIP4P/2005 are in satisfactory agreement with the reported experimental results in the supercooled region [279], this figure seems to indicate that the line of maxima in κ_T (and other extrema in the response functions) might be accessible to experiment only in the doubly metastable region.

to -30 MPa [299, 322, 323]. Negative pressure studies seem to come into focus about every twenty years. In 1950 Briggs [339] reached -25 MPa for water (compared with -50 MPa for mercury), while Winnick and Cho [340] developed a clever centrifugal force method in 1971, but were still unable to get beyond Briggs' limit. Henderson and Speedy's outstanding works of 1987 were slightly ahead of the pattern. They reported the line of density maxima

1
2
3 to -20.3 MPa [324] and the melting temperature of ice to -24 MPa [325]. They both lie on
4 a natural extension of the positive pressure data, but cavitation prevented to follow these
5 properties to larger negative pressure.
6
7

8
9 The 20 year cycle for negative pressure studies was restored in 1991 by Green et al.
10 [341], and Zheng et al. [329, 342] who broke new ground. They showed that, with a
11 microscopic version of the original (1850) Berthelot tube approach, unprecedented tensions,
12 in the vicinity of -150 MPa, could be reached before their water-filled $\simeq 5$ by $15 \mu\text{m}$ dimension
13 vesicles in quartz crystals, cavitated. Since these tensions are close to the values predicted
14 for the same temperature 40-47 °C by classical nucleation theory nearly 70 years ago [343]
15 and quantitatively supported by more recent theory [105, 344], it appeared that a major
16 barrier had been crossed.
17
18

19
20 What was of high significance in these studies was the finding of a tension maximum,
21 identified by the "schizophrenic" behavior at 40-47 °C of the vesicles in a preparation of
22 density 0.91 g/cm^3 , and the failure to cavitate at any temperature for inclusions of higher
23 densities. {Different vesicles in the same sample which, at other densities would all behave
24 in the same manner, would sometimes cavitate during cooling but at different temperatures
25 in the range 40-47 °C, and sometimes not at all. Any inclusion that survived cavitation
26 to 40 °C would never cavitate, making it clear that a tension maximum, very close to the
27 limiting tension for that sample, had been traversed.} This suggested the existence of a
28 density maximum at this low density. However, since the cavitation probability depends on
29 a combination of negative pressure and surface tension, a more refined analysis is needed,
30 see below. In the measurements of the 90s era were also the first direct measurements of a
31 physical property in the new high tension range made available by the micro-Berthelot tube.
32 Alvarenga et al. [330] showed it was possible, using micro-Brillouin scattering methods, to
33 obtain the isochoric velocity of sound and hence the adiabatic compressibility along the
34 isochore.
35
36
37
38
39
40
41
42
43
44
45
46
47
48
49

50 After a further two decade lapse, a new set of experiments has emerged since 2010 from
51 the Caupin laboratory. Using an acoustic wave to stretch water, an experimental equation of
52 state was measured at ambient temperature to -26 MPa [326]. It agrees with the extrapola-
53 tion of the recommended formulation of the equation of state measured at positive pressure
54 [327, 328]. Later, using the same autoclaving method established by geochemists [346] and
55 used by Zheng et al. [329] and Schmulovich et al. [331], El Mekki et al. [332] obtained a
56
57
58
59
60

1
2
3 perfectly formed vesicle with which they were able to study the statistics of cavitation in
4 a single vesicle as function of temperature and thereby to estimate the temperature of the
5 minimum energy barrier for cavitation, around 320 K. This must, however, be corrected
6 for the variation of surface tension with temperature, in order to locate the temperature of
7 the tension maximum for the isochore of the studied density, 0,922 g/cm³. The correction
8 depends on the model chosen to express the energy barrier for cavitation. Using classical
9 nucleation theory with a Tolman length correction to the surface tension, the results are not
10 inconsistent with the extrapolation of the positive pressure equation of state [327, 328], that
11 is a temperature of density maximum near 296 K at 0,922 g/cm³. Obviously more direct
12 measurements would be useful.
13
14
15
16
17
18
19
20

21 Another line of research uses the fact that some of the water inclusions are able to survive
22 cooling without any bubble nucleation [39, 329], which gives access to the doubly metastable
23 region. Revisiting the work of Alvarenga et al. [330], Pallares et al. recently measured the
24 sound velocity in two doubly metastable samples [39]. An estimate of the path followed in
25 the phase diagram is given in Fig.23. This study suggests that: (i) the experimental equation
26 of state deviates from the extrapolation of positive pressure data at low temperature, (ii)
27 the adiabatic compressibility passes through a maximum when the temperature varies at
28 constant density, and (iii) the sound velocity vs. density at constant temperature becomes
29 non-monotonic at low temperature.
30
31
32
33
34
35
36

37 These features are consistent both with the liquid-liquid critical point scenario [19] and
38 the singularity-free interpretation [23]. It has also been suggested that the experiments might
39 have found the liquid-liquid transition [333]; although not impossible, this does not seem
40 likely [39]. More measurements on water in the doubly metastable region would certainly
41 help to shed light on the origin of its anomalies.
42
43
44
45
46
47
48

49 X. THERMODYNAMICS AND DYNAMICS OF CONFINED WATER

50
51
52 The dynamical properties of water in restricted geometries and at interfaces have been
53 studied intensely because of the important effects in systems of interest to biology, chem-
54 istry, and geophysics, the behavior of which depends on how the pore size and structure
55 influence the diffusion of water. Those properties are particularly relevant for understand-
56 ing phenomena like the mobility of water in biological channels or the dynamics of hydrated
57
58
59
60

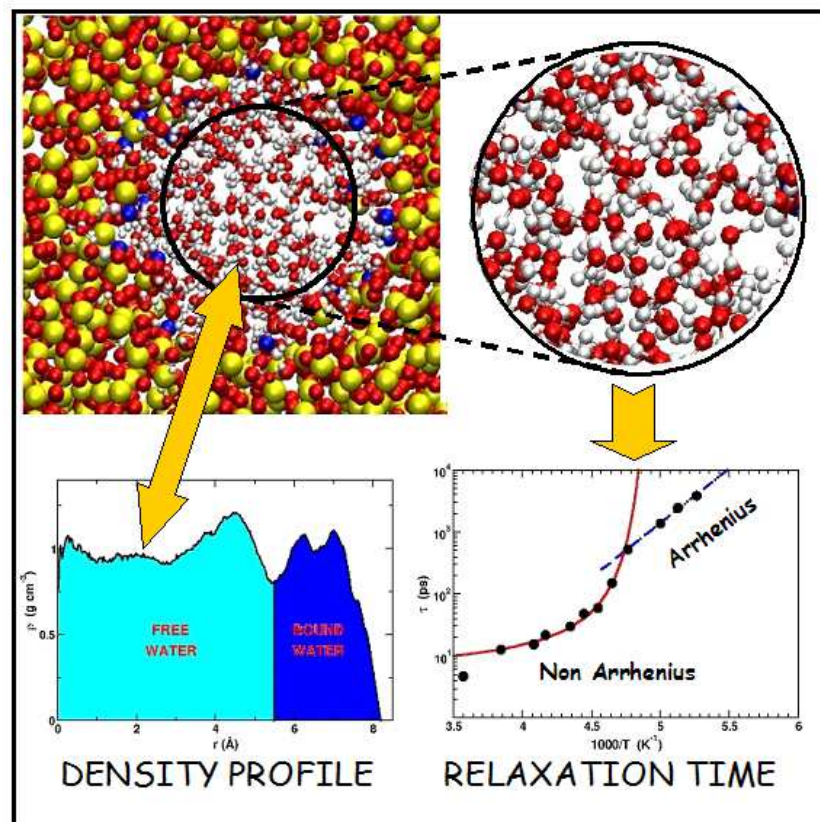


FIG. 24. Molecular dynamics simulations of water in MCM-41. In the picture we can see the difference between bound and free water which show distinct dynamical behavior and the behavior of the relaxation time of free water that shows the FTS transition that coincides with the Widom line (not shown). Reproduced from ref. [296].

proteins [8–10] also in connection with cryopreservation, see for example ref. [347].

Of all this vast field we will here focus only on the relation between dynamics and thermodynamics in confinement and in particular on to what extent confinement can be of help to shed light on the thermodynamics of bulk water in the supercooled region.

Molecular dynamics studies on water confined in hydrophilic silica porous glasses like Vycor [348, 349] and MCM-41 [296–298] upon supercooling have evidenced that for this kind of pores and hydrophilic surfaces the dynamics of water can be split in two ranges: (i) the dynamics of the bound water, close to the surface of the pores, and (ii) the dynamics of the inner water, often called free water, which is more bulk-like. The dynamics of the bulk-like inner part follows the MCT in the region of mild supercooling and upon further supercooling shows a FTS [296–298, 348, 349].

1
2
3 Experiments show that it is easier to avoid crystallization of water in confinement than
4 in bulk. In particular, by confining water in nanopores of mesoporous silica MCM-41-S
5 with cylindrical pores of 14 Å diameter it was possible to study its dynamical behavior in a
6 temperature range down to 160 K, without crystallization [285, 350].
7
8

9
10 Quasielastic neutron scattering (QENS) is the most suitable technique to study transla-
11 tional dynamics as its cross section is directly related to the (Q, ω) Fourier transform of the
12 density-density correlation function. Care must instead be taken when analyzing relaxation
13 times with techniques that probe orientational degrees of freedom as the FTS transition is
14 only translational in nature. QENS experiments are sensitive only to the more mobile water
15 contained in the inner part of the pores as the sluggish water close to the surface of the
16 strongly hydrophilic pores gives a signal which is buried in the resolution of the instrument.
17 The experiments performed on supercooled water in confinement found evidence of a FTS
18 dynamic crossover [285, 350] already hypothesized in bulk water, and in analogy with other
19 network-forming liquids [231].
20
21
22
23
24
25
26
27

28 Most important is that it was found that the FTS line, as function of pressure, points to
29 the zone where the LLC is supposed to exist [34, 285, 351]. After that the FTS transition
30 line was identified to coincide with the Widom line in simulations of bulk water [34], Gallo
31 et al. simulated water in MCM-41 and obtained the same results as in the experiments, see
32 Fig. 24, further finding that the FTS crossover coincides with a peak in the specific heat
33 that identifies the Widom line [296, 298] and thus bridging the gap between experiments
34 in confinement [285, 350] and MD results in the bulk [34]. This link between Widom line
35 and FTS crossover described in these last two sections shows that for water the Widom
36 line appears to also be a switching line for hopping, favored on the side where water is less
37 dense. Another typical feature of glass forming materials that has recently been related
38 to the crossing of the Widom line and consequent stiffening of the hydrogen-bond network
39 [352] is the appearance of the Boson peak which is an excess of intensity in the low-frequency
40 range of the vibrational spectrum.
41
42
43
44
45
46
47
48
49
50
51
52
53

54 XI. THERMODYNAMICS AND DYNAMICS OF AQUEOUS SOLUTIONS

55
56
57 In this section we will discuss how and to what extent aqueous solutions can be used
58 as route to reach the “no-man’s land”. Similar to confinement, many aqueous solutions
59
60

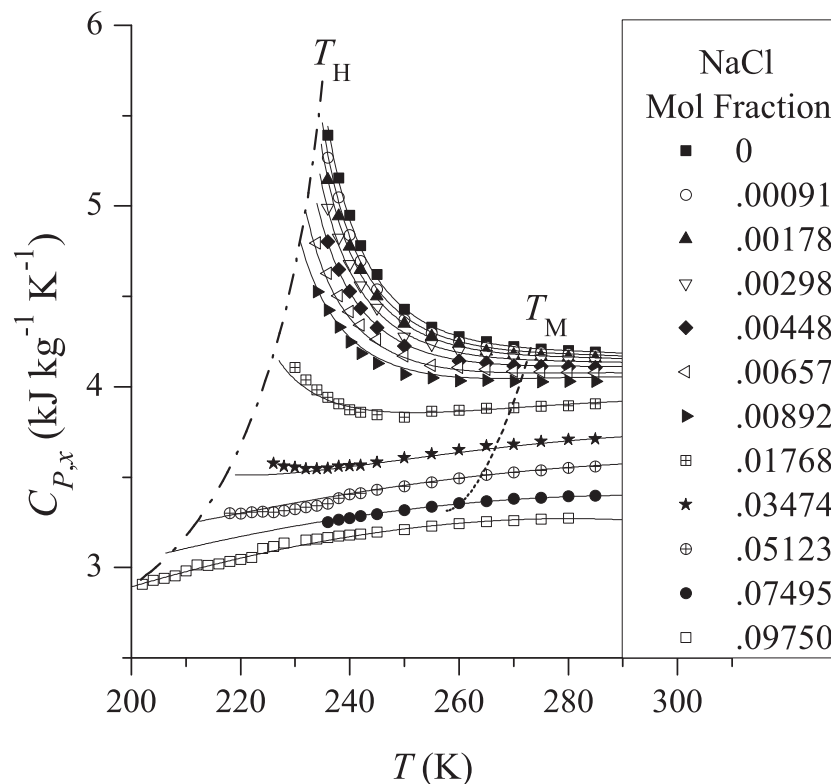


FIG. 25. Suppression of the anomaly of the heat capacity in aqueous solutions of sodium chloride. Symbols: experimental data of Archer and Carter [356, 357]. Solid curves: predictions based on two-state thermodynamics [134]. Dashed curve shows the positions of the melting temperatures. Dashed-dotted curve shows the temperatures of homogeneous ice formation.

have the invaluable advantage that they can be supercooled more than the bulk [353–355]. Besides, in the natural environment water is almost always found as solvent in a mixture of two or more components.

Archer and Carter showed that in NaCl(aq) solution the heat capacity and the density anomalies are still present in dilute solutions [356, 357], while at higher concentration of NaCl the heat-capacity anomaly disappears, as seen in Fig. 25. This fact does not contradict the possibility of a liquid-liquid transition in supercooled aqueous solutions of NaCl, stemming from the liquid-liquid transition in pure water. Moreover, the suppression of the heat-capacity anomaly measured at constant composition is predicted by thermodynamics and, as seen in Fig. 25, is well described by the two-state model [134].

Later Mishima performed experiments on LiCl aqueous solutions where the observed decompression-induced volumetric change of dilute LiCl aqueous solution can be interpreted

1
2
3 by the polyamorphic viewpoint about the solvent water and can be regarded as the expected
4 polyamorphic phase separation [358, 359]. This finding is supported by later experiments
5 [360] and by simulations [361, 362]. Kobayashi and Tanaka [169, 170] studied the glass-
6 forming ability of LiCl-water mixtures and found that it is maximized near the eutectic
7 point. Furthermore, it was demonstrated that the dependence of the viscosity and the
8 Raman spectra on salt concentration can be explained by a simple two-state model.
9

10
11
12 Chatterjee and Debenedetti studied the thermodynamics of solvophobic aqueous-like so-
13 lutions. In the presence of an LLCP for the aqueous-like component, critical lines will stem
14 from the LLCP of the pure substance upon increasing the solute content [363, 364].
15

16
17
18 Given these evidences, if an LLCP in water exists then it could be found with a properly
19 tuned aqueous solution. Indeed, a LLCP was claimed for the glycerol-water system by
20 Suzuki and Mishima at 0.12–0.15 mole fraction, 150 K and 30–50 MPa [365]. Murata and
21 Tanaka have also reported the observation of a liquid-liquid transition in supercooled aqueous
22 solutions of glycerol [366] and also in many other aqueous organic solutions [367]. This
23 interpretation has, however, been questioned for water-glycerol mixtures and ice formation
24 suggested as the origin [365, 368, 369].
25
26
27
28
29
30
31

32
33 Corradini et al. studied with MD simulations NaCl dissolved in TIP4P water with con-
34 centrations ranging from $c=0.67$ to 2.10 mol/kg [107, 288]. The liquid-liquid critical point
35 is present both in the bulk and in the solutions and its position in the thermodynamic plane
36 shifts to higher temperature and lower pressure upon adding salt. Comparison with avail-
37 able experimental data allowed to produce the phase diagrams of both bulk water and the
38 aqueous solution as should be measurable in experiments as shown in Fig. 26. Given the
39 position of the liquid-liquid critical point in the solution as obtained in these simulations,
40 the experimental determination of the hypothesized liquid-liquid critical point of water in
41 aqueous solutions of salts appears possible. For the experimental $c=0.67$ mol/kg NaCl(aq)
42 the LLCP is predicted to be at around $T_c = 230$ K and $P_c = -120$ MPa. In NaCl(aq) with
43 concentration $c=0.8$ mol/kg experiments have shown that rupture occurs at $P = -140$ MPa
44 [341]. More recently a series of aqueous solution was studied [331] and cavitation pressures
45 beyond -100 MPa were also observed. From refs. [321] and [354] the homogeneous nucle-
46 ation temperature position can be estimated to be slightly below that of the LLCP of $c=0.67$
47 mol/kg.
48
49
50
51
52
53
54
55
56
57
58

59
60 Upon further adding salt (Fig. 26) the LDL region shrinks more and more as ions are

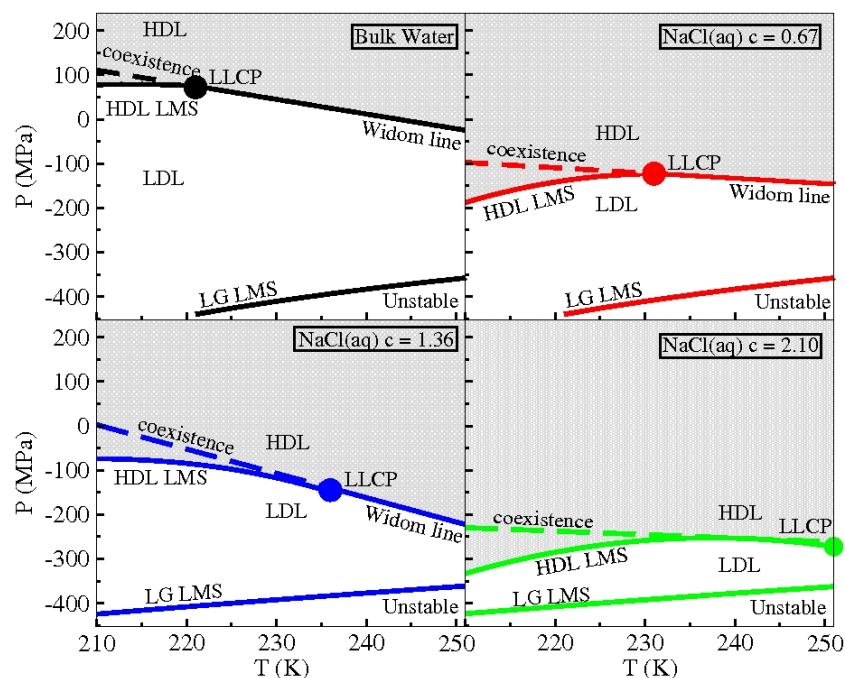


FIG. 26. Phase diagram of NaCl aqueous solutions of supercooled water as obtained from molecular dynamics simulations properly matched to the experimental data. Upon increasing salt content the LDL region shrinks and the LLCP is shifted to lower pressures and higher temperatures. Reproduced from ref. [288].

more favorably solvated by the high density liquid [362, 371].

To complete the picture of low concentration solutions of NaCl in water an MCT behavior and a FTS transition was found upon supercooling and the FTS transition happens on crossing the Widom line, see Fig. 27, confirming also for the solution the link between dynamics and thermodynamics found in the bulk [290, 291]. The excess entropy, approximated by the two-body terms extracted from MD simulations of NaCl(aq), shows the same FTS transition as the diffusion coefficient [198] and this means that from a direct experimental measurement of the $g(r)$ the FTS should be measurable also in solutions.

Small angle x-ray scattering experiments of NaCl aqueous solutions also demonstrate the persistence of the anomalous behavior in the solution since they show that the correlation length can be fit with a power law, similar to the bulk, upon cooling [372].

Biddle et al. [134] have compared their equation of state for solutions based on the ideas described in sec. IV, with the MD results of NaCl(aq) [107, 288] and found agreement.

Recent experiments on melting of precipitated ice IV in supercooled LiCl-H₂O solution

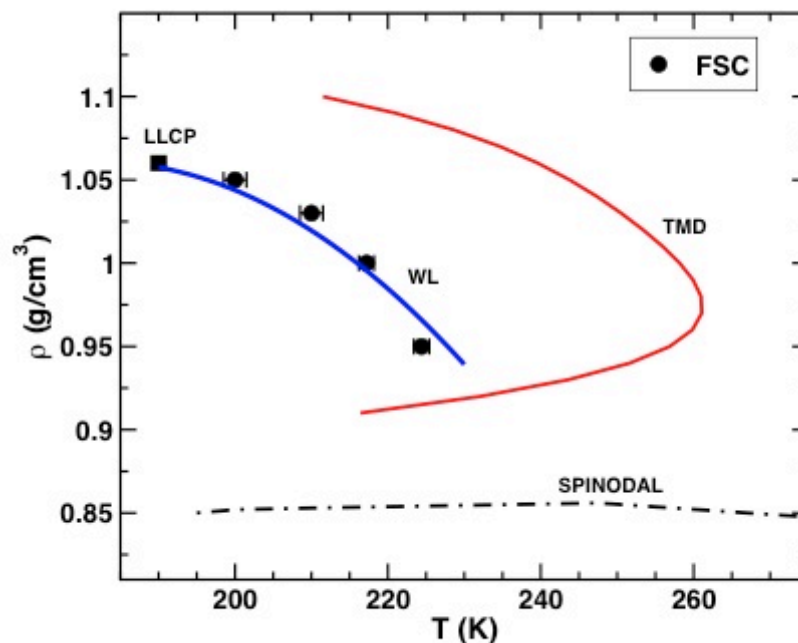


FIG. 27. FTS transition points (circles) and Widom line (line) in a NaCl aqueous solution as obtained from molecular dynamics simulations. The nose-shaped line is the TMD [290].

by Mishima [373, 374] can be explained presuming existence of polymorphism in water, and by the simple assumption that LiCl is dissolved mainly in high-density liquid water as also found in simulation on NaCl(aq) [371].

A similar picture to that of electrolytes appears for the phase diagram of the small amphiphilic methanol molecule. The phase diagram is shifted down in pressure (but not in temperature) and the LLCP is still found for low concentrations [375]. A FTS was measured in methanol solutions at different concentrations [376].

Also a model potential like Jagla shows, upon addition of a solvophobic solute, the same phenomenology described so far. In particular, solutions of Jagla water upon insertion of

1
2
3 hard spheres show a shift of the LLCPP to higher pressures and lower temperatures and a
4 dynamic transition upon crossing the Widom line [289, 293].
5

6 Experiments, theory and simulations thus indicate that aqueous solutions are a viable
7 route to solve the mysteries of supercooled water.
8
9

10 11 12 13 **XII. FUTURE DIRECTIONS** 14

15
16 The foregoing review makes clear that, despite many, often highly sophisticated, experi-
17 mental and computational efforts to obtain a full understanding of the complex behavior of
18 water, there remain many gaps in our knowledge and understanding of this most anomalous
19 liquid. In this section we seek to identify the most serious of these gaps, and to explore
20 how they might be dealt with. The biggest problem faced is that of the "crystallization
21 curtain" that has until recently blocked our knowledge of behavior below the homogeneous
22 nucleation temperature. How best to capitalize on the success of Nilsson and coworkers
23 [209] in penetrating this barrier by means of microdroplet streams and pulsed x-ray laser
24 interrogation, is obviously one line of study to be explored and this is the first issue that
25 will be considered below.
26
27

28
29 But there are other possibilities for circumventing the crystallization problem to be con-
30 sidered. Each has its own set of difficulties and uncertainties but also promise. There is,
31 for instance, the approach outlined by Koop and coworkers [385] to effectively mimic the
32 raising of pressure on water by introduction of second components. Although this usually
33 results in the wiping-out of the anomalies at the same time as it removes the crystallization
34 event (Figs. 25 and 26), it now seems it is possible to decouple the two effects by using the
35 right kind of solute. This approach should be worthy of detailed study since it is basically
36 simple.
37
38

39
40 Then there is the prospect raised by recent studies of water under high tension [39, 299],
41 which have suggested that the anomalous domain can be elevated above the fast crystal-
42 lization domain, perhaps due to competition between ice Ih and various empty clathrate
43 structures that frustrate the generation of critical nuclei of any one crystal form. The nega-
44 tive pressure domain is the only remaining unexplored region of metastable water's existence,
45 and although the challenges in sample production, and in exploring anything other than iso-
46 choric behavior are many, the rewards might be great. It has been argued [299, 336] that it
47
48
49
50
51
52
53
54
55
56
57
58
59
60

1
2
3 is in this domain that the observations needed to distinguish between the different scenarios
4 of section II, will need to be made.
5
6

7 Also, of course, there are developments and refinements in the field of computer simula-
8 tions that are much needed for the understanding of deeply supercooled water. The need is
9 illustrated by a comparison of laboratory data for the fundamental thermodynamic proper-
10 ties, isothermal compressibility and constant pressure heat capacity, with those determined
11 by calculations with the best pair potential currently available. The comparison of ambient
12 pressure compressibility obtained with the pair-potential given most attention in this review,
13 viz. TIP4P/2005 is shown in Figure 28. The agreement is quite good for the first 20°C of
14 supercooling, but then becomes rapidly poorer at lower temperatures where the simulations
15 go through a mild maximum and the experimental quantity shows a strong tendency to
16 diverge at about the same temperature. The power law behavior is seen not only for the
17 compressibility, but also for the heat capacity (Fig. 1), and even more clearly for various
18 transport properties such as viscosity, dielectric relaxation, spin-lattice relaxation and the
19 related reorientation relaxation time, all measured by different authors, so is probably a
20 reliable representation of the observable data. The divergence temperature which has not
21 been confirmed because it lies in "no-man's land", falls in the range 223-228 K, depending
22 on range of data fitted and nature of background corrections.
23
24
25
26
27
28
29
30
31
32
33
34

35 We now consider each of these in sequence.
36
37
38
39

40 **A. Ultrafast probing.** 41 42

43 As described in section V there has been a development in terms of a general method
44 for studying liquid structures below T_H based on fast cooling and ultrafast probing using
45 femtosecond short x-ray pulses by exploiting the unique capabilities of the x-ray laser LCLS
46 [209, 265]. This needs to be further developed to allow other types of measurements both
47 at ambient pressure and eventually at elevated pressures. It will be essential to measure
48 the thermodynamic response functions, such as C_P and κ_T , on small water droplets into
49 "no-mans land" and also the correlation length (ξ). If direct temperature measurements on
50 the droplets can be developed and a heat source introduced to induce a temperature rise,
51 then potentially C_P could be determined.
52
53
54
55
56
57
58

59 SAXS is the most direct probe of density variations or fluctuations on different length
60

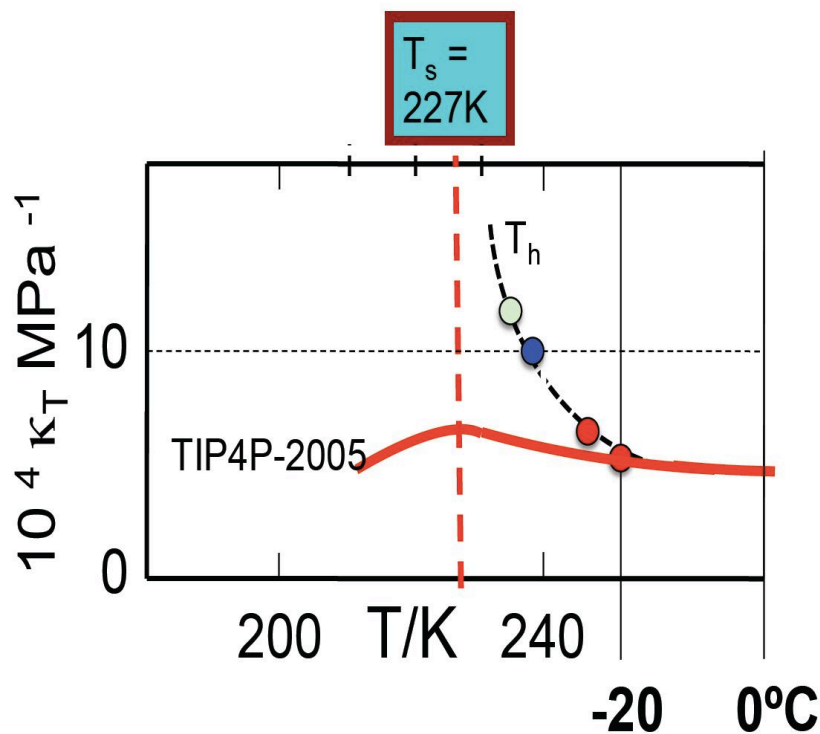


FIG. 28. Comparison of the compressibility-temperature relation at 0.1 MPa obtained with the TIP4P/2005 pair-potential (heavy red curve), with the experimental findings and their extensions, as follows: $-20\text{ }^{\circ}\text{C}$ (253 K): combination of fluctuation based data (Huang et al.) and direct p - V data (Speedy et al.) that are in close agreement: $-24\text{ }^{\circ}\text{C}$ (249 K) lowest temperature direct measurement of Speedy et al. (239 K limit of Holten and Anisimov extrapolation of ambient pressure fitted data: 235 K (based on low T limit of heat capacity measurements, that follow the power law with same divergence temperature).

scales in a liquid and from such measurements both κ_T and ξ could be determined using x-ray lasers. There is a thermodynamic relationship that relates κ_T to the structure factor at $q = 0$ as $S(0) = nk_B T \kappa_T$, where k_B is the Boltzmann constant, T is the absolute temperature, and n is the molecular number density [377]. We can then test the hypothesis that neither ξ , C_P nor κ_T will diverge to infinity but will reach a maximum at T_s i.e., within the LLCPh hypothesis, at the Widom line. Depending on how flat the temperature-dependent region around T_s is, this could provide further insight into the validity of the various scenarios and if there exists an LLCPh. It will also be essential to follow ξ and κ_T to lower temperature below T_s . Furthermore it would be valuable to conduct the experiment using D_2O in order

1
2
3 to probe isotope effects as well as use NaCl solution, since the latter has an effect similar
4 to pressure [372, 378] as discussed in section XI. It could also be possible to determine the
5 density variation from Wide-Angle X-ray Scattering (WAXS) at very high q . The scattering
6 intensity will have weak q -dependence and become proportional to the density of the liquid.
7 From such measurements it could also be possible to derive the thermal expansivity α . Here
8 it will be essential to observe if there is a minimum in α close to the Widom line. Eventually
9 all these classes of experiments should be developed to also involve higher pressures. This
10 will become a major experimental challenge but it is essential that an effort will be devoted
11 to this since it could provide a final answer as to which of the various scenarios best describes
12 real water.
13
14
15
16
17
18
19
20

21 Another essential question to address is the proposed scenario that there is only a liquid
22 to solid transition and that an LDL liquid crystallizes faster than the relaxation time of the
23 liquid [35, 108]. Could we then observe at which temperature the time-scale of liquid equi-
24 libration becomes longer than the time scale for ice crystallization? By directly comparing
25 these time scales we could establish if and at which temperature the liquid could no longer
26 equilibrate relative to fast ice nucleation. We would expect that the structural fluctuations
27 significantly slow down entering into the supercooled regime and maybe in the "no-man's
28 land" region could become on the order of 10 ps or 100 ps. This could also be related to the
29 much discussed fragile to strong transition in the temperature dependence of the viscosity of
30 water both above and below "no-man's land" [24, 238, 241, 294, 379]. It has been suggested
31 that there is a dynamic transition at 228 K that would coincide with the temperature of the
32 T_s or Widom line [241].
33
34
35
36
37
38
39
40
41
42
43
44

45 **B. Second component studies.**

46
47
48 Koop et al. [385] showed that ice nucleation commences at a temperature determined by
49 the water activity irrespective of whether the water activity is reduced by increase of pressure
50 or by addition of a second component that dissolves in the water. The more hydrophilic the
51 solute the less of it is required to reduce the nucleation temperature to a target value, or
52 alternatively to remove the possibility of crystallization altogether.
53
54
55
56

57 Hydrophilic solutes like LiCl or MgCl₂ lower the nucleation temperature rapidly, leading
58 to non-crystallizing solutions. On computational time scales, NaCl behaves the same way
59
60

1
2
3 [288]. The general consequence of high hydrophilicity is that the structures responsible for
4 the interesting anomalies of water are quickly dismantled (or at least are pushed out of
5 sight to negative pressures (see Fig. 26, and ref. [288]). There are other solutes, however,
6 which do not lower the activity of water very rapidly, in fact lead to demonstrably ideal
7 solution behavior according to melting point depression criteria, and it is found that in
8 these cases the low temperature behavior retains the anomalies of water, indeed in enhanced
9 form. This behavior is only recently recognized, and not yet much exploited. It might
10 provide a convincing demonstration of how water would behave during cooling in absence of
11 crystallization. Its relation to the studies of Murata and Tanaka [367] needs to be clarified
12 in future work. However, because second component incorporation is a proxy for increasing
13 pressure, neither provides clear answers to the burning question of pure water behavior at
14 ambient pressure, in absence of crystallization. This may be more easily approached from
15 the other end of the pressure scale, namely at high states of tension or negative pressure.
16
17
18
19
20
21
22
23
24
25
26
27
28

29 **C. Studies at negative pressure.**

30
31
32 Studies of water at large negative pressures have been sparse because of the difficulty
33 of preparing the microscopic samples of water in mineral matrices needed to evaluate the
34 behavior of water in this exotic state, and the difficulty of studying them once success-
35 fully formed. Regrettably the fluid inclusion strategy seems to offer the only feasible way
36 of obtaining samples suitable for evaluating the behavior of water in this interesting do-
37 main. The constraint to constant volume over the temperature range of study is another
38 problem. Nevertheless the difficulties have been mastered by different groups, and Caupin
39 and coworkers, [39, 299] in particular, have given evidence that the anomalous behavior can
40 emerge from, and be studied outside of, the fast crystallization zone ("no-man's land"), see
41 section IX. Clearly this provides a challenge to future workers to perform measurements
42 additional to the velocity of sound studies that have so far been performed, and to design
43 sampling procedures that permit more variable pVT conditions.
44
45
46
47
48
49
50
51
52
53

54 Although most workers are of the opinion that the critical zone in real water lies fully
55 at positive pressures, and that scenario B of section II is the appropriate description of
56 real water behavior, the issue is not yet settled. Although it has not been discussed in the
57 body of the review, there is a powerful argument by Binder (see ref. [387]) to the effect that
58
59
60

1
2
3 in a metastable system a true critical point cannot exist because the diverging time scale
4 needed for its ergodic manifestation would cross the finite lifetime for the liquid imposed by
5 crystallization kinetics. This difficult-to-deny argument which, however, only concerns the
6 immediate vicinity of the critical point, leads us to refer to a critical "zone" within which
7 ergodicity in principle cannot be established, but on either side of which a liquid-liquid line
8 or a Widom line could exist and could play a role in the physics of the liquid.
9

10
11
12
13
14 The arguments given by Speedy for an essentially continuous line of compressibility in-
15 finities from a negative pressure extreme to strong positive pressures, and the similarity to
16 the engineering equations of state, coupled with the lack of any isochore crossing point for
17 the available isochores from the IAPWS-95 equation of state in the positive pressure range
18 (such as that seen so clearly for ST2 water [94]), leaves the situation with real water in some
19 doubt. While this can be rationalized by locating the critical point very close to ambient
20 pressure, as fitted by Holten and Anisimov [31], the fact that the "most likely" second crit-
21 ical point pressure has moved steadily to lower pressures with passing time over some two
22 decades, keeps the final location of the critical point and liquid-liquid line, or HDL spinodal
23 vs Widom line at ambient pressure, a matter for continuing debate and future work. An
24 important part of this debate concerns the behavior of the line of density maxima (LDM),
25 which itself passes through a maximum at negative pressures according to all pair-potential
26 models, but does the opposite in the case of the empirical equations of state and the scenario
27 C of section II. A positive identification of the behavior of the LMD is badly needed as the
28 TMD claimed in the original study of Zheng et al. 1991 is now subject to adjustment by a
29 surface tension argument given earlier in section IX. Two possibilities are identified here for
30 future work.
31
32
33
34
35
36
37
38
39
40
41
42
43

44 Firstly, the existence of a density maximum can be identified directly from the Brillouin
45 light scattering measurement by the vanishing of the central line intensity since the Landau-
46 Placzek ratio must go to zero at a density maximum. The Landau-Placzek ratio connects
47 the intensities of the Brillouin peaks, I_B , and of the elastic peak, I_R , in light scattering with
48 the specific heat at constant volume and that at constant pressure according to the following
49 equation:
50
51
52
53
54

$$\frac{I_R}{2I_B} = \frac{C_P - C_V}{C_V} \quad (9)$$

55
56
57
58
59 However, in the quartz inclusion milieu presently used, the stray light is far too intense for
60

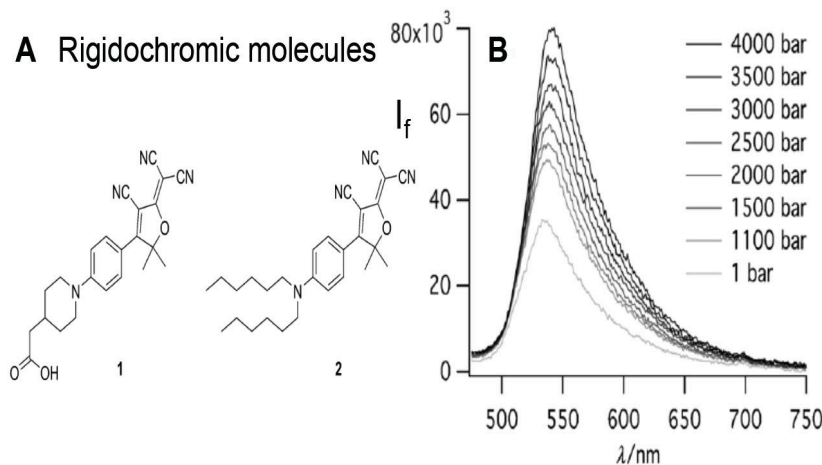


FIG. 29. **A.** Fluorescent molecules whose intensities I_f have high sensitivity to pressure or viscosity. **B.** Pressure dependence of the fluorescence intensity of molecule 1 in 1M solution in acetone. Reproduced from Ref. [381] with permission.

this observation to be a possibility. Further developments of stray light canceling strategies, or ways of producing a single perfect vesicle in a perfect quartz crystal, may eventually permit this simple measurement to generate an unambiguous line of density maxima that will end the debate one way or another.

Secondly, and more immediately, the introduction of small reporter dye molecules, sensitive to pressure, offer the possibility of direct spectroscopic determination of a density maximum. For instance, there is the water-soluble dyestuff molecules of the type recently used for analyzing friction patterns on sliding surfaces [380]. These studies depended on the sensitivity of the fluorescence spectrum to pressure or viscosity or both [381].

The fluorescence intensity of molecule 1 of Fig. 29A is depicted in Fig. 29B. The sensitivity to pressure is seen to be quite high, and although the isochoric nature of the projected experiment will possibly complicate the interpretation, the likelihood of a null result at the tension maximum seems small. In any case, this is not the only pressure sensitive dyestuff that is available. If the pressure sensitivity is due to a pressure dependent viscosity, so much the better since the diffusivity of water is known to decrease with great rapidity as pressure decreases in the direction of the tensile domain [382].

Of course, the molecule must first survive the autoclaving procedure used to produce the samples but there is precedence for this in the successful introduction of a water-insoluble polyphenyl, orthoterphenyl, into the vesicles prepared by Zheng (and only reported in ref.

1
2
3 [384]). We expect that a water soluble version of the molecule seen in Fig. 29 will likewise
4 survive as it need only be present in very low concentrations.
5

6
7 If the temperature of maximum density detected by such fluorescence intensity studies
8 confirms the reversal of TMD trajectory in pressure, then the existence of the second critical
9 point at zero pressure or thereabouts will find strong support.
10

11
12 But what will it imply if such a study confirms the high values of the TMD reported
13 from the original inclusion measurements or their successor studies? Firstly, it will confirm
14 the great sensitivity of the equation of state parameters to the choice of L-L coexistence
15 data which was pointed out by the authors of ref. [31], and secondly it will support the
16 qualitative validity of engineering equations of state for water, which to date have been
17 given little credence by the metastable water community.
18
19

20
21 The origin of the sensitivity can be found in the way the TMD is approaching the liquid-
22 gas spinodal limit. This can be seen from the work of Vashist et al. [117] on liquid Si in
23 the Stillinger-Weber (S-W) model where the point of reversal of the TMD with increasing
24 tension is extremely close to the spinodal limit for the liquid state. Since the latter cannot
25 be penetrated, the said reversal must suddenly switch in the opposite direction if the λ
26 parameter of the S-W model is made any larger. Indeed if it is raised to the value 23 used
27 by Molinero and Moore [124] in their successful adaptation of the S-W form of potential to
28 the description of water, then the isochore minima, *which determine the TMD*, no longer
29 reverse their direction with increasing temperature, but rather behave in the manner given
30 by, for instance, the HGK, or IAPWS-95 equations of state for water. This is demonstrated
31 by current assessments of the isochores of the tuned S-W model seen in Fig. 30 LH panel
32 which no longer cross at a critical point as they do for values of λ of 21 and lower (Kapko
33 and Angell to be published).
34
35

36
37 More importantly, it might also require recognition that, not only have the critical point-
38 related anomalies emerged from "no-man's land" (as suggested by the negative pressure
39 studies of Caupin and co-authors [39, 299]), but that the critical point itself has disappeared
40 into the liquid-gas spinodal and become a virtual phenomenon. It would mean that the
41 Widom line does not exist but rather that the anomalies of water are provoked by close
42 approach to a line of spinodal instabilities of the high density liquid that lies just a few K
43 on the low temperature side of a line of liquid-liquid transitions that itself lies close to but
44 below the line of homogeneous nucleation temperatures. This is now called the "critical
45
46
47
48
49
50
51
52
53
54
55
56
57
58
59
60

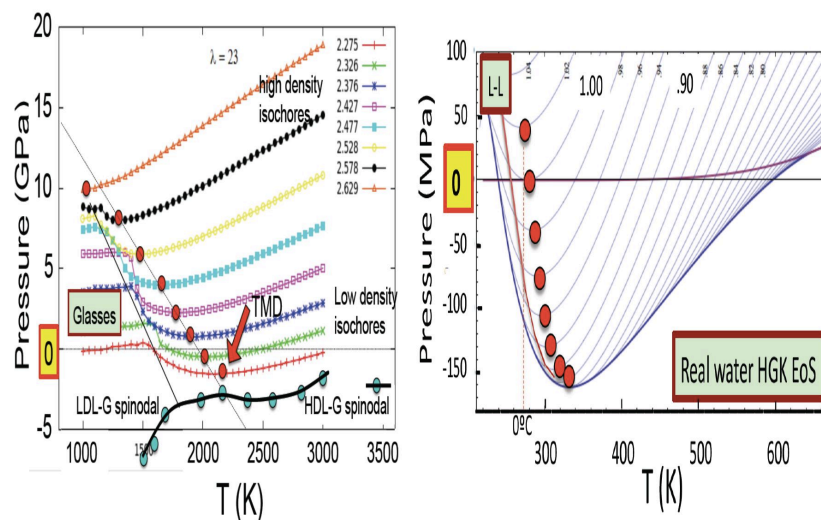


FIG. 30. **LH panel.** Behavior of the isochores, and the TMD, with isochose density in the tuned S-W model with λ parameter = 23. The TMD does not reverse as it does for the silicon potential $\lambda=21$. The flattened segments at lower temperatures correspond to broken ergodicity states (glasses on the simulation time scale). **RH panel.** Isochores and density maxima behavior of the HGK equation of state for water.

point-free" scenario [24] (diagram C in Fig. 2).

Thus in light of Figure 1 above and the latter challenges, there seems to be a need for more work on water models that will provide better agreement with experiment in these extreme conditions.

Why have pair-potential models not yet acquired the ability to show the above sequence of possibilities? According to the x-ray laser data shown in Fig. 12, the TIP4P-2005 model is not "going tetrahedral" quickly enough with decreasing temperature (see Fig. 12). Perhaps, as in mW water [108] they need the additional drive to tetrahedrality that is provided by potentials of the S-W form, in which a departure from tetrahedrality is penalized by a repulsive energy component that opposes the pairwise additive attraction component of the total potential. In water this would act on the O-O-O alignments which need to be tetrahedral in an LDA-like structure. While such possibilities as the above remain uninvestigated, water is likely to maintain its mystique as the most anomalous and least understood liquid.

XIII. ACKNOWLEDGEMENTS

This review was initiated during the Nordita (Nordic Institute for Theoretical Physics) scientific program "Water - the Most Anomalous Liquid". Additional financial support for this program was provided by the Royal Swedish Academy of Sciences through its Nobel Institutes for Physics and Chemistry, by the Swedish Research Council and by the Department of Physics at Stockholm University. We would like to acknowledge helpful suggestions by Prof. Pablo Debenedetti. We are grateful to Stephan Fuhrmann for providing Fig. 3. CAA wishes to acknowledge support from the NSF under collaborative grant No. CHE 12-13265. FC acknowledges funding by the European Research Council under the European Community's FP7 Grant Agreement 240113, and by the Agence Nationale de la Recherche Grant 09-BLAN-0404-01. CC would like to thank Department of Science and Technology, New Delhi for financial support. TL is grateful for funding to the European Research Council (ERC Starting Grant SULIWA), the Austrian Science Fund FWF (bilateral project I1392) and the Alexander von Humboldt Foundation (Bessel award). AZP would like to acknowledge support for this work by the Department of Energy, Office of Basic Energy Sciences, under Award No. DE-SC0002128. HT acknowledges supports from Grants-in-Aid for Scientific Research (S) (Grand No. 21224011) and Specially Promoted Research (Grand No. 25000002) from the Japan Society for the Promotion of Science. CV acknowledges project FIS2013-43209-P for funding. LX acknowledges the support from National Science Foundation of China (Grant No.: 11174006, 11290162, 11525520) and MOST (Grant No.: 2012CB921404, 2015CB856801).

-
- 1
2
3
4
5
6
7 [1] Angell, C. A. Water and Aqueous Solutions at Subzero Temperatures, in *Water: A Comprehensive Treatise* Vol.7. New York: Plenum, 1982.
8
9
10
11 [2] Debenedetti, P. G. *Metastable Liquids: Concepts and Principles*. Princeton: Princeton University Press, 1996.
12
13
14 [3] Franks, F. *Water: A Matrix of Life*. Cambridge: Royal Society of Chemistry, 2000.
15
16 [4] Debenedetti, P. G. Supercooled and glassy water. *J. Phys: Condens Matter* **2003**, *15*, R1669–
17 R1726.
18
19 [5] Debenedetti, P. G.; Stanley, H. E. Supercooled and Glassy Water. *Physics Today* **2003**, *56*,
20 40–46.
21
22 [6] Angell, C. A. Amorphous water. *Ann. Rev. Phys. Chem.* **2004**, *55*, 559–583.
23
24 [7] Ball, P. Water as an active constituent in cell biology. *Chem. Rev.* **2008**, *108*, 74–108.
25
26 [8] Bellissent-Funel, M.-C. *Hydration Processes in Biology: Theoretical and Experimental Approaches*. Amsterdam: ISO Press, 1999.
27
28 [9] Robinson, G. W.; Zhu, S. B.; Singh, S.; Evans, M. W. *Water in Biology, Chemistry, and*
29 *Physics: Experimental Overviews and Computational Methodologies*. Singapore: World Scientific, 1996.
30
31 [10] Workshop on “Water”: Structure and Dynamics of Water and Aqueous Solutions — Anomalies
32 and their Possible Implications in Biology. Grenoble: Proc. of Inst. Laue-Langevin, 1984.
33
34 [11] Angell, C. A.; Shuppert, J.; Tucker, J. C. Anomalous properties of supercooled water. Heat
35 capacity, expansivity, and proton magnetic resonance chemical shift from 0 to -38°C. *J. Phys.*
36 *Chem.* **1973**, *77*, 3092–3099.
37
38 [12] Speedy, R. J.; Angell, C. A. Isothermal compressibility of supercooled water and evidence
39 for a thermodynamic singularity at 45°C. *J. Chem. Phys.* **1976**, *65*, 851–858.
40
41 [13] Stanley, H. E. *Introduction to phase transitions and critical phenomena*. New York: Oxford
42 University Press, 1971.
43
44 [14] Kumar, P.; Stanley, H. E. Thermal conductivity minimum: A new water anomaly. *J. Phys.*
45 *Chem. B* **2011**, *115*, 14269–14273.
46
47 [15] Angell, C. A.; Oguni, M.; Sichina, W. J. Heat capacity of water at extremes of supercooling
48 and superheating. *J. Phys. Chem.* **1982**, *86*, 998–1002.
49
50
51
52
53
54
55
56
57
58
59
60

- 1
2
3 [16] Sato, H.; Watanabe, K.; Levelt-Sengers, J. M. H.; Gallagher, J. S.; Hill, P. G.; Straub, J.;
4 Wagner, W. Sixteen Thousand evaluated experimental thermodynamic property data for
5 water and steam. *J. Phys. Chem. Ref. Data* **1991**, *20*, 1023–1044.
6
7
8 [17] Conde, O.; Teixeira, J.; Papon, P. Analysis of sound velocity in supercooled H₂O, D₂O, and
9 water-ethanol mixtures. *J. Chem. Phys.* **1982**, *76*, 3747–3753.
10
11 [18] Kanno, H.; Angell, C. A. Water: Anomalous compressibilities to 1.9 kbar and correlation
12 with supercooling limits. *J. Chem. Phys.* **1979**, *70*, 4008–4016.
13
14 [19] Poole, P. H.; Sciortino, F.; Essmann, U.; Stanley, H.E. Phase Behavior of Metastable Water.
15 *Nature* **1992**, *360*, 324–328.
16
17 [20] Poole, P. H.; Sciortino, F.; Essmann, U.; Stanley, H. E. The Spinodal of Liquid Water. *Phys.*
18 *Rev. E* **1993**, *48*, 3799–3817.
19
20 [21] Poole, P. H.; Essmann, U.; Sciortino, F.; Stanley, H. E. Phase Diagram for Amorphous Solid
21 Water. *Phys. Rev. E* **1993**, *48*, 4605–4610.
22
23 [22] Sciortino, F.; Poole, P. H.; Essmann, U.; Stanley, H. E. Line of Compressibility Maxima in
24 the Phase Diagram of Supercooled Water. *Phys. Rev. E* **1997**, *55*, 727–737.
25
26 [23] Sastry, S.; Debenedetti, P. G.; Sciortino, F.; Stanley, H. E. Singularity-Free Interpretation
27 of the Thermodynamics of Supercooled Water. *Phys. Rev. E* **1996**, *53*, 6144–6154.
28
29 [24] Angell, C. A. Insights into liquid water phases from study of its unusual glass-forming prop-
30 erties. *Science* **2008**, *319*, 582–587.
31
32 [25] Speedy, R. J. Stability-limit conjecture. *J. Phys. Chem.* **1982**, *86*, 982–989.
33
34 [26] Tanaka, H. Simple physical model of liquid water. *J. Chem. Phys.* **2000**, *112*, 799–809.
35
36 [27] Tanaka, H. Simple view of waterlike anomalies of atomic liquids with directional bonding.
37 *Phys. Rev. B* **2002**, *66*, 064202.
38
39 [28] Tanaka, H. Bond orientational order in liquids: Towards a unified description of water-like
40 anomalies, liquid-liquid transition, glass transition, and crystallization. *Eur. Phys. J. E* **2012**,
41 *35*, 113.
42
43 [29] Fuentesvilla, D. A.; Anisimov, M. A. Scaled equation of state for supercooled water near the
44 liquid-liquid critical point. *Phys. Rev. Lett.* **2006**, *97*, 195702.
45
46 [30] Bertrand, C. E.; Anisimov, M. A. Peculiar thermodynamics of the second critical point in
47 supercooled water. *J. Phys. Chem. B* **2011**, *115*, 14099–14111.
48
49
50
51
52
53
54
55
56
57
58
59
60

- 1
2
3 [31] Holten, V.; Anisimov, M. A. Entropy-driven liquid-liquid separation in supercooled water.
4
5 *Sci. Rep.* **2012**, *2*, 713.
6
- 7 [32] Stanley, H. E.; Kumar, P.; Franzese, G.; Xu, L.; Yan, Z.; Mazza, M. G.; Buldyrev, S. V.;
8
9 Chen, S.-H.; Mallamace, F. Liquid Polyamorphism: Possible Relation to the Anomalous
10
11 Behavior of Water. *Eur. Phys. J. Special Topics* **2008**, *161*, 1–17.
12
- 13 [33] Mishima, O.; Stanley, H. E. The relationship between liquid, supercooled and glassy water.
14
15 *Nature* **1998**, *396*, 329–335.
16
- 17 [34] Xu, L.; Kumar, P.; Buldyrev, S. V.; Chen, S.-H.; Poole, P. H.; Sciortino, F.; Stanley, H. E.
18
19 Relation between the Widom line and the dynamic crossover in systems with a liquid-liquid
20
21 phase transition. *Proc. Natl. Acad. Sci. (USA)* **2005**, *102*, 16558–16562.
22
- 23 [35] Limmer, D.T.; Chandler, D. The putative liquid-liquid transition is a liquid-solid transition
24
25 in atomistic models of water. *J. Chem. Phys.* **2011**, *135*, 134503.
26
- 27 [36] Limmer, D. T.; Chandler, D. The putative liquid-liquid transition is a liquid-solid transition
28
29 in atomistic models of water. II. *J. Chem. Phys.* **2013**, *138*, 214504.
30
- 31 [37] Nilsson, A.; Pettersson, L. G. M. The Structural Origin of Anomalous Properties of Liquid
32
33 Water. *Nature Commun.* **2015**, *6*, 8998.
34
- 35 [38] Poole, P. H. ; Sciortino, F.; Grande, T.; Stanley, H. E.; Angell, C. A. Effect of Hydrogen
36
37 Bonds on the Thermodynamic Behavior of Liquid Water. *Phys. Rev. Lett.* **1994**, *73*, 1632–
38
39 1635.
40
- 41 [39] Pallares, G.; El Mekki Azouzi, M.; González, M. A.; Aragonés, J. L.; Abascal, J. L. F.;
42
43 Valeriani, C.; Caupin, F. Anomalies of water at negative pressure. *Proc. Natl. Acad. Sci.*
44
45 *(USA)* **2014**, *111*, 7936–7941.
46
- 47 [40] Mishima, O.; Stanley, H. E. Decompression-Induced Melting of Ice IV and the Liquid-Liquid
48
49 Transition in Water. *Nature* **1998**, *392*, 164–168.
50
- 51 [41] Sciortino, F.; La Nave, E.; Tartaglia, P. Physics of the liquid-liquid critical point. *Phys. Rev.*
52
53 *Lett.* **2003**, *91*, 155701.
54
- 55 [42] Sivakumar, T. C.; Rice, S. A.; Sceats, M. G. Raman spectroscopic studies of the OH stretch-
56
57 ing region of low density amorphous solid water and of polycrystalline ice Ih. *J. Chem. Phys.*
58
59 **2000**, *69*, 3468–3476.
60
- 60 [43] Maruyama, S.; Wakabayashi, K.; Oguni, M. Thermal properties of supercooled water con-
61
62 fined within silica gel pores. *American Institute of Physics Conference Proceedings* **2004**,

- 1
2
3 708, 675–676.
4
5 [44] Mishima, O.; Calvert, L. D.; Whalley, E. 'Melting ice' I at 77 K and 10 kbar: a new method
6 of making amorphous solids. *Nature* **1984**, *310*, 393–395.
7
8 [45] Mishima, O.; Calvert, L. D.; Whalley, E. An apparently first-order transition between two
9 amorphous phases of ice induced by pressure. *Nature* **1985**, *314*, 76–78.
10
11 [46] Finney, J. L.; Bowron, D. T.; Soper, A. K.; Loerting, T.; Mayer, E.; Hallbrucker, A. Structure
12 of a New Dense Amorphous Ice. *Phys. Rev. Lett.* **2002**, *89*, 205503.
13
14 [47] Bellissent-Funel, M.-C.; Bove, L.E.; Nilsson, A.; Paciaroni, A.; Schlesinger, D.; Skinner, L.B.;
15 Amann-Winkel, K. X-ray and Neutron Scattering of Water, *Chem. Rev.* **2015**, *XX*, YY–ZZ.
16
17 [48] Whiting, H. A new theory of cohesion applied to the thermodynamics of liquids and
18 solids, *Proc. Am. Acad. Arts Sci.* **1884**, *19*, 353–431.
19
20 [49] Röntgen, W. K. Ueber die constitution des flüssigen wassers. *Ann. Phys.* **1892**, *45*, 91–97.
21
22 [50] Davis, C. M., Jr.; Litovitz, T. A. Two-State Theory of the Structure of Water. *J. Chem.*
23 *Phys.* **1965**, *42*, 2563–2576.
24
25 [51] Angell, C. A. Two-state thermodynamics and transport properties for water from "bond
26 lattice" model, *J. Phys. Chem.* **1971**, *75*, 3698–3705.
27
28 [52] Vedamuthu, M.; Singh, S.; Robinson, G. W. Properties of Liquid Water: Origin of the
29 Density Anomalies. *J. Phys. Chem.* **1994**, *98*, 2222–2230.
30
31 [53] Mishima, O. Reversible first-order transition between two H₂O amorphs at 0.2 GPa and
32 135K. *J. Chem. Phys.* **1994**, *100*, 5910–5912.
33
34 [54] Bellissent-Funel, M.- C.; Bosio, L.; Hallbrucker, A.; Mayer, E.; Sridi-Dorbez, R. X-ray and
35 neutron scattering studies of the structure of hyperquenched glassy water. *J. Chem. Phys.*
36 **1992**, *97*, 1282–1286.
37
38 [55] Bellissent-Funel, M.- C.; Bosio, L. A neutron scattering study of liquid D₂O under pressure
39 and at various temperatures. *J. Chem. Phys.* **1995**, *102*, 3727–3735.
40
41 [56] Anderson, O. Glass-liquid transition of water at high pressure. *Proc. Natl. Acad. Sci. (USA)*
42 **2011**, *108*, 11013–11016.
43
44 [57] Soper, A. K.; Ricci, M. A. Structures of high-density and low-density water. *Phys. Rev. Lett.*
45 **2000**, *84*, 2881–2884.
46
47 [58] Bellissent-Funel, M. C. Is there a liquid-liquid phase transition in supercooled water? *Euro-*
48 *phys. Lett.* **1998**, *42*, 161–166.
49
50
51
52
53
54
55
56
57
58
59
60

- 1
2
3 [59] Head-Gordon, T.; Stillinger, F. H. An Orientational Perturbation Theory for Pure Liquid
4 Water. *J. Chem. Phys.* **1993**, *98*, 3313–3327.
5
6
7 [60] Stanley, H. E.; "Mysteries of Water" [Opening Course, 1998 Les Houches School], in Hydrata-
8 tion Processes in Biology: Theoretical and Experimental Approaches [Proc. NATO Advanced
9 Study Institutes, Vol. 305], edited by M.-C. Bellissent-Funel (IOS Press, Amsterdam, 1999),
10 Chapter 1.
11
12
13 [61] Giovambattista, N.; Loerting, T.; Lukanov, B. R.; Starr, F. W. Interplay of the glass transi-
14 tion and the liquid-liquid phase transition in water. *Sci. Rep.* **2012**, *2*, 1–8.
15
16
17 [62] Loerting, T.; Fuentes-Landete, V.; Handle, P. H.; Seidl, M.; Amann-Winkel, K.; Gainaru,
18 C.; Böhmer, R. The glass transition in high-density amorphous ice. *J. Non-Crystalline Solids*
19 **2015**, *407*, 423–430.
20
21
22 [63] Mishima, O.; Suzuki, Y. Propagation of the polyamorphic transition of ice and the liquid-
23 liquid critical point. *Nature* **2002**, *419*, 599–603.
24
25
26 [64] Klotz, S.; Strässle, Th.; Nelmes, R. J.; Loveday, J. S.; Hamel, G.; Rouse, G.; Canny, B.;
27 Chervin, J. C.; Saitta, A. M. Nature of the Polyamorphic Transition in Ice under Pressure.
28 *Phys. Rev. Lett.* **2005**, *94*, 025506.
29
30
31 [65] Yoshimura, Y.; Mao, H. K.; Hemley, R. J. An in situ Raman spectroscopic study on the
32 reversible transition between low-density and high-density amorphous ices at 135 K. *J. Phys.:
33 Condens. Matter* **2007**, *19*, 425214 .
34
35
36 [66] Winkel, K.; Elsaesser, M. S.; Mayer, E.; Loerting, T. Water polyamorphism: reversibility
37 and (dis)continuity. *J. Chem. Phys.* **2008**, *128*, 044510.
38
39
40 [67] Winkel, K.; Mayer, E.; Loerting, T. Equilibrated high-density amorphous ice and its first-
41 order transition to the low-density form. *J. Phys. Chem. B* **2011**, *115*, 14141–14148.
42
43
44 [68] Andersson, O. Glass-liquid transition of water at high pressure. *Proc. Natl. Acad. Sci. (USA)*
45 **2011**, *108*, 11013–11016.
46
47
48 [69] Johari, G. P.; Hallbrucker, A.; Mayer, E. The glass-liquid transition of hyperquenched water.
49 *Nature* **1987**, *330*, 552–553.
50
51
52 [70] Hallbrucker, A.; Mayer, E.; Johari, G. P. Glass-liquid transition and the enthalpy of devit-
53 rification of annealed vapor-deposited amorphous solid water - A comparison with hyper-
54 quenched glassy water. *J. Phys. Chem.* **1989**, *93*, 4986–4990.
55
56
57
58
59
60

- 1
2
3 [71] Elsaesser, M. S.; Winkel, K.; Mayer, E.; Loerting, T. Reversibility and isotope effect of the
4 calorimetric glass – liquid transition of low-density amorphous ice. *Phys. Chem. Chem. Phys.*
5 **2010**, *12*, 708–712.
6
7
8
9 [72] Kohl, I.; Bachmann, L.; Hallbrucker, A.; Mayer, E.; Loerting, T. Liquid- like Relaxation in
10 Hyperquenched Water at ≤ 140 K. *Phys. Chem. Chem. Phys.* **2005**, *7*, 3210–3220.
11
12 [73] Angell, C. A.; Moynihan, C. T.; Hemmati, M. 'Strong' and 'superstrong' liquids, and an
13 approach to the perfect glass state via phase transition. *J. Non-Crystalline Solids* **2000**, *274*,
14 319–331.
15
16
17
18 [74] Shephard, J. J.; Evans, J. S. O.; Salzman, C. G. Structural Relaxation of Low-Density
19 Amorphous Ice upon Thermal Annealing. *J. Phys. Chem. Lett.* **2013**, *4*, 3672–3676.
20
21 [75] Smith, R. S.; Kay, B. D. The existence of supercooled liquid water at 150 K. *Nature* **1999**,
22 *398*, 788–791.
23
24
25 [76] Fisher, M.; Devlin, J. P. Defect activity in amorphous ice from isotopic exchange data -
26 Insight into the glass-transition. *J. Phys. Chem.* **1995**, *99*, 11584–11590.
27
28
29 [77] Angell, C. A. Glass transition dynamics in water and other tetrahedral liquids: 'order-
30 disorder' transitions versus 'normal' glass transitions. *J. Phys.: Condens. Matter* **2007**, *19*,
31 205112.
32
33
34 [78] Capaccioli, S.; Ngai, K. L. Resolving the controversy on the glass transition temperature of
35 water? *J. Chem. Phys.* **2011**, *135*, 104504.
36
37
38 [79] Amann-Winkel, K.; Böhmer, R.; Fujara, F.; Gainaru, C.; Geil, B.; Loerting, T. Water's
39 Controversial Glass Transitions, *Rev. Mod. Phys.* **2015**, in press.
40
41
42 [80] Sepulveda, A.; Leon-Gutierrez, E.; Gonzalez-Silveira, M.; Rodriguez-Tinoco, C.; Clavaguera-
43 Mora, M. T.; Rodriguez-Viejo, J. Glass transition in ultrathin films of amorphous solid water.
44 *J. Chem. Phys.* **2012**, *137*, 244506.
45
46
47 [81] Amann-Winkel, K.; Gainaru, C.; Handle, P. H.; Seidl, M.; Nelson, H.; Böhmer, R.; Loerting,
48 T. Water's second glass transition. *Proc. Natl. Acad. Sci. (USA)* **2013**, *110*, 17720–17725.
49
50
51 [82] Gainaru, C.; Agapov, A. L.; Fuentes-Landete, V.; Amann-Winkel, K.; Nelson, H.; Köster,
52 K. W.; Kolesnikov, A. I.; Novikov, V. N.; Richert, R.; Böhmer, R.; Loerting, T.; Sokolov, A.
53 P. Anomalously large isotope effect in the glass transition of water. *Proc. Natl. Acad. Sci.*
54 *(USA)* **2014**, *111*, 17402–17407.
55
56
57
58
59
60

- 1
2
3 [83] Mishima, O.; Suzuki, Y. Vitrification of emulsified liquid water under pressure. *J. Chem.*
4 *Phys.* **2001**, *115*, 4199–4202.
5
6
7 [84] Mishima, O. The glass-to-liquid transition of the emulsified high-density amorphous ice made
8 by pressure-induced amorphization. *J. Chem. Phys.* **2004**, *121*, 3161–3164.
9
10 [85] Andersson, O. Relaxation time of water's high-density amorphous ice phase. *Phys. Rev. Lett.*
11 **2005**, *95*, 205503.
12
13 [86] Andersson, O.; Inaba, A. Dielectric properties of high-density amorphous ice under pressure.
14 *Phys. Rev. B* **2006**, *74*, 184201.
15
16 [87] Seidl, M.; Elsaesser, M. S.; Winkel, K.; Zifferer, G.; Mayer, E.; Loerting, T. Volumetric study
17 consistent with a glass-to-liquid transition in amorphous ices under pressure. *Phys. Rev. B*
18 **2011**, *83*, 100201.
19
20 [88] Handle, P. H.; Seidl, M.; Loerting, T. Relaxation Time of High-Density Amorphous Ice.
21 *Phys. Rev. Lett.* **2012**, *108*, 225901.
22
23 [89] Floriano, M. A.; Handa, Y. P.; Klug, D. D.; Whalley, E. Nature of the transformations of
24 ice-I and low-density amorphous ice to high-density amorphous ice. *J. Chem. Phys.* **1989**,
25 *91*, 7187–7192.
26
27 [90] Xu, L.; Buldyrev, S. V.; Giovambattista, N.; Angell, C. A.; Stanley, H. E. A monatomic system
28 with a liquid-liquid critical point and two distinct glassy states. *J. Chem. Phys.* **2009**, *130*,
29 054505.
30
31 [91] Xu, L.; Giovambattista, N.; Buldyrev, S. V.; Debenedetti, P. G.; Stanley, H. E. Waterlike
32 glass polyamorphism in a monoatomic isotropic Jagla model. *J. Chem. Phys.* **2011**, *134*,
33 064507.
34
35 [92] Harrington, S.; Poole, P. H.; Sciortino, F.; Stanley, H. E. Equation of state of supercooled
36 water simulated using the extended simple point charge intermolecular potential. *J. Chem.*
37 *Phys.* **1997**, *107*, 7443–7450.
38
39 [93] Yamada, M.; Mossa, S.; Stanley, H. E.; Sciortino, F. Interplay between Time-Temperature-
40 Transformation and the Liquid-Liquid Phase Transition in Water. *Phys. Rev. Lett.* **2002**, *88*,
41 195701.
42
43 [94] Poole, P. H.; Saika-Voivod, I.; Sciortino, F. Density minimum and liquid-liquid phase tran-
44 sition. *J. Phys.: Condens. Matter* **2005**, *17*, L431–L437.
45
46
47
48
49
50
51
52
53
54
55
56
57
58
59
60

- 1
2
3 [95] Paschek, D. How the liquid-liquid transition affects hydrophobic hydration in deeply super-
4 cooled water. *Phys. Rev. Lett.* **2004**, *94*, 217802.
5
6
7 [96] Paschek, D.; Ruppert, A.; Geiger, A. Thermodynamic and structural characterization of the
8 transformation from a metastable low-density to a very high-density form of supercooled
9 TIP4P-Ew model water. *Chem. Phys. Chem.* **2008**, *18*, 2737–2741.
10
11
12 [97] Liu, Y.; Panagiotopoulos, A. Z.; Debenedetti, P. G. Low-temperature fluid-phase behavior
13 of ST2 water. *J. Chem. Phys.* **2009**, *131*, 104508.
14
15
16 [98] Abascal, J. L. F.; Vega, C. Widom line and the liquid-liquid critical point for the TIP4P/2005
17 water model. *J. Chem. Phys.* **2010**, *133*, 234502.
18
19
20 [99] Meyer, M.; Stanley, H. E. Liquid-liquid phase transition in confined water: A Monte-Carlo
21 study. *J. Phys. Chem. B* **1999**, *103*, 9728–9730.
22
23
24 [100] Stokely, K.; Mazza, M. G.; Stanley, H. E.; Franzese, G. Effect of Hydrogen Bond Coopera-
25 tivity on the Behavior of Water. *Proc. Natl. Acad. Sci. (USA)* **2010**, *107*, 1301–1306.
26
27
28 [101] Li, Y.; Li, J.; Wang, F. Liquid-liquid transition in supercooled water suggested by microsec-
29 ond simulations. *Proc. Natl. Acad. Sci. (USA)* **2013**, *110*, 12209–12212.
30
31
32 [102] Corsetti, F.; Artacho, E.; Soler, J. M.; Alexandre, S. S.; Fernández-Serra, M.-V. Room
33 temperature compressibility and the diffusivity anomaly of liquid water from first principles. *J.*
34 *Chem. Phys.* **2013**, *139*, 194502.
35
36
37 [103] Jeffery, C. A.; Austin, P. H. A new analytic equation of state for liquid water. *J. Chem.*
38 *Phys.* **1999**, *110*, 484–496.
39
40
41 [104] Kiselev, S. B. Physical Limit of Stability in Supercooled Liquids. *Int. J. Thermophys.* **2001**,
42 *22*, 1421–1433.
43
44
45 [105] Kiselev, S. B.; Ely, J. F. Parametric crossover model and physical limit of stability in super-
46 cooled water. *J. Chem. Phys.* **2002**, *116*, 5657–5665.
47
48
49 [106] Kalová, J.; Mares, R. Crossover Equation and the Vapor Pressure of Supercooled Water. *Int.*
50 *J. Thermophys.* **2010**, *31*, 756–765.
51
52
53 [107] Corradini, D.; Rovere, M.; Gallo, P. A route to explain water anomalies from results on an
54 aqueous solution of salt. *J. Chem. Phys.* **2010**, *132*, 134508.
55
56
57 [108] Moore, E. B.; Molinero, V. Structural transformation in supercooled water controls the
58 crystallization rate of ice. *Nature* **2011**, *479*, 506–508.
59
60

- 1
2
3 [109] Holten, V.; Limmer, D. T.; Molinero, V.; Anisimov, M. A. Nature of the anomalies in
4 supercooled liquid state of the mW model of water. *J. Chem. Phys.* **2013**, *138*, 174501.
5
6
7 [110] Xu, L.; Buldyrev, S. V.; Angell, C. A.; Stanley, H. E. Thermodynamics and dynamics of the
8 two-scale spherically symmetric Jagla ramp model of anomalous liquids. *Phys. Rev. E* **2006**,
9 *74*, 031108.
10
11
12 [111] Gallo, P.; Sciortino, F. Ising Universality Class for the Liquid-Liquid Critical Point of a One
13 Component Fluid: A Finite-Size Scaling Test. *Phys. Rev. Lett.* **2012**, *109*, 177801.
14
15
16 [112] Liu, Y.; Palmer, J. C.; Panagiotopoulos, A. Z.; Debenedetti, P. G. Liquid-liquid transition
17 in ST2 water. *J. Chem. Phys.* **2012**, *137*, 214505.
18
19
20 [113] Liu, Y.; Panagiotopoulos, A. Z.; Debenedetti, P. G. Low-temperature fluid-phase behavior
21 of ST2 water. *J. Chem. Phys.* **2009**, *131*, 104508.
22
23
24 [114] Franzese, G.; Malescio, G.; Skibinsky, A.; Buldyrev, S. V.; Stanley, H. E. Generic mechanism
25 for generating a liquid-liquid phase transition. *Nature* **2001**, *409*, 692–695.
26
27
28 [115] Smallenburg, F.; Filion, L.; Sciortino, F. Erasing no-man’s land by thermodynamically sta-
29 bilizing the liquid-liquid transition in tetrahedral particles. *Nature Phys.* **2014**, *10*, 653–657.
30
31
32 [116] Saika-Voivod, I.; Sciortino, F.; Poole, P. H. Computer simulations of liquid silica: equation
33 of state and liquid-liquid phase transition. *Phys. Rev. E* **2001**, *63*, 011202.
34
35
36 [117] Vasisht, V. V.; Saw, S.; Sastry, S. Liquid-liquid critical point in supercooled silicon. *Nature*
37 *Phys.* **2011**, *7*, 549–553.
38
39
40 [118] Glosli, J. N.; Ree, F. H. Liquid-liquid phase transformation in carbon. *Phys. Rev. Lett.* **1999**,
41 *82*, 4659–4662.
42
43
44 [119] Li, R. Z.; Chen, J.; Li, X. Z.; Wang, E. G.; Xu, L. Supercritical phenomenon of hydrogen
45 beyond the liquid-liquid phase transition. *New J. Phys.* **2015**, *17*, 063023.
46
47
48 [120] Stillinger, F. H.; Rahman, A. Improved simulation of liquid water by molecular dynamics.
49 *J. Chem. Phys.* **1974**, *60*, 1545–1557.
50
51
52 [121] Palmer, J. C.; Martelli, F.; Liu, Y.; Car, R.; Panagiotopoulos, A. Z.; Debenedetti, P. G.
53 Metastable liquid–liquid transition in a molecular model of water. *Nature* **2014**, *510*, 385–
54 388.
55
56 [122] Cuthbertson, M. J.; Poole, P. H. Mixturelike Behavior Near a Liquid-Liquid Phase Transition
57 in Simulations of Supercooled Water. *Phys. Rev. Lett.* **2011**, *106*, 115706.
58
59
60

- 1
2
3 [123] Poole, P. H.; Bowles, R. K.; Saika-Voivod, I.; Sciortino, F. Free energy surface of ST2 water
4 near the liquid-liquid phase transition. *J. Chem. Phys.* **2013**, *138*, 034505.
5
6 [124] Molinero, V.; Moore, E. B. Water Modeled As an Intermediate Element between Carbon
7 and Silicon. *J. Phys. Chem. B* **2009**, *113*, 4008–4016.
8
9 [125] Yagasaki, T.; Matsumoto, M.; Tanaka, H. Spontaneous liquid-liquid phase separation of
10 water. *Phys. Rev. E* **2014**, *89*, 020301.
11
12 [126] Overduin, S. D.; Patey, G. N. Fluctuations and local ice structure in model supercooled
13 water. *J. Chem. Phys.* **2015**, *143*, 094504.
14
15 [127] Kesselring, T. A.; Franzese, G.; Buldyrev, S. V.; Herrmann, H. J.; Stanley, H. E. Nanoscale
16 Dynamics of Phase Flipping in Water near its Hypothesized Liquid-Liquid Critical Point.
17 *Sci. Rep.* **2012**, *2*, 474.
18
19 [128] Kesselring, T. A.; Lascaris, E.; Franzese, G.; Buldyrev, S. V.; Herrmann, H. J.; Stanley, H.
20 E. Finite-size scaling investigation of the liquid-liquid critical point in ST2 water and its
21 stability with respect to crystallization. *J. Chem. Phys.* **2013**, *138*, 244506.
22
23 [129] Ghiringhelli, L. M.; Valeriani, C.; Los, J.H.; Meijer, E.J.; Fasolino, A.; Frenkel, D. State-of-
24 the-art models for the phase diagram of carbon and diamond nucleation. *Mol. Phys.* **2008**,
25 *106*, 2011–2038.
26
27 [130] Smallenburg, F.; Sciortino, F. Tuning the Liquid-Liquid Transition by Modulating the
28 Hydrogen-Bond Angular Flexibility in a Model for Water. *Phys. Rev. Lett.* **2015**, *115*, 015701.
29
30 [131] Palmer, J. C.; Debenedetti, P. G.; Car, R.; Panagiotopoulos, A. Z. Response to “Comment
31 [arXiv:1407.6854] on Palmer et al., Nature, 510, 385, 2014”. *arXiv:1407.7884* [cond-mat.stat-
32 mech], **2014**.
33
34 [132] Jagla, E. A. Core-softened potentials and the anomalous properties of water. *J. Chem. Phys.*
35 **1999**, *111*, 8980–8986.
36
37 [133] Tanaka, H. Thermodynamic anomaly and polyamorphism of water *Europhys. Lett.* **2000**, *50*,
38 340–346.
39
40 [134] Biddle, J. W.; Holten, V.; Anisimov, M. A. Behavior of supercooled aqueous solutions stem-
41 ming from hidden liquid-liquid transition in water. *J. Chem. Phys.* **2014**, *141*, 074504.
42
43 [135] Holten, V.; Sengers, J. V.; Anisimov, M. A. Equation of state for supercooled water at
44 pressures up to 400 MPa. *J. Phys. Chem. Ref. Data* **2014**, *43*, 043101.
45
46
47
48
49
50
51
52
53
54
55
56
57
58
59
60

- 1
2
3 [136] Hare, D. E.; Sorensen, C. M. The density of supercooled water. II. Bulk samples cooled to
4 the homogeneous nucleation limit. *J. Chem. Phys.* **1987**, *87*, 4840–4845.
5
6
7 [137] Mishima, O. Volume of supercooled water under pressure and the liquid-liquid critical point.
8 *J. Chem. Phys.* **2010**, *133*, 144503.
9
10
11 [138] Sotani, T.; Arabas, J.; Kubota, H.; Kijima, M. Volumetric behaviour of water under high
12 pressure at subzero temperature. *High Temp. High Pressures* **2000**, *32*, 433.
13
14 [139] Abascal, J. L. F.; Vega, C. A general purpose model for the condensed phases of water. *J.*
15 *Chem. Phys.* **2005**, *123*, 234505.
16
17
18 [140] Overduin, S. D.; Patey, G. N. An analysis of fluctuations in supercooled TIP4P/2005 water.
19 *J. Chem. Phys.* **2013**, *138*, 184502.
20
21
22 [141] Huang, C.; Wikfeldt, K. T.; Tokushima, T.; Nordlund, D.; Harada, Y.; Bergmann, U.;
23 Niebuhr, M.; Weiss, T. M.; Horikawa, Y.; Leetmaa, M. et al. The Inhomogeneous Structure
24 of Water at Ambient Conditions, *Proc. Natl. Acad. Sci. (USA)* **2009**, *106*, 15214–15218.
25
26
27 [142] Huang, C.; Weiss, T. M.; Nordlund, D.; Wikfeldt, K. T.; Pettersson, L. G. M.; Nilsson, A.
28 Increasing correlation length in bulk supercooled H₂O, D₂O and NaCl solution determined
29 from small angle x-ray scattering, *J. Chem. Phys.* **2010**, *133*, 134504.
30
31
32 [143] Huang, C.; Wikfeldt, K.T.; Tokushima, T.; Nordlund, D.; Harada, Y.; Bergmann, U.;
33 Niebuhr, M.; Weiss, T. M.; Horikawa, Y.; Leetmaa, et al. Reply to Soper “Fluctuations
34 in water around a bimodal distribution of local hydrogen bonded structural motifs”, *Proc.*
35 *Natl. Acad. Sci. (USA)* **2010**, *107*, E45.
36
37
38 [144] Soper, A. K.; Teixeira, J.; Head-Gordon, T. Is ambient water inhomogeneous on the
39 nanometer-length scale? *Proc. Natl. Acad. Sci. (USA)* **2010**, *107*, E44.
40
41
42 [145] Clark, G. N. I.; Hura, G. L.; Teixeira, J.; Soper, A. K.; Head-Gordon, T. Small-angle
43 scattering and the structure of ambient liquid water. *Proc. Natl. Acad. Sci. (USA)* **2010**,
44 *107*, 14003–14007.
45
46
47 [146] Overduin, S. D.; Patey, G. N. Understanding the Structure Factor and Isothermal Com-
48 pressibility of Ambient Water in Terms of Local Structural Environments. *J. Phys. Chem. B*
49 **2012**, *116*, 12014–12020.
50
51
52 [147] Wernet, Ph.; Nordlund, D.; Bergmann, U.; Ogasawara, H.; Cavalleri, M.; Näslund, L.-Å.;
53 Hirsch, T. K.; Ojamäe, L.; Glatzel, P.; Odellius, M.; Pettersson, L. G.M.; Nilsson, A. The
54 structure of the first coordination shell in liquid water. *Science* **2004**, *304*, 995–999.
55
56
57
58
59
60

- 1
2
3 [148] Myneni, S.; Luo, Y.; Näslund, L.-Å.; Cavalleri, M.; Ojamäe, L.; Ogasawara, H.; Pelmen-
4 schikov, A.; Wernet, Ph.; Väterlein, P.; Heske, C.; Hussain, Z.; Pettersson, L. G. M.; Nils-
5 son, A. Spectroscopic probing of local hydrogen bonding structures in liquid water, *J. Phys.:*
6 *Condens. Mat.* **2002**, *14*, L213–L219.
- 7
8
9
10 [149] Nilsson, A.; Nordlund, D.; Waluyo, I.; Huang, N.; Ogasawara, H.; Kaya, S.; H.; Bergmann,
11 U.; Näslund, L.-Å.; Öström, H.; Wernet, Ph.; Andersson, K.; Schiros, T.; Pettersson, L. G.
12 M. X-ray Absorption Spectroscopy and X-ray Raman Scattering of Water; An Experimental
13 View, *J. Electron Spec. Rel. Phen.* **2010**, *177*, 99–129.
- 14
15
16 [150] Chen, W.; Wu, X.; Car, R. X-ray absorption signatures of the molecular environment in
17 water and ice. *Phys. Rev. Lett.* **2010**, *105*, 017802.
- 18
19
20 [151] Nordlund, D.; Ogasawara, H.; Andersson, K. J.; Tatarkhanov, M.; Salmerón, M.; Petters-
21 son, L. G. M.; Nilsson, A. Sensitivity of X-ray Absorption Spectroscopy to Hydrogen Bond
22 Topology. *Phys. Rev. B* **2009**, *80*, 233404.
- 23
24
25 [152] Kühne, T. D.; Khaliullin, R. Z. Electronic signature of the instantaneous asymmetry in the
26 first coordination shell in liquid water. *Nature Commun.* **2013**, *4*, 1450.
- 27
28
29 [153] Clark, G. N. I.; Cappa, C. D.; Smith, J. D.; Saykally, R. J.; Head-Gordon, T. The structure
30 of ambient water. *Mol. Phys.* **2010**, *108*, 1415–1433.
- 31
32
33 [154] Fernandez-Serra, M.-V.; Artacho, E. Electrons and hydrogen-bond connectivity in liquid
34 water. *Phys. Rev. Lett.* **2006**, *96*, 016404.
- 35
36
37 [155] Soper, A. K. Recent Water Myths. *Pure Appl. Chem.* **2010**, *82*, 1855–1867.
- 38
39
40 [156] Nilsson, A.; Huang, C.; Pettersson, L. G. M. Fluctuations in ambient water. *J. Mol. Liq.*
41 **2012**, *176*, 2–16.
- 42
43
44 [157] Pettersson, L. G. M.; Nilsson, A. The Structure of Water; from Ambient to Deeply Super-
45 cooled. *J. Non-Crystalline Solids* **2015**, *407*, 399–417.
- 46
47
48 [158] Fuchs, O.; Zharnikov, M.; Weinhardt, L.; Blum, M.; Weigand, M.; Zubavichus, Y.; Bär, M.;
49 Maier, F.; Denlinger, J. D.; Heske, C.; Grunze, M.; Umbach, E. Isotope and temperature
50 effects in liquid water probed by x-ray absorption and resonant x-ray emission spectroscopy.
51 *Phys. Rev. Lett.* **2008**, *100*, 027801.
- 52
53
54 [159] Weinhardt, L.; Benkert, A.; Meyer, F.; Blum, M.; Wilks, R. G.; Yang, W.; Bär, M.; Reinert,
55 F.; Heske, C. Nuclear dynamics and spectator effects in resonant inelastic soft x-ray scattering
56 of gas- phase water molecules, *J. Chem. Phys.* **2012**, *136*, 144311.
- 57
58
59
60

- 1
2
3 [160] Lange, K. M.; Könecke, R.; Ghadimi, S.; Golnak, R.; Soldatov, M. A.; Hodeck, K. F.;
4 Soldatov, A.; Aziz, E. F. High resolution X-ray emission spectroscopy of water and aqueous
5 ions using the micro-jet technique. *Chem. Phys.* **2010**, *377*, 1-5.
6
7
8 [161] Lange, K. M.; Soldatov, M.; Golnak, R.; Gotz, M.; Engel, N.; Könecke, R.; Rubensson,
9 J.-E.; Aziz, E. F. X-ray emission from pure and dilute H₂O and D₂O in a liquid microjet:
10 Hydrogen bonds and nuclear dynamics. *Phys. Rev. B* **2012**, *85*, 155104.
11
12
13 [162] Tokushima, T.; Harada, Y.; Takahashi, O.; Senba, Y.; Ohashi, H.; Pettersson, L. G. M.;
14 Nilsson, A.; Shin, S. High Resolution X-ray Emission Spectroscopy of Liquid Water: The
15 Observation of Two Structural Motifs. *Chem. Phys. Lett.* **2008**, *460*, 387–400.
16
17
18 [163] Tokushima, T.; Harada, Y.; Horikawa, Y.; Takahashi, O.; Senba, Y.; Ohashi, H.; Pettersson,
19 L. G. M.; Nilsson, A.; Shin, S. High resolution X-ray emission spectroscopy of water and its
20 assignment based on two structural motifs. *J. Electron Spec. Rel. Phen.* **2010**, *177*, 192–205.
21
22
23 [164] Gilberg, E.; Hanus, M. J.; Foltz, B. Investigation of the electronic structure of ice by high
24 resolution x-ray spectroscopy. *J. Chem. Phys.* **1982**, *76*, 5093–5097.
25
26
27 [165] Pettersson, L. G. M.; Tokushima, T.; Harada, Y.; Takahashi, O.; Shin, S.; Nilsson, A.
28 Comment on “Isotope and Temperature Effects in Liquid Water Probed by X-ray Absorption
29 and Resonant X-ray Emission Spectroscopy”. *Phys. Rev. Lett.* **2008**, *100*, 249801.
30
31
32 [166] Fuchs, O.; Zharnikov, M.; Weinhardt, L.; Blum, M.; Weigand, M.; Zubavichus, Y.; Bär,
33 M.; Maier, F.; Denlinger, J. D.; Heske, C.; Grunze, M.; Umbach, E. Reply to Comment
34 on “Isotope and Temperature Effects in Liquid Water Probed by X-Ray Absorption and
35 Resonant X-Ray Emission Spectroscopy”. *Phys. Rev. Lett.* **2008**, *100*, 249802.
36
37
38 [167] Nilsson, A.; Tokushima, T.; Horikawa, Y.; Harada, Y.; Ljungberg, M. P.; Shin, S.; Pettersson,
39 L. G. M. Resonant inelastic x-ray scattering of water. *J. Electron. Spectrosc. Relat. Phenom.*
40 **2013**, *188*, 84–100.
41
42
43 [168] Taschin, A.; Bartolini, P.; Eramo, R.; Righini, R.; Torre, R. Evidence of two distinct local
44 structures of water from ambient to supercooled conditions. *Nature Commun.* **2013**, *4*, 2401.
45
46
47 [169] Kobayashi, M.; Tanaka, H. Relationship between the phase diagram, the glass-forming ability,
48 and the fragility of a water/salt mixture. *J. Phys. Chem. B* **2011**, *115*, 14077–14090.
49
50
51 [170] Kobayashi, M.; Tanaka, H. Possible Link of the V-Shaped Phase Diagram to the Glass-
52 Forming Ability and Fragility in a Water-Salt Mixture. *Phys. Rev. Lett.* **2011**, *106*, 125703.
53
54
55
56
57
58
59
60

- 1
2
3 [171] Torquato, S.; Truskett, T. M.; Debenedetti, P. G. Is Random Close Packing of Spheres Well
4 Defined? *Phys.Rev. Lett.* **2000**, *84*, 2064–2067.
5
6
7 [172] Errington, J. R.; Debenedetti, P. G. Relationship between structural order and the anomalies
8 of liquid water. *Nature* **2001**, *409*, 318–321.
9
10 [173] Vega, C.; Abascal, J. L. F. Relation between the melting temperature and the temperature of
11 maximum density for the most common models of water. *J. Chem. Phys.* **2005**, *123*, 144504.
12
13 [174] Vega, C.; Abascal, J. L. F.; Conde, M. M.; Aragoes, J. L. What ice can teach us about water
14 interactions: a critical comparison of the performance of different water models. *Faraday*
15 *Discuss.* **2009**, *141*, 251–276.
16
17 [175] Agarwal, M.; Alam, M. P.; Chakravarty, C. Thermodynamic, diffusional, and structural
18 anomalies in rigid-body water models. *J. Phys. Chem. B* **2011**, *115*, 6935–6945.
19
20 [176] Fine, R. A.; Millero, F. J. The high pressure P V T properties of deuterium oxide. *J. Chem.*
21 *Phys.* **1975**, *63*, 89–95.
22
23 [177] Shell, M. S.; Debenedetti, P. G.; Panagiotopoulos, A. Z. Molecular structural order and
24 anomalies in liquid silica. *Phys. Rev. E* **2002**, *66*, 011202.
25
26 [178] Nayar, D.; Chakravarty, C. Water and water-like liquids: relationships between structure,
27 entropy and mobility. *Phys. Chem. Chem. Phys.* **2013**, *15*, 14162–14177.
28
29 [179] Barros de Oliveira, A.; Salcedo, E.; Chakravarty, C.; Barbosa, M. C. Entropy, diffusivity and
30 the energy landscape of a waterlike fluid. *J. Chem. Phys.* **2010**, *132*, 234509.
31
32 [180] Green, H. S. *The Molecular Theory of Fluids*; North-Holland: Amsterdam, 1952.
33
34 [181] Schlitter, and J. R. Estimation of absolute and relative entropies of macromolecules using
35 the covariance matrix. *Chem. Phys. Lett.* **1993**, *215*, 617–621.
36
37 [182] Andricioaei, I.; Karplus, M. On the calculation of entropy from covariance matrices of the
38 atomic fluctuations. *J. Chem. Phys.*, **2001**, *115*, 6289–6292.
39
40 [183] Lin, S. T.; Blanco, M.; Goddard III, W. A. The two-phase model for calculating thermody-
41 namic properties of liquids from molecular dynamics: Validation for the phase diagram of
42 Lennard-Jones fluids *J. Chem. Phys.* **2003**, *119*, 11792–11805.
43
44 [184] Henchman, R. H.; Cockram, S. J. Water's non-tetrahedral side *Faraday Discuss.* **2013**, *167*,
45 529–550.
46
47 [185] Hensen, U.; Gräter, F.; Henchman, R. H. Macromolecular entropy can be accurately com-
48 puted from force. *J. Chem. Theory Comput.* **2014**, *10*, 4777–4781.
49
50
51
52
53
54
55
56
57
58
59
60

- 1
2
3 [186] Henchman, R. H.; Irudayam, S. J. Hydrogen-Bond Definition to Characterize the Structure
4 and Dynamics of Liquid Water. *J. Phys. Chem. B* **2010**, *114*, 16792–16810.
5
6
7 [187] Raveché, H. J. Entropy and Molecular Correlation Functions in Open Systems. I. Derivation.
8
9 *J. Chem. Phys.* **1971**, *55*, 2242–2250.
10
11 [188] Mountain, R. D.; Raveché, H. J. Entropy and Molecular Correlation Functions in Open
12 Systems. II Two- and Three-Body Correlations. *J. Chem. Phys.* **1971**, *55*, 2250–2255.
13
14 [189] Wallace, D. C. On the role of density fluctuations in the entropy of a fluid. *J. Chem. Phys.*
15 **1987**, *87*, 2282–2285.
16
17
18 [190] Baranyai, A.; Evans, D. J. Direct entropy calculation from computer simulation of liquids.
19 *Phys. Rev. A* **1989**, *40*, 3817–3822.
20
21 [191] Arisawa, T.; Arai, T.; Yokoyama, I. Pair and triplet correlation entropies based on the hard
22 sphere solution of the PercusYevick equation. *Physica B* **1999**, *262*, 190–198.
23
24 [192] Sastry, S.; Angell, C. A. Liquidliquid phase transition in supercooled silicon. *Nature Mater.*
25 **2003**, *2*, 739–743.
26
27 [193] Molinero, V.; Sastry, S.; Angell, C. A. Tuning of Tetrahedrality in a Silicon Potential Yields
28 a Series of Monatomic (Metal-like) Glass Formers of Very High Fragility. *Phys. Rev. Lett.*
29 **2006**, *97*, 075701.
30
31 [194] Bhat, M. H.; Molinero, V.; Soignard, E.; Solomon, V. C.; Sastry, S.; Yarger, J. L.; Angell,
32 C. A. Vitrification of a monatomic metallic liquid. *Nature* **2007**, *448*, 787–790.
33
34 [195] Hujo, W.; Jabes, B. S.; Rana, V. K.; Chakravarty, C.; Molinero, V. The Rise and Fall of
35 Anomalies in Tetrahedral Liquids *J. Stat. Phys.* **2011**, *145*, 293–312.
36
37 [196] Singh, M.; Dhabal, D.; Nguyen, A. H.; Molinero, V.; Chakravarty, C. Triplet Correlations
38 Dominate the Transition from Simple to Tetrahedral Liquids *Phys. Rev. Lett.* **2014**, *112*,
39 147801.
40
41 [197] Dhabal, D.; Singh, M.; Wikfeldt, K. T.; Chakravarty, C. Triplet correlation functions in
42 liquid water. *J. Chem. Phys.*, **2014**, *141*, 174504.
43
44 [198] Gallo, P.; Corradini, D.; Rovere, M. Excess entropy of water in a supercooled solution of
45 salt. *Mol. Phys.* **2011**, *109*, 2969–2979.
46
47 [199] Gallo, P.; Rovere, M. Relation between the two body entropy and the relaxation time in
48 supercooled water. *Phys. Rev. E* **2015**, *91*, 012107.
49
50
51
52
53
54
55
56
57
58
59
60

- 1
2
3 [200] Tanaka, H. Importance of many-body orientational correlations in the physical description
4 of liquids. *Faraday Discuss.* **2013**, *167*, 9–76.
5
6
7 [201] Woodcock, L. V.; Angell, C. A.; Cheeseman, P. Molecular dynamics studies of the vitreous
8 state: Simple ionic systems and silica. *J. Chem. Phys.* **1976**, *65*, 1565–1577.
9
10 [202] Lascaris, E. Tunable liquid-liquid critical point in an ionic model of silica.
11 <http://arxiv.org/abs/1510.08088> **2015**.
12
13 [203] Lascaris, E.; Hemmati, M.; Buldyrev, S. V.; Stanley, H. E.; Angell, C. A. Search for a
14 liquid-liquid critical point in models of silica. *J. Chem. Phys.* **2014**, *140*, 224502.
15
16 [204] McMillan, P. F. Polyamorphic transformations in liquids and glasses *J. Mater. Chem.* **2004**,
17 *14*, 1506–1512.
18
19 [205] Wilding, M. C.; Wilson, M.; McMillan, P. F. Structural studies and polymorphism in amor-
20 phous solids and liquids at high pressure. *Chem. Soc. Rev.* **2006**, *35*, 964–986.
21
22 [206] Mishima, O. Polyamorphism in water. *Proc. Jpn. Acad., Ser. B* **2010**, *86*, 165–175.
23
24 [207] H. Tanaka, General view of a liquid-liquid phase transition *Phys. Rev. E* **2000**, *62*, 6968–6976.
25
26 [208] Harada, Y.; Tokushima, T.; Horikawa, Y.; Takahashi, O.; Niwa, H.; Kobayashi, M.; Oshima,
27 M.; Senba, Y.; Ohashi, H.; Wikfeldt, K. T.; Nilsson, A.; Pettersson, L. G. M.; Shin, S.
28 Selective Probing of OH/OD Stretch Vibrations in Liquid Water using Resonant Inelastic
29 Soft X-ray Scattering. *Phys. Rev. Lett.* **2013**, *111*, 193001.
30
31 [209] Sellberg, J. A.; Huang, C.; McQueen, T. A.; Loh, N. D.; Laksmono, H.; Schlesinger, D.;
32 Sierra, R. G.; Nordlund, D.; Hampton, C. Y.; Starodub, D. et al. Ultrafast X-ray probing
33 of water structure below the homogeneous ice nucleation temperature. *Nature* **2014**, *510*,
34 381–384.
35
36 [210] Bowron, D. T.; Finney, J. L.; Hallbrucker, A.; Kohl, I.; Loerting, T.; Mayer, E.; Soper, A. K.
37 The local and intermediate range structures of the five amorphous ices at 80K and ambient
38 pressure: A Faber-Ziman and Bhatia-Thornton analysis. *J. Chem. Phys.* **2006**, *125*, 194502.
39
40 [211] *Liquid Polymorphism*, edited by Stanley H.E. Adv. Chem. Phys, vol. 152 (Wiley, NY, 2013).
41
42 [212] Mayer, E. Hyperquenching of Water and Dilute Aqueous Solutions into Their Glassy States:
43 An Approach to Cryofixation. *Cryo-Letters* **1988**, *9*, 66–77.
44
45 [213] Mayer, E. New Method for Vitriifying Water and Other Liquids by Rapid Cooling of Their
46 Aerosols. *J. Appl. Phys.* **1985**, *58*, 663–667.
47
48
49
50
51
52
53
54
55
56
57
58
59
60

- 1
2
3 [214] Mayer, E.; Brüggeller, P. Vitrification of Pure Liquid Water by High Pressure Jet Freezing.
4
5 *Nature* **1982**, *298*, 715–718.
6
7 [215] Brüggeller, P.; Mayer, E. Complete Vitrification in Pure Liquid Water and Dilute Aqueous
8
9 Solutions. *Nature* **1980**, *288*, 569–571.
10
11 [216] Tu, Y.; Buldyrev, S. V.; Liu, Z.; Fang, H.; Stanley, H. E. Different water scenarios for a
12
13 primitive model with two types of hydrogen bonds *Europhys. Lett.* **2012**, *97*, 56005.
14
15 [217] Ponyatovsky, E. G.; Sinitsyn, V. V.; Pozdnyakova, T. A. The metastable T–P phase diagram
16
17 and anomalous thermodynamic properties of supercooled water. *J. Chem. Phys.* **1998**, *109*,
18
19 2413–2422.
20
21 [218] Moynihan, C. T. Two Species/Nonideal Solution Model for Amorphous/Amorphous Phase
22
23 Transitions. *Mater. Res. Soc. Symp. Proc.* **1996**, *455*, 411.
24
25 [219] Holten, V.; Palmer, J. C.; Poole, P. H.; Debenedetti, P. G.; Anisimov, M. A. Two-state
26
27 thermodynamics of the ST2 model for supercooled water. *J. Chem. Phys.* **2014**, *140*, 104502.
28
29 [220] Russo, J.; Tanaka, H. Understanding waters anomalies with locally favoured structures.
30
31 *Nature Commun.* **2014**, *5*, 3556.
32
33 [221] Shiratani, E.; Sasai, M. Growth and collapse of structural patterns in the hydrogen bond
34
35 network in liquid water. *J. Chem. Phys.* **1996**, *104*, 7671–7680.
36
37 [222] Shiratani, E.; Sasai, M. Molecular scale precursor of the liquid–liquid phase transition of
38
39 water. *J. Chem. Phys.* **1998**, *108*, 3264–3276.
40
41 [223] Appignanesi, G. A.; Rodriguez Fris, J. A.; Sciortino, F. Evidence of a two-state picture
42
43 for supercooled water and its connections with glassy dynamics. *Eur. Phys. J. E* **2009**, *29*,
44
45 305–310.
46
47 [224] Wikfeldt, K. T.; Nilsson, A.; Pettersson, L. G. M. Spatially Inhomogeneous Bimodal Inherent
48
49 Structure in Simulated Liquid Water. *Phys. Chem. Chem. Phys.* **2011**, *13*, 19918–19924.
50
51 [225] Accordino, S. R.; Rodriguez Friz, J. A.; Sciortino, F.; Appignanesi, G. A. Quantitative
52
53 investigation of the two-state picture for water in the normal liquid and the supercooled
54
55 regime. *Eur. Phys. J. E* **2011**, *34*, 48.
56
57 [226] Russo, J.; Tanaka, H. The microscopic pathway to crystallization in supercooled liquids. *Sci.*
58
59 *Rep.* **2012**, *2*, 505.
60
[227] Debenedetti, P. G.; Stillinger, F. H. Supercooled liquids and the glass transition. *Nature*
2001, *410*, 259–267.

- 1
2
3 [228] Gallo, P.; Sciortino, F.; Tartaglia, P.; Chen, S.-H. Slow Dynamics of Water Molecules in
4 Supercooled States. *Phys. Rev. Lett.* **1996**, *76*, 2730–2733.
5
6
7 [229] Sciortino, F.; Gallo, P.; ; Tartaglia, P.; Chen, S.-H. Supercooled water and the kinetic glass
8 transition *Phys. Rev. E* **1996**, *54*, 6331–6343.
9
10 [230] Götze, W. *Complex Dynamics of Glass-Forming Liquids: A Mode-Coupling Theory*; Oxford
11 University Press: Oxford, 2008.
12
13
14 [231] Saika-Voivod, I.; Poole, P. H.; Sciortino, F. Fragile-to-strong transition and polyamorphism
15 in the energy landscape of liquid silica. *Nature* **2001**, *412*, 514–517.
16
17 [232] Angell, C. A. Formation of Glasses from Liquids and Biopolymers. *Science* **1995**, *267*, 1924–
18 1935.
19
20
21 [233] Martinez, L. M.; Angell, C. A.; A thermodynamic connection to the fragility of glass-forming
22 liquids. *Nature* **2001**, *410*, 663–667.
23
24 [234] Sun, Q.; Zhou, C.; Yue, Y.; Hu, L. A Direct Link between the Fragile-to-Strong Transition
25 and Relaxation in Supercooled Liquids *J. Phys. Chem. Lett.* **2014**, *5*, 1170–1174.
26
27 [235] Mallamace, F.; Branca, C.; Corsaro, C.; Leone, N.; Spooren, J.; Chen, S.-H.; Stanley, H. E.
28 Transport properties of glass-forming liquids suggest that dynamic crossover temperature is
29 as important as the glass transition temperature. *Proc. Natl. Acad. Sci.* **2010**, *107*, 22457–
30 22462.
31
32 [236] Prielmeier, F. X.; Lang, E. W.; Speedy, R. J.; Lüdemann, H.-D. Diffusion in supercooled
33 water to 300 MPa. *Phys. Rev. Lett.* **1987**, *59*, 1128–1131.
34
35 [237] Sokolov, A. P.; Hurst, J.; Quitmann, D. Dynamics of supercooled water: Mode-coupling
36 theory approach. *Phys. Rev. B* **1995**, *51*, 12865–12868 (R).
37
38 [238] Torre, R.; Bartolini, P.; Righini, R. Structural relaxation in supercooled water by time-
39 resolved spectroscopy. *Nature* **2004**, *428*, 296–299.
40
41 [239] Dehaoui, A.; Issenmann, B.; Caupin, F. Viscosity of deeply supercooled water and its cou-
42 pling to molecular diffusion. *Proc. Natl. Acad. Sci. (USA)* **2015**, *112*, 12020–12025.
43
44 [240] Starr, F. W.; Nielsen J.K., Stanley, H. E. Fast and Slow Dynamics of Hydrogen Bonds in
45 Liquid Water. *Phys. Rev. Lett.* **1999**, *82*, 2294–2297.
46
47 [241] Ito, K.; Moynihan, C. T.; Angell, C. A. Thermodynamic determination of fragility in liquids
48 and a fragile-to-strong liquid transition in water. *Nature* **1999**, *398*, 492–495.
49
50
51
52
53
54
55
56
57
58
59
60

- 1
2
3 [242] Starr, F.W.; Sciortino, F. ; Stanley, H.E. Dynamics of simulated water under pressure *Phys.*
4 *Rev. E* **1999**, *60*, 6757–6768.
5
6
7 [243] Fraux, G.; Doye, J. P. K. Note: Heterogeneous ice nucleation on silver-iodide-like surfaces.
8 *J. Chem. Phys.* **2014**, *141*, 216101.
9
10 [244] Atkinson, J. D.; Murray, B. J.; Woodhouse, M. T.; Whale, T. F.; Baustian, K. J.; Carslaw,
11 K. S.; Dobbie, S.; O’Sullivan, D.; Malkin, T. L. The importance of feldspar for ice nucleation
12 by mineral dust in mixed-phase clouds. *Nature* **2013**, *498*, 355–358.
13
14 [245] Cwilong, B. M. Sublimation in a Wilson Chamber. *Proc. Roy. Soc. A* **1947**, *190*, 137–143.
15
16 [246] Mossop, S. C. The Freezing of Supercooled Water. *Proc. Phys. Soc. B* **1955**, *68*,193–208.
17
18 [247] Mason, B. J. The supercooling and nucleation of water. *Adv. Phys.* **1958**, *7*, 221–234.
19
20 [248] Kelton, K. F. *Crystal Nucleation in Liquids and Glasses*; Vol. 45 Academic Press: Boston,
21 1991; p. 75.
22
23 [249] Auer, S.; Frenkel, D. Numerical prediction of absolute crystallization rates in hard-sphere
24 colloids. *J. Chem. Phys.* **2004**, *120*, 3015–3029.
25
26 [250] Valeriani, C.; Sanz, E.; Frenkel, D. Rate of homogeneous crystal nucleation in molten NaCl.
27 *J. Chem. Phys.* **2005**, *122*, 194501.
28
29 [251] Hardy, S. C. A grain boundary groove measurement of the surface tension between ice and
30 water. *Philos. Mag.* **1977**, *35*, 471–484.
31
32 [252] Gránásy, L.; Pusztai, T.; James, P. F. Interfacial properties deduced from nucleation exper-
33 iments: A CahnHilliard analysis. *J. Chem. Phys.* **2002**, *117*, 6157–6168.
34
35 [253] Sanz,E.; Vega, C.; Espinosa, J. R.; Caballero-Bernal, R.; Abascal, J. L. F.; Valeriani, C. *J.*
36 *Am. Chem. Soc.* **2013**, *135*, 15008.
37
38 [254] Espinosa, J. R.; Sanz, E.; Valeriani,C.; Vega, C. Homogeneous ice nucleation evaluated for
39 several water models, *J. Chem. Phys.* **2014**, *141*, 18C529.
40
41 [255] Matsumoto, M.; Saito, S.; Ohmine, I. Molecular dynamics simulation of the ice nucleation
42 and growth process leading to water freezing. *Nature* **2002**, *416*, 409–413.
43
44 [256] Radhakrishnan, R.; Trout, B. L. Nucleation of Crystalline Phases of Water in Homogeneous
45 and Inhomogeneous Environments. *Phys. Rev. Lett.* **2003**, *90*, 158301.
46
47 [257] Quigley, D.; Rodger, P. M. Metadynamics simulations of ice nucleation and growth. *J. Chem.*
48 *Phys.* **2008**, *128*, 154518.
49
50
51
52
53
54
55
56
57
58
59
60

- 1
2
3 [258] Brukhno, A. V.; Anwar, J.; Davidchack, R.; Handel, R. Challenges in molecular simulation
4 of homogeneous ice nucleation. *J. Phys.: Condens. Matter* **2008**, *20*, 494243.
5
6 [259] Reinhardt, A.; Doye, J. P. K. Free energy landscapes for homogeneous nucleation of ice for
7 a monatomic water model. *J. Chem. Phys.* **2012**, *136*, 054501.
8
9 [260] Li, T.; Donadio, D.; Russo, G.; Galli, G. Homogeneous ice nucleation from supercooled water.
10 *Phys. Chem. Chem. Phys.* **2011**, *13*, 19807–19813.
11
12 [261] Russo, J.; Romano, F.; Tanaka, H. New metastable form of ice and its role in the homo-
13 geneous crystallization of water. *Nature Materials* **2014**, *13*, 733–739.
14
15 [262] **Stan, C. A. et al.** A microfluidic apparatus for the study of ice nucleation in supercooled
16 water drops. *Lab. Chip* **2009**, *9*, 2293–2305.
17
18 [263] Riechers, B.; Wittbracht, F.; Hütten, A.; Koop, T. The homogeneous ice nucleation rate
19 of water droplets produced in a microfluidic device and the role of temperature uncertainty.
20 *Phys. Chem. Chem. Phys.* **2013**, *15*, 5873–5887.
21
22 [264] Hagen, D. E.; Anderson, R. J.; Kassner, J. L. Homogeneous Condensation–Freezing Nucle-
23 ation Rate Measurements for Small Water Droplets in an Expansion Cloud Chamber. *J.*
24 *Atmos. Sci.* **1981**, *38*, 1236–1243.
25
26 [265] Laksmono, H.; McQueen, T. A.; Sellberg, J. A.; Loh, N. D.; Huang, C.; Schlesinger, D.;
27 Sierra, R. G.; Hampton, C. Y.; Nordlund, D.; Beye, M. et al. Anomalous Behavior of the
28 Homogeneous Ice Nucleation Rate in “No-Man’s Land”, *J. Phys. Chem. Lett.* **2015**, *6*, 2826–
29 2832.
30
31 [266] Huang, J. F.; Bartell, L. S. Kinetics of Homogeneous Nucleation in the Freezing of Large
32 Water Clusters. *J. Phys. Chem.* **1995**, *99*, 3924–3931.
33
34 [267] Bhabhe, A.; Pathak, H.; Wyslouzil, B. E. Freezing of Heavy Water (D₂O) Nanodroplets. *J.*
35 *Phys. Chem. A* **2013**, *117*, 5472–5482.
36
37 [268] Jenniskens, P.; Blake, D. F. Crystallization of Amorphous Water Ice in the Solar System.
38 *Astrophys. J.* **1996**, *473*, 1104–1113.
39
40 [269] Safarik, D. J.; Mullins, C. B. The nucleation rate of crystalline ice in amorphous solid water.
41 *J. Chem. Phys.* **2004**, *121*, 6003–6010.
42
43 [270] Hage, W.; Hallbrucker, A.; Mayer, E.; Johari, G. P. Crystallization Kinetics of Water below
44 150 K. *Chem. Phys.* **1994**, *100*, 2743–2747.
45
46
47
48
49
50
51
52
53
54
55
56
57
58
59
60

- 1
2
3 [271] Hage, W.; Hallbrucker, A.; Mayer, E.; Johari, G. P. Kinetics of Crystallizing D₂O Water near
4 150 K by Fourier Transform Infrared Spectroscopy and a Comparison with the Corresponding
5 Calorimetric Studies on H₂O Water. *J. Chem. Phys.* **1995**, *103*, 545–550.
6
7
8 [272] Stöckel, P.; Weidinger, I. M.; Baumgärtel, H.; Leisner, T. Rates of homogeneous ice nucle-
9 ation in levitated H₂O and D₂O droplets. *J. Phys. Chem. A* **2005**, *109*, 2540–2546.
10
11 [273] Murray, B. J.; Broadley, S. L.; Wilson, T. W.; Bull, S. J.; Wills, R. H.; Christenson, H.
12 K.; Murray, E. J. Kinetics of the homogeneous freezing of water. *Phys. Chem. Chem. Phys.*
13 **2010**, *12*, 10380–10387.
14
15 [274] Pruppacher, H. R. A New Look at Homogeneous Ice Nucleation in Supercooled Water Drops.
16 *J. Atmosph. Sci.* **1995**, *52*, 1924–1933.
17
18 [275] Manka, A.; Pathak, H.; Tanimura, S.; Wolk, J.; Strey, R.; Wyslouzil, B. E. Freezing water
19 in no-man’s land. *Phys. Chem. Chem. Phys.* **2012**, *14*, 4505–4516.
20
21 [276] McMillan, J. A.; Los, S. C. Vitreous ice: Irreversible transformations during warm-up. *Nature*
22 **1965**, *206*, 806–807.
23
24 [277] Rozmanov, D.; Kusalik, P. G. Temperature dependence of crystal growth of hexagonal ice
25 (*I_h*). *Phys. Chem. Chem. Phys.* **2011**, *13*, 15501–15511.
26
27 [278] Avrami, M. Kinetics of Phase Change. I General Theory. *J. Chem. Phys.* **1939**, *7*, 1103–1112.
28
29 [279] Abascal, J. L. F.; Vega, C. Note: Equation of state and compressibility of supercooled water:
30 Simulations and experiment. *J. Chem. Phys.* **2011**, *134*, 186101.
31
32 [280] Wikfeldt, K. T.; Huang, C.; Nilsson, A.; Pettersson, L. G. M. Enhanced small-angle scattering
33 connected to the Widom line in simulations of supercooled water. *J. Chem. Phys.* **2011**, *134*,
34 214506.
35
36 [281] Bresme, F.; Biddle, J. W.; Sengers, J. V.; Anisimov, M. A. Communication: Minimum in the
37 thermal conductivity of supercooled water: A computer simulation study. *J. Chem. Phys.*
38 **2014**, *140*, 161104.
39
40 [282] Berg, B. A.; Dubey, S. Finite Volume Kolmogorov-Johnson-Mehl-Avrami Theory. *Phys. Rev.*
41 *Lett.* **2008**, *100*, 165702.
42
43 [283] Ostwald, W. Studien über die Bildung und Umwandlung fester Körper. *Z. Phys. Chem.*
44 **1897**, *22*, 289–330.
45
46 [284] van Santen, R. A. The Ostwald Step Rule. *J. Phys. Chem.* **1984**, *88*, 5768–5769.
47
48
49
50
51
52
53
54
55
56
57
58
59
60

- 1
2
3 [285] Liu, L.; Chen, S. H.; Faraone, A.; Yen, C.-W.; Mou, C.-Y. Pressure Dependence of Fragile-
4 to-Strong Transition and a Possible Second Critical Point in Supercooled Confined Water.
5 *Phys. Rev. Lett.* **2005**, *95*, 117802.
6
7
8
9 [286] Xu, I.; Ehrenberg, I.; Buldyrev, S. V.; Stanley, H. E. Relationship between the liquid-liquid
10 phase transition and dynamic behavior in the Jagla model. *J. Phys.: Condens. Matter* **2006**,
11 *18*, S2239–S2246.
12
13
14 [287] Franzese, G.; Stanley, H. E. The Widom line of supercooled water. *J. Phys. Condens. Matter*
15 **19**, 205126 (2007).
16
17
18 [288] Corradini, D.; Gallo, P. Liquid-Liquid critical point in NaCl aqueous solutions: concentration
19 effects. *J. Phys. Chem. B* **2011**, *115*, 14161–14166.
20
21
22 [289] Corradini, D.; Buldyrev, S. V.; Gallo, P.; Stanley, H. E. Effects of hydrophobic solutes on
23 the liquid-liquid critical point. *Phys. Rev. E* **2010**, *81*, 061504.
24
25
26 [290] Gallo, P.; Corradini, D.; Rovere, M. Fragile to strong crossover at the Widom line in super-
27 cooled aqueous solutions of NaCl. *J. Chem. Phys.* **2013**, *139*, 204503.
28
29
30 [291] Gallo, P.; Rovere, M. Mode Coupling and fragile to strong transition in supercooled TIP4P
31 water. *J. Chem. Phys.* **2012**, *137*, 164503.
32
33 [292] De Marzio M.; Camisasca G.; Rovere M.; Gallo P. Mode Coupling Theory and Fragile to
34 Strong Transition in Supercooled TIP4P/2005 Water *Submitted (2015)*.
35
36
37 [293] Corradini, D.; Gallo, P.; Buldyrev, S. V.; Stanley, H. E. Fragile to strong crossover coupled
38 to liquid-liquid transition in hydrophobic solutions. *Phys. Rev. E* **2012**, *85*, 051503.
39
40
41 [294] Xu, L.; Mallamace, M.; Yan, Z.; Starr, F. W.; Buldyrev, S. V.; Stanley, H. E. Appearance
42 of a fractional Stokes–Einstein relation in water and a structural interpretation of its onset.
43 *Nature Phys.* **2009**, *5*, 565–569.
44
45
46 [295] Soper, A. K. Radical re-appraisal of water structure in hydrophilic confinement. *Chem. Phys.*
47 *Lett.* **2013**, *590*, 1-15.
48
49
50 [296] Gallo, P.; Rovere, M.; Chen, S.-H. Dynamic crossover in supercooled confined water: under-
51 standing bulk properties through confinement. *J. Phys. Chem. Lett.* **2010**, *1*, 729–733.
52
53
54 [297] Gallo, P.; Rovere, M.; Chen, S.-H. Anomalous dynamics of water confined in MCM-41 at
55 different hydrations. *J. Phys.: Condens. Matter* **2010**, *22*, 284102.
56
57
58 [298] Gallo, P.; Rovere, M.; Chen, S.-H. Water confined in MCM-41: a Mode Coupling Theory
59 analysis. *J. Phys.: Condens. Matter* **2012**, *24*, 064109.
60

- 1
2
3 [299] Caupin, F. Escaping the no man's land: Recent experiments on metastable liquid water. *J.*
4 *Non-Crystalline Solids* **2015**, *407*, 441–448.
5
6
7 [300] Rosenfeld, Y. Relation between the transport coefficients and the internal entropy of simple
8 systems. *Phys. Rev. A* **1977**, *15*, 2545–2549.
9
10 [301] Rosenfeld, Y. A quasi-universal scaling law for atomic transport in simple fluids. *J. Phys.:*
11 *Condens. Matter* **1999**, *11*, 5415–5427.
12
13 [302] Dzugutov, M. A universal scaling law for atomic diffusion in condensed matter. *Nature* **1996**,
14 *381*, 137–139.
15
16 [303] Hoyt, J. J.; Asta, M.; Sadigh, B. Test of the Universal Scaling Law for the Diffusion Coeffi-
17 cient in Liquid Metals. *Phys. Rev. Lett.* **2000**, *85*, 594–597.
18
19 [304] Sharma, R.; Chakraborty, S. N.; Chakravarty, C. Entropy, diffusivity, and structural order
20 in liquids with waterlike anomalies. *J. Chem. Phys.* **2006**, *125*, 204501.
21
22 [305] Errington, J. R.; Truskett, T. M.; Mittal, J. Excess-entropy-based anomalies for a waterlike
23 fluid. *J. Chem. Phys.* **2006**, *125*, 244502.
24
25 [306] Agarwal, M.; Singh, M.; Sharma, R.; Alam, M. P.; Chakravarty, C. Relationship between
26 Structure, Entropy, and Diffusivity in Water and Water-Like Liquids. *J. Phys. Chem. B*
27 **2010**, *114*, 6995–7001.
28
29 [307] Abramson, E. H. Viscosity of water measured to pressures of 6 GPa and temperatures of 300
30 °C. *Phys. Rev. E* **2007**, *76*, 051203.
31
32 [308] Agarwal, M.; Chakravarty, C. Relationship between structure, entropy, and mobility in
33 network-forming ionic melts. *Phys. Rev. E* **2009**, *79*, 030202(R).
34
35 [309] de Oliveira, A. B.; Franzese, G.; Netz, P. A.; Barbosa, M. C. Waterlike hierarchy of anomalies
36 in a continuous spherical shouldered potential. *J. Chem. Phys.* **2008**, *128*, 064901.
37
38 [310] Mittal, J.; Errington, J. R.; Truskett, T. M. Relationship between thermodynamics and
39 dynamics of supercooled liquids. *J. Chem. Phys.* **2006**, *125*, 076102.
40
41 [311] Krekelberg, W. P.; Kumar, T.; Mittal, J.; Errington, J. R.; Truskett, T. M. Anomalous
42 structure and dynamics of the Gaussian-core fluid. *Phys. Rev. E* **2009**, *79*, 031203.
43
44 [312] Goel, T.; Patra, C. N.; Mukherjee, T.; Chakravarty, C. Excess entropy scaling of transport
45 properties of Lennard-Jones chains. *J. Chem. Phys.* **2008**, *129*, 164904.
46
47 [313] Malvaldi, M.; Chiappe, C. Excess entropy scaling of diffusion in room-temperature ionic
48 liquids. *J. Chem. Phys.* **2010**, *132*, 244502.
49
50
51
52
53
54
55
56
57
58
59
60

- 1
2
3
4 [314] Chopra, R.; Truskett, T. M.; Errington, J. R. On the Use of Excess Entropy Scaling to
5 Describe the Dynamic Properties of Water. *J. Phys. Chem. B* **2010**, *114*, 10558–10566.
6
7 [315] Chopra, R.; Truskett, T. M.; Errington, J. R. Excess entropy scaling of dynamic quantities
8 for fluids of dumbbell-shaped particles. *J. Chem. Phys.* **2010**, *133*, 104506.
9
10 [316] Gallo, P.; Corradini, D.; Rovere, M. Widom line and dynamical crossovers: routes to under-
11 stand supercritical water. *Nature Commun.* **2014**, *5*, 5806.
12
13 [317] Simeoni, G. G.; Bryk, T.; Gorelli, F. A.; Krisch, M.; Ruocco, G.; Santoro, M.; Scopigno, T.
14 The Widom line as the crossover between liquid-like and gas-like behavior in supercritical
15 fluids. *Nature Phys.* **2010**, *6*, 503–507.
16
17 [318] Brazhkin, V. V.; Fomin, Yu. D.; Lyapin, A. G.; Ryzhov, V. N.; Tsiok, E. N. Widom Line for
18 the Liquid-Gas Transition in Lennard-Jones System. *J. Phys. Chem. B* **2011**, *115*, 14112–
19 14115.
20
21 [319] Gallo, P.; Corradini, D.; Rovere, M. The Widom line and dynamical crossover in supercritical
22 water: Popular water models versus experiments *J. Chem. Phys.* **2015**, *143*, 114502.
23
24 [320] Tanaka, H. A new scenario of the apparent fragile-to-strong transition in tetrahedral liquids:
25 water as an example. *J. Phys: Condens. Matter* **2003**, *15*, L703-L711.
26
27 [321] Kanno, H.; Speedy, R. J.; Angell, C. A. Supercooling of water to -92 °C under pressure.
28 *Science* **1975**, *189*, 880–881.
29
30 [322] Caupin, F.; Herbert, E. Cavitation in water: a review. *C. R. Phys.* **2006**, *7*, 1000–1017.
31
32 [323] Caupin, F.; Stroock, A. D. The stability limit and other open questions on water at negative
33 pressure, in: H.E. Stanley, S. Rice (Eds.), *Liquid Polymorphism*; Advances in Chemical
34 Physics **152**, Wiley: New York, 2013.
35
36 [324] Henderson, S. J.; Speedy, R. J. Temperature of maximum density in water at negative
37 pressure. *J. Phys. Chem.* **1987**, *91*, 3062–3068.
38
39 [325] Henderson, S. J.; Speedy, R. J. Melting temperature of ice at positive and negative pressures.
40 *J. Phys. Chem.* **1987**, *91*, 3069–3072.
41
42 [326] Davitt, K.; Rolley, E.; Caupin, F.; Arvengas, A.; Balibar, S. Equation of state of water under
43 negative pressure. (2010) 174507.
44
45 [327] Wagner, W.; Pruß, A. The IAPWS formulation 1995 for the thermodynamic properties of
46 ordinary water substance for general and scientific use. *J. Phys. Chem. Ref. Data* **2002**, *31*,
47 387–535.
48
49
50
51
52
53
54
55
56
57
58
59
60

- 1
2
3 [328] The International Association for the Properties of Water and Steam, Revised Release on the
4 IAPWS Formulation 1995 for the Thermodynamic Properties of Ordinary Water Substance
5 for General and Scientific Use, 2009.
6
7
8
9 [329] Zheng, Q.; Durben, D. J.; Wolf, G. H.; Angell, C. A. Liquids at large negative pressures:
10 water at the homogeneous nucleation limit. *Science* **1991**, *254*, 829–832.
11
12 [330] Alvarenga, A. D.; Grimsditch, M.; Bodnar, R. J. Elastic properties of water under negative
13 pressures. *J. Chem. Phys.* **1993**, *98*, 8392–8396.
14
15
16 [331] Shmulovich, K. I.; Mercury, L.; Thiéry, R.; Ramboz, C.; El Mekki, M. Experimental super-
17 heating of water and aqueous solutions. *Geochim. Cosmochim. Acta* **2009**, *73*, 2457–2470.
18
19 [332] El Mekki Azouzi, M.; Ramboz, C.; Lenain, J.-F.; Caupin, F. A coherent picture of water at
20 extreme negative pressure. *Nature Phys.* **2013**, *9*, 38–41.
21
22
23 [333] Angell, C. A.; Supercooled water: Two phases? *Nature Materials* **2014**, *13*, 673–675.
24
25 [334] Ronceray, P.; Harrowell, P., Favoured local structures in liquids and solids: a 3D lattice
26 model. *Soft Matter* **2015**, *11*, 3322–3331.
27
28 [335] Velikov, V.; Borick, S.; Angell, C. A. The glass transition of water, based on hyperquenching
29 experiments. *Science* **2001**, *294*, 2335–2338.
30
31
32 [336] Meadley, S. L.; Angell, C. A. Water and its relatives: The stable, supercooled and particu-
33 larly the stretched, regimes. Proceedings of the International School of Physics Enrico Fermi:
34 "Water: Fundamentals as the basis for understanding the environment and promoting tech-
35 nology" Course 187, edited by P. G. Debenedetti, M. A Ricci and F. Bruni; IOS Press,
36 Amsterdam; SIF, Bologna, 2015; p 19–44.
37
38
39 [337] Birch, F. Finite Elastic Strain of Cubic Crystals. *Phys. Rev. E* **1947**, *71*, 809–824.
40
41 [338] Murnaghan, F. D. The Compressibility of Media under Extreme Pressures. *Proc. Natl. Acad.*
42 *Sci. (USA)* **1944**, *30*, 244–247.
43
44 [339] Briggs, L. J. Limiting negative pressure of water. *J. Appl. Phys.* **1950**, *21*, 721–722.
45
46 [340] Winnick, J.; Cho, S. J. PVT behavior of water at negative pressures. *J. Chem. Phys.* **1971**,
47 *55*, 2092–2097.
48
49 [341] Green, J. L.; Durben, D. J.; Wolf, G. H.; Angell, C. A. Water and Solutions at Negative
50 Pressure: Raman Spectroscopic Study to -80 Megapascals. *Science* **1990**, *249*, 649–652.
51
52 [342] Zheng, Q. Liquids under tension and glasses under stress. Ph. D. Thesis, Purdue University,
53 1991.
54
55
56
57
58
59
60

- 1
2
3 [343] Fisher, J. C. The Fracture of Liquids. *J. Appl. Phys.* **1948**, *19*, 1062–1067.
4
5 [344] Caupin, F. Liquid-vapor interface, cavitation, and the phase diagram of water *Phys. Rev. E*,
6
7 **2005**, *71*, 051605, 1-5.
8
9 [345] Davitt, K.; Arvengas, A.; Caupin, F. Water at the cavitation limit: density of the metastable
10
11 liquid and size of the critical bubble. *Euro. Phys. Lett.* **2010**, *90*, 16002.
12
13 [346] Bodnar, R. J.; Sterner, S. M. Synthetic fluid inclusions in natural quartz I. Compositional
14
15 types synthesized and applications to experimental geochemistry. *Geochim. Cosmochim. Acta*
16
17 **1984**, *48*, 2659–2668.
18
19 [347] Corradini, D.; Strelakova, E.; Stanley, H. E.; Gallo, P. Microscopic mechanism of protein
20
21 cryopreservation in an aqueous solution with trehalose. *Sci. Rep.* **2013**, *3*, 1218.
22
23 [348] Gallo, P.; Rovere, M.; Spohr, E. Supercooled confined water and the Mode Coupling
24
25 Crossover Temperature. *Phys. Rev. Lett.* **2000**, *85*, 4317.
26
27 [349] Gallo, P.; Rovere, M.; Spohr, E. Glass transition and layering effect in confined water: a
28
29 computer simulation study. *J. Chem. Phys.* **2000**, *113*, 11324–11335.
30
31 [350] Faraone, A.; Liu, L.; Mou, C.-Y.; Yen, C.-W.; Chen, S.-H. Fragile-to-strong liquid transition
32
33 in deeply supercooled confined water. *J. Chem. Phys.* **2004**, *121*, 10843–10846.
34
35 [351] Luo, J.; Xu, L.; Lascaris, E.; Stanley, H. E.; Buldyrev, S. V. Behavior of the Widom Line in
36
37 Critical Phenomena. *Phys. Rev. Lett.* **2014**, *112*, 135701.
38
39 [352] Kumar, P.; Wikfeldt, K. T.; Schlesinger, D.; Pettersson, L. G. M.; Stanley, H. E. The Boson
40
41 peak in supercooled water. *Sci. Rep.* **2013**, *3*, 1980.
42
43 [353] Kanno, H.; Angell, C. A. Homogeneous nucleation and glass formation in aqueous alkali
44
45 halide solutions at high pressures. *J. Phys. Chem.* **1977**, *81*, 2639–2643.
46
47 [354] Miyata, K.; Kanno, H.; Niino, T.; Tomizawa, K. Cationic and anionic effects on the homo-
48
49 geneous nucleation of ice in aqueous alkali halide solutions. *Chem. Phys. Lett.* **2002**, *354*,
50
51 51–55.
52
53 [355] Miyata, K.; Kanno, H. Supercooling behavior of aqueous solutions of alcohols and saccha-
54
55 rides. *J. Mol. Liq.* **2005**, *119*, 189–193.
56
57 [356] Archer, D. G.; Carter, R. W. Thermodynamic Properties of the NaCl + H₂O System. 4. Heat
58
59 Capacities of H₂O and NaCl(aq) in Cold-Stable and Supercooled States. *J. Phys. Chem. B*
60
2000, *104*, 8563–8584.

- 1
2
3 [357] Carter, R. W.; Archer, D. G. Heat capacity of $\text{NaNO}_3(\text{aq})$ in stable and supercooled states.
4 Ion association in the supercooled solution. *Phys. Chem. Chem. Phys.* **2000**, *2*, 5138–5145.
5
6
7 [358] Mishima, O. Application of polyamorphism in water to spontaneous crystallization of emul-
8 sified $\text{LiCl-H}_2\text{O}$ solution. *J. Chem. Phys.* **2005**, *123*, 154506.
9
10 [359] Mishima, O. Phase separation in dilute $\text{LiCl-H}_2\text{O}$ solution related to the polyamorphism of
11 liquid water. *J. Chem. Phys.* **2007**, *126*, 244507.
12
13
14 [360] Guadalupe, N. R.; Bove, L. E.; Corti, H. R.; Loerting, T. Pressure-induced transformations
15 in $\text{LiCl-H}_2\text{O}$ at 77 K. *Phys. Chem. Chem. Phys.* **2014**, *16*, 18553–18562.
16
17
18 [361] Paschek, D. How the Liquid-Liquid Transition Affects Hydrophobic Hydration in Deeply
19 Supercooled Water. *Phys. Rev. Lett.* **2005**, *94*, 217802.
20
21
22 [362] Le, L.; Molinero, V. Nanophase Segregation in Supercooled Aqueous Solutions and their
23 Glasses Driven by the Polyamorphism of Water. *J. Phys. Chem. A* **2011**, *115*, 5900–5907.
24
25
26 [363] Chatterjee, S.; Debenedetti, P. G. Fluid-Phase Behavior of Binary Mixtures in which One
27 Component Can Have Two Critical Points. *J. Chem. Phys.* **2006**, *124*, 154503.
28
29
30 [364] Anisimov, M. A. Cold and supercooled water: a novel supercritical-fluid solvent. *Russ. J.*
31 *Phys. Chem. B* **2012**, *6*, 861–867.
32
33 [365] Suzuki, Y.; Mishima, O. Experimentally proven liquid-liquid critical point of dilute of dilute
34 glycerol-water solutions at 150 K. *J. Chem. Phys.* **2014**, *141*, 094505.
35
36
37 [366] Murata, K.; Tanaka, H. Liquid–liquid transition without macroscopic phase separation in a
38 water–glycerol mixture. *Nature Materials* **2012**, *11*, 436–443.
39
40
41 [367] Murata, K.-I.; Tanaka, H. General nature of liquid–liquid transition in aqueous organic
42 solutions. *Nature Commun.* **2013**, *4*, 2844.
43
44 [368] Popov, I.; Greenbaum (Gutina), A.; Sokolov, A. P.; Feldman, Y. The puzzling first-order
45 phase transition in water–glycerol mixtures. *Phys. Chem. Chem. Phys.* **2015**, *17*, 18063–
46 18071.
47
48
49 [369] Zhao, L.-S.; Cao, Z.-X.; Wang, Q. Glass transition of aqueous solutions involving annealing-
50 induced ice recrystallization resolves liquid-liquid transition puzzle of water. *Sci. Rep.* **2015**,
51 *5*, 15714.
52
53
54
55 [370] Miyata, K.; Kanno, H.; Niino, T.; Tomizawa, K. Cationic and anionic effects on the homo-
56 geneous nucleation of ice in aqueous alkali halide solutions, *Chem. Phys. Lett.* **2002**, *354*,
57 51–55.
58
59
60

- 1
2
3 [371] Corradini, D.; Rovere, M.; Gallo, P. Structural properties of high density and low density
4 water in supercooled aqueous solutions of salt. *J. Phys. Chem. B* **2011**, *115*, 1461–1468.
5
6
7 [372] Huang, C.; Weiss, T. M.; Nordlund, D.; Wikfeldt, K. T.; Pettersson, L. G. M.; Nilsson, A.
8 Increasing correlation length in bulk supercooled H₂O, D₂O, and NaCl solution determined
9 from small angle x-ray scattering. *J. Chem. Phys.* **2010**, *133*, 134504.
10
11 [373] Mishima, O. Melting of the Precipitated Ice IV in LiCl Aqueous Solution and Polyamorphism
12 of Water. *J. Phys. Chem. B* **2011**, *115*, 14064–14067.
13
14
15 [374] Suzuki, Y.; Mishima, O. Sudden switchover between the polyamorphic phase separation and
16 the glass-to-liquid transition in glassy LiCl aqueous solutions. *J. Chem. Phys.* **2013**, *138*,
17 084507.
18
19 [375] Corradini, D.; Su, Z.; Stanley, H. E.; Gallo, P. A molecular dynamics study of the equation
20 of state and structure of supercooled aqueous solutions of methanol. *J. Chem. Phys.* **2012**,
21 *137*, 184503.
22
23 [376] Mallamace, F.; Branca, C.; Corsaro, C.; Leone, N.; Spooren, J.; Stanley, H. E.; Chen, S.-H.
24 Dynamical crossover and breakdown of the Stokes-Einstein relation in confined water and in
25 methanol-diluted bulk water. *J. Phys. Chem. B* **2010**, *114*, 1870–1878.
26
27 [377] Hendricks, R. W., Mardon, P. G. and Shaffer, L. B. X-Ray Zero-Angle Scattering Cross-
28 Section of Water. *J. Chem. Phys.* **1974**, *61*, 319–322.
29
30 [378] Leberman, R.; Soper, A. K. Effect of High-Salt Concentrations on Water-Structure. *Nature*
31 **1995**, *378*, 364–366.
32
33 [379] Mallamace, F.; Corsaro, C.; Baglioni, P.; Fratini, E.; Chen, S.-H. The dynamical crossover
34 phenomenon in bulk water, confined water and protein hydration water. *J. Phys.: Condens.*
35 *Matter* **2012**, *24*, 064103.
36
37 [380] Suhina, T.; Weber, B.; Carpentier, C. E.; Lorincz, K.; Schall, P.; Bonn, D.; M., B. A.
38 Fluorescence Microscopy Visualization of Contacts Between Objects. *Angew. Chemie Int.*
39 *Ed.* **2015**, *54*, 3688–3691.
40
41 [381] Holmberg, K.; Andersson, P.; Erdemir, A. Global energy consumption due to friction in
42 passenger cars. *Tribol. Int.* **2012**, *47*, 221–234.
43
44 [382] Poole, P. H.; Becker, S. R.; Sciortino, F.; Starr, F. W. Dynamical Behavior Near a Liquid-
45 Liquid Phase Transition in Simulations of Supercooled Water. *J. Phys. Chem. B* **2011**, *115*,
46 1417614183.
47
48
49
50
51
52
53
54
55
56
57
58
59
60

- 1
2
3 [383] Prielmeier, F. X.; Lang, E. W.; Speedy, R. J.; Lüdemann, H.-D. The Pressure Dependence of
4 Self Diffusion in Supercooled Light and Heavy Water. *Ber. Bunsenges. Phys. Chem.* **1988**,
5 *92*, 1111–1117.
6
7
8
9 [384] Zheng, Q.; Green, J.; Kieffer, J.; Poole, P. H.; Shao, J.; Wolf, G. H.; Angell, C. A. Limiting
10 tensions for liquids and glasses from laboratory and MD studies. NATO-ASI Series *Liquids*
11 *under Negative pressure*, Kluwer Academic Pub, 2002; p. 1–46.
12
13
14 [385] Koop, T.; Luo, B.-P.; Tsias, A.; Peter, T. Water activity as the determinant for homogeneous
15 ice nucleation in aqueous solutions. *Nature* **2000**, *406*, 611–614.
16
17
18 [386] Waluyo, I.; Nordlund, D.; Bergmann, U.; Schlesinger, D.; Pettersson, L. G. M.; Nilsson,
19 A. Different View of Structure-Making and Structure-Breaking in Alkali Halide Aqueous
20 Solutions through X-ray Absorption Spectroscopy. *J. Chem. Phys.* **2014**, *140*, 244506.
21
22
23 [387] Binder, K. Simulations clarify when supercooled water freezes into glassy structures. *Proc*
24 *Natl. Acad. Sci. (USA)* **2014**, *111*, 9374–9375.
25
26
27
28
29
30
31
32
33
34
35
36
37
38
39
40
41
42
43
44
45
46
47
48
49
50
51
52
53
54
55
56
57
58
59
60